JAN. - APR. 2002
Volume VIII Number I
ISSN 0859 144X

THE ASEAN JOURNAL OF RADIOLOGY

Published by The Radiological Society and
The Royal College of Radiologists of Thailand,
Bangkok, Thailand

Started through an educational grant from Bracco since 1995

Toshiba Medical Systems Group

contributes to the health and welfare of people all over the world through the development, production and servicing of advanced medical equipment. Toshiba Medical Systems Company has grown into one of the world's leading diagnostic imaging manufacturers, contributing to the advancement of medicine.

Its operations include Research & Development design, production, sales & services and support of diagnostic imaging equipment and systems. Based on the concept that only R & D carried out in full collaboration with worldwide medical circles can truly contribute to health care progress, Toshiba maintains constant contact with the real world of daily medical practice, receiving feed-back on clinical needs and incorporating it into R & D actvities. These and other activities have won the highest praise in the global medical market.

It is our commitment to bring high technology plus experience through the supply of a wide-range of Diagnostic X-ray, Ultrasound, Computerised Tomography and Magnetic Resonance Imaging Systems. Toshiba's vision is to provide solutions to the medical professionals that help save the patient's lives while offering reliable products with a long service life.

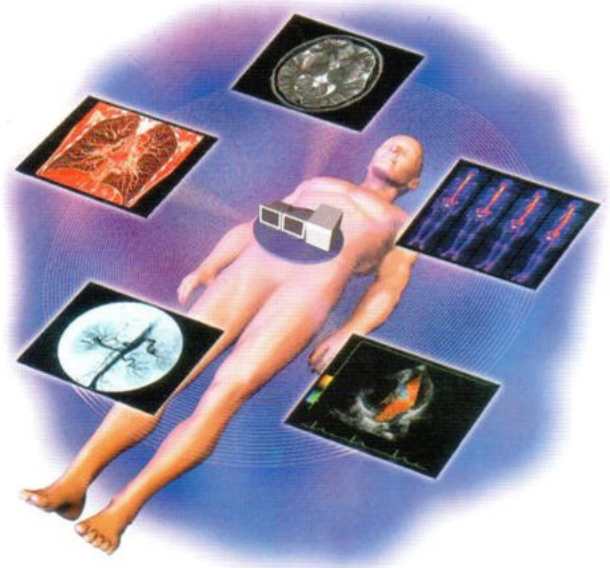

TOSHIBA
MEDICAL SYSTEMS

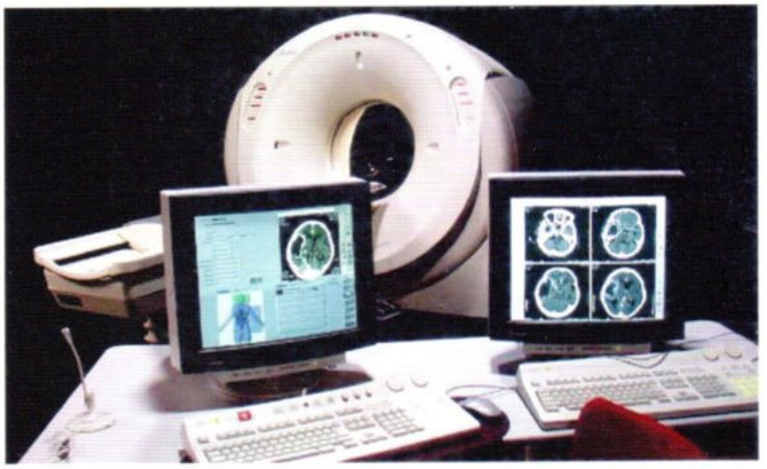

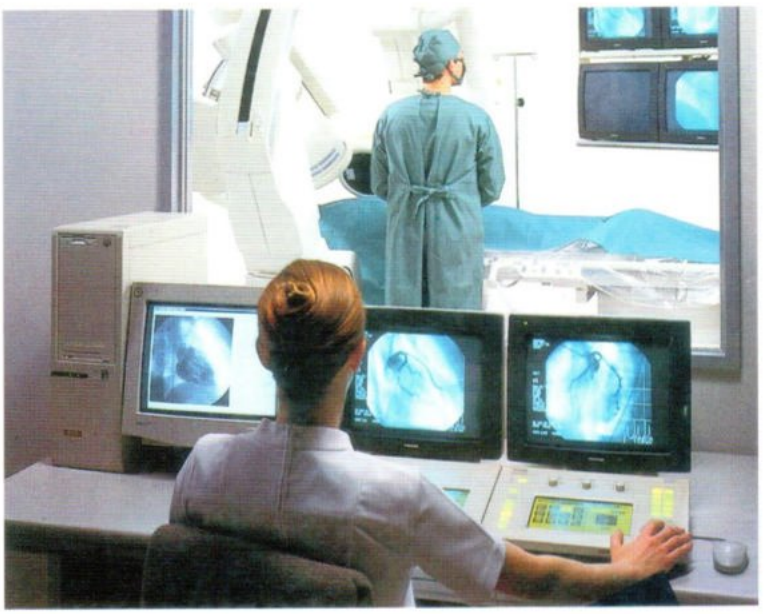

Sole Distributor

CMC Biotech Co., Ltd.

364 Muban Town-in-Town, Soi Ladphrao 94
Ladphrao Road, Wangthonglang, Bangkok 10310
Tel : 66 (0) 2530-4995 (Hunting 8 lines)
Fax: 66 (0) 2539-6903
E-mail address : cmcsales@cmcbiotech.co.th

- **Central Branch (Bangkok)**

Tel : 66 (0) 2530-4689, 2530-4995 Ext. 601
E-mail address: cmccb@cmcbiotech.co.th

- **Northern Branch (Chiangmai)**

Tel : 66 (0) 5328-3261 Fax : 66 (0) 5320-4463
E-mail address: cmcnb@cmcbiotech.co.th

- **North Eastern Branch (Khon Kaen)**

Tel : 66 (0) 4334-1642 Fax : 66 (0) 4334-1643
E-mail address: cmcneb@cmcbiotech.co.th

- **Southern Branch (Hadyai)**

Tel : 66 (0) 7442-9803 Fax : 66 (0) 7442-9804
E-mail address: cmcsb@cmcbiotech.co.th

Service Excellence with Professionalism

Made for Life

JAN. - APR. 2002
Volume VIII Number I

ISSN 0859 144X

THE ASEAN JOURNAL OF RADIOLOGY

**Published by The Radiological Society and
The Royal College of Radiologists of Thailand,
Bangkok, Thailand**

Started through an educational grant from Bracco since 1995

www.bracco.com/imaging

Chief Editor

Professor Kawee Tungsubutra
Kaweevej Hospital, 318 Taksin Road, Dhonburi, Bangkok 10600, Thailand.

Asean Journal of Radiology.
Instructions for Authors.

1. The Asean Journal of Radiology publishes the papers on Radiological Sciences, such as research work, review articles, case reports, innovations in Medical Sciences related to all branches of Radiology, and letters to the editor. The aforementioned materials can be written in English only.

2. The authors have to submit 2 copies of the manuscript and a diskette: **to Prof. Dr. Kawee Tungsubutra.** 318 Kaweevej Hospital, Taksin Road, Dhonburi, Bangkok 10600, Thailand.

3. The original copy to be submitted must be typed in a double space on one side of the page of 8.1/2" x 11.1/2" paper.

4. The format of the article must include :

a. Title page and address of the author (s)
b. Abstract
c. Introduction (Background)
d. Material and Method
e. Results and discussion (Tables and Illustrations)
f. Acknowledgement (if any)
g. References (Follow the Vancouver style developed by ICMJE)

5. We will provide 5 copies of reprints for the author (s) who submit (s) an article for publication in the Asean Journal.

6. The illustrations and tables must be clearly prepared with legends in English as they are the art works to be reproduced.

7. The authors are responsible for the contents of the article as to its facts and findings.

8. Ethics.

Paper reporting studies which might be interpreted as human experimentation (e.g. controlled trials) should conform to the standards of the Declaration of Helsinki (see British Medical Journal 1964:2:177) and should indicate that, approval that such studies may proceed, has been granted by the local or hospital Ethics Committee.

When reporting experiments on animals indicate whether the institution's or the National Research Council's guide for, or any national law on, the care and use of laboratory animals was followed.

BRACCO EDUCATION

Asia - Oceania

AO

Asian-Oceanian Seminars on Diagnostic and Interventional Radiology 2002

Uroradiology and Obstetrics & Gynaecology Imaging: current issues and new modalities

May 18 - 19
Seoul, Korea

Programme Leader:
Prof K S Cho

For further information please contact:

ASDIR Secretariat
Huntington Consultancy Pte Ltd
47 Hill Street #06-04
S.C.C.C.I. Building
Singapore 179365
Tel: +65-339 2883
Fax: +65-339 2272
E-mail: asdir.secretariat@huntington.com.sg

BRACCO
THE IMAGE OF INNOVATION

www.bracco.com/imaging

THE ASEAN JOURNAL OF RADIOLOGY

Volume VIII Number I JAN. - APR. 2002

CONTENTS

THE ASEAN JOURNAL OF RADIOLOGY

Volume VIII Number I JAN. - APR. 2002

CONTENTS

SELECTIVE TRANSCATHETER EMBOLIZATION FOR TREATMENT OF HEMOBILIA CAUSED BY POST-TRAUMATIC HEPATIC PSEUDOANEURYSM

VALLOP LAOPAIBOON[1] NITTAYA CHAMADOL[1]
JIRAPORN SRINAKARIN[1] WARINTHORN PHUTHARUK[1] AKE PUGKHEM[2]

ABSTRACT

Post-traumatic hepatic pseudoaneurysms are rare. Hepatic pseudoaneurysm is one of the causes of hemobilia, which can be treated via transarterial embolization. Two cases of post-traumatic hepatic pseudoaneurysm causing hemobilia were treated using selective transcatheter embolization in Srinagarind Hospital, Khon Kaen, Thailand. There was no further hemobilia after transcatheter embolization.

INTRODUCTION

Post-traumatic hepatic artery pseudoaneurysms that develop following penetrating or blunt traumas are rare.[1,2] Other reported etiologies for hepatic pseudoaneurysms include percutaneous liver biopsies, percutaneous transhepatic cholangiograms, and infection or inflammation due to septic emboli or pancreatitis.[3,4] Hepatic artery pseudoaneurysms are one cause of hemobilia[5] and hemobilia can be treated via transarterial embolization.

In this report, we present two cases of hepatic artery pseudoaneurysm, which resulted in a clinical presentation of hemobilia. These two pseudoaneurysms were treated with transcatheter embolization.

MATERIALS AND METHODS

We retrospectively reviewed the medical records and imaging studies of two cases of hepatic artery pseudoaneurysms at Srinagarind Hospital. Follow-up clinical findings, ultrasonograms and CT were recorded prospectively.

CASE REPORTS

CASE 1

A 23 year-old man fell from a machine at work. At the referring hospital, he was diagnosed with fractures of the mandible, cervical spine, femur and a blunt abdominal injury. Two months later, the patient developed hemobilia and was referred to our hospital.

Abdominal computed tomography (CT) was performed and it revealed low attenuation areas with internal high density in the right lobe of the liver, diagnosed as an hepatic hematoma (Figure 1A). Contrast enhanced CT revealed a central area of contrast enhancement isodense with the aorta representing a hepatic pseudoaneurysm (Figure 1B). A Doppler sonogram demonstrated a hypoechoic area in the right lobe of the liver, with a central jet flow consistent with a pseudoaneurysm (Figure 1C). Digital subtraction angiography (DSA) confirmed a pseudoaneurysm arising from a branch of the right hepatic artery (Figure 1D,1E). A simple curve 4-French catheter was introduced into the branch supplying the aneurysm and on into the aneurysm. Four

[1] Department of Radiology, Faculty of Medicine, Khon Kaen University, Thailand.
[2] Department of Surgery, Faculty of Medicine, Khon Kaen University, Thailand.

embolization coils (Cook, Bloomington) were deposited in the pseudoaneurysm. Gelfoam embolization into the aneurysm was the performed. Afterwards an embolization coil was deposited proximal to the aneurysm at the neck. Repeat contrast medium injection into the right hepatic artery demonstrated no contrast filling of the pseudoaneurysm (Figure 1F).

A follow-up Doppler sonogram was performed one week later and no remaining flow from the pseudoaneurysm was observed (Figure 1G). Four and eight months later, no remaining pseudoaneurysm was seen on the follow-up contrast enhanced CTs (Figure 1H). The patient remained asymptomatic during the entire follow-up period.

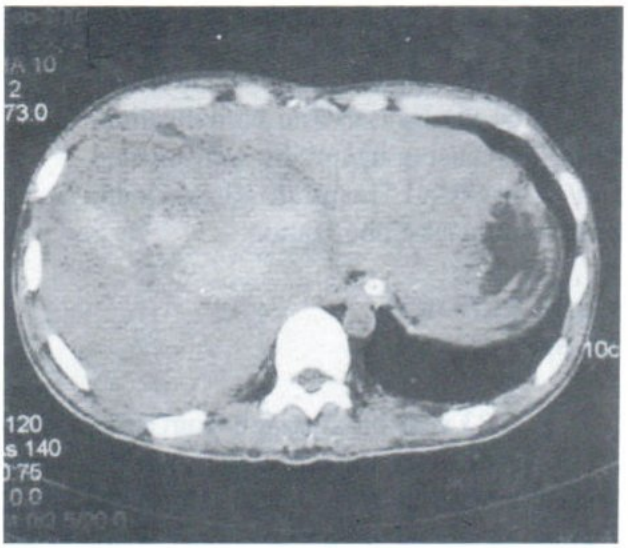

1A

Fig. 1A. Noncontrast enhanced CT demonstrates low density areas with internal high density in the right lobe of the liver, indicating a hepatic hematoma.

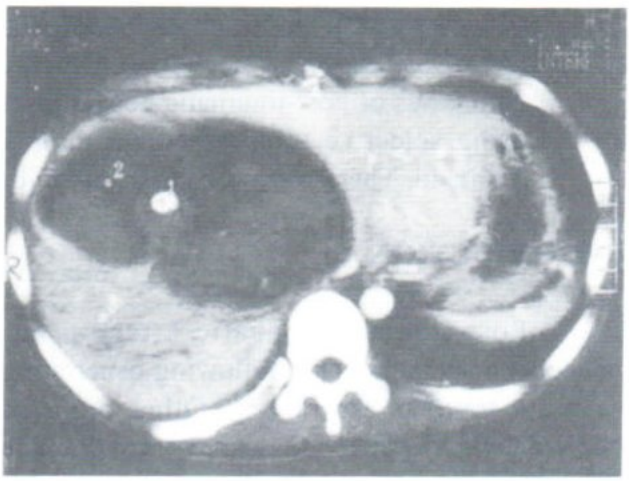

1B

Fig. 1B. Contrast enhanced CT demonstrates a central area of contrast enhancement isodense with the aorta indicates a hepatic pseudoaneurysm.

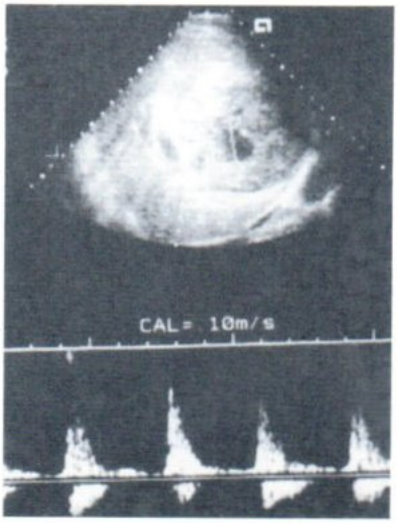

1C

Fig. 1C. Doppler ultrasound demonstrates hypoechoic areas in the right lobe of liver with a central jet of flow consistent with a pseudoaneurysm.

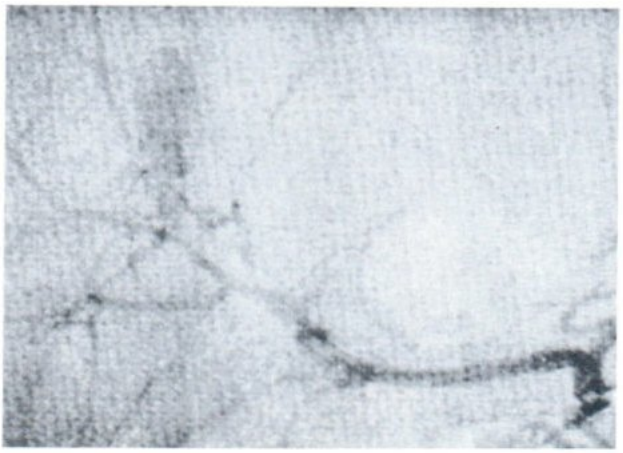

1D

Fig. 1D. Digital subtraction angiography confirms the presence of a pseudoaneurysm arising from a branch of the hepatic artery.

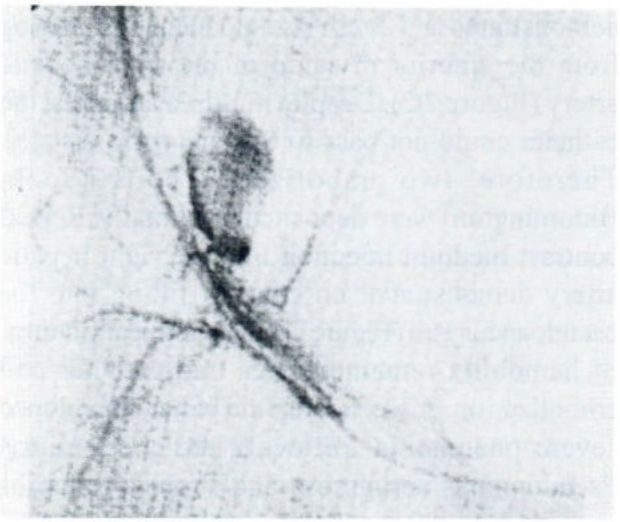

1E

Fig. 1E. Selective feeding artery branch digital substraction angiography shows pseudoaneurysm.

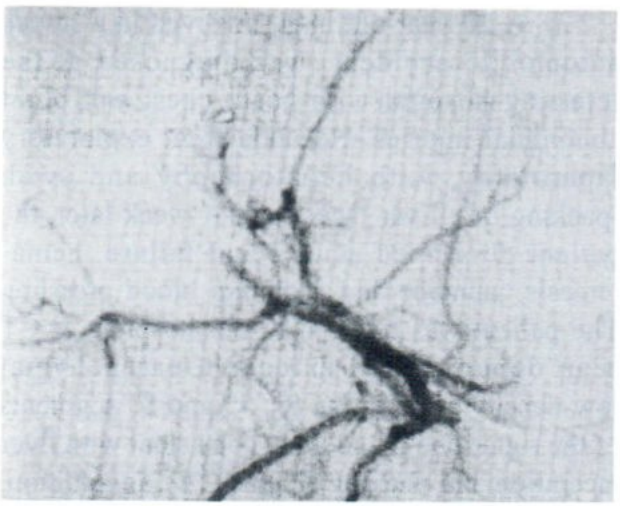

1E

Fig. 1F. Repeat contrast injection after coils and gelfoam embolization demonstrates no further filling of the pseudoaneurysm.

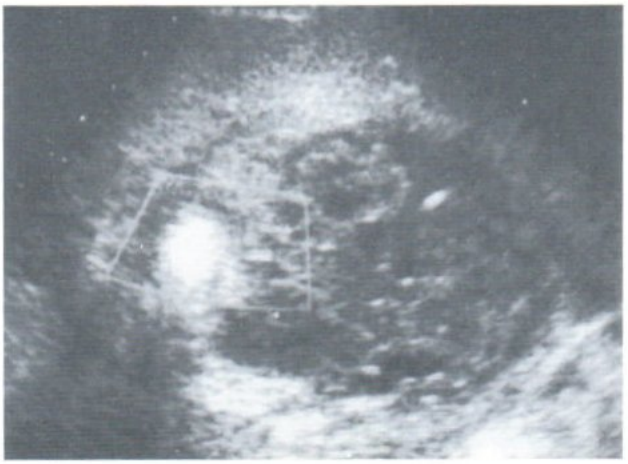

1G

Fig. 1G. Follow-up sonogram eight months later, no remaining area of central jet of flow of the pseudoaneurysm is demonstrated.

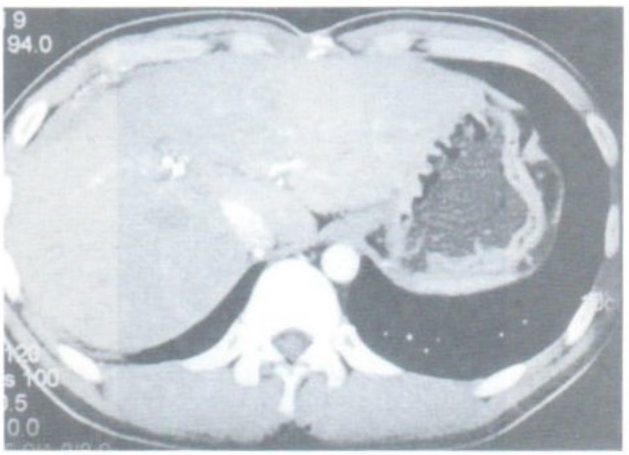

1H

Fig. 1H. Follow-up contrast enhanced CT eight months later, no remaining aneurysm is evident.

CASE 2

A 20-year-old man, involved in a severe automobile accident, was diagnosed at the referring hospital with head, chest and blunt abdominal injuries. He underwent exploratory laparotomy, with hepatorhaphy and swab -packing of a liver laceration. A week later, the patient developed acute renal failure, hematemesis, jaundice and declining blood pressure. The patient was referred to our hospital. A CT scan demonstrated extensive parenchymal low-density areas in the 5th, 7th and 8th segments of the right lobe of the liver, consistent with liver laceration and packing (Figure 2A). In addition, an enhancing lesion was seen in the anterior segment of the right lobe of the liver consistent with a pseudoaneurysm (Figure 2B). An adjacent low-density area was consistent with hematoma (Figure 2B). The DSA of the hepatic artery demonstrated a 1.5 cm pseudoaneurysm arising from the anterior division of the right hepatic artery (Figure 2C). Despite multiple attempts, the catheter could not pass to the aneurysm distally. Therefore, two embolization coils (Cook, Bloomington) were deposited proximally. Repeat contrast medium injection into the right hepatic artery demonstrated no contrast filling into the pseudoaneurysm (Figure 2D). No clinical findings of hemobilia remained after transcatheter coil embolization. A week later, the patient developed severe pneumonia following the chest injury. Pseudomonas aeruginosa and Proteus mirabilis were cultured from the tracheal specimen. The patient's relatives declined further hospital treatment preferring to take the patient home for last rites.

2A

Fig. 2A. Contrast enhanced CT demonstrates areas of low and high density in the anterior segment of the right lobe consistent with a liver laceration.

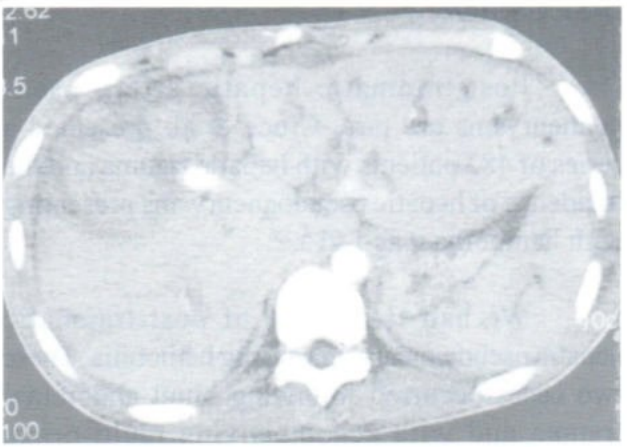

2B

Fig. 2B. Contrast enhanced CT demonstrates an enhanced lesion in the anterior segment of the right lobe consistent with a hepatic aneurysm.

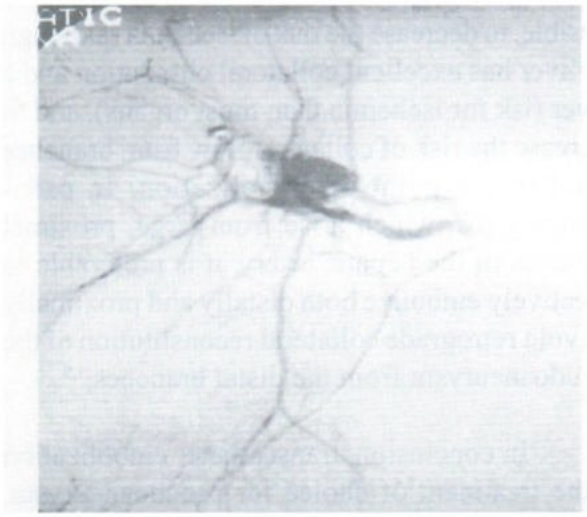

2C

Fig. 2C. Digital subtraction angiography of the hepatic artery demonstrates a pseudoaneurysm arising from a branch of the right hepatic artery.

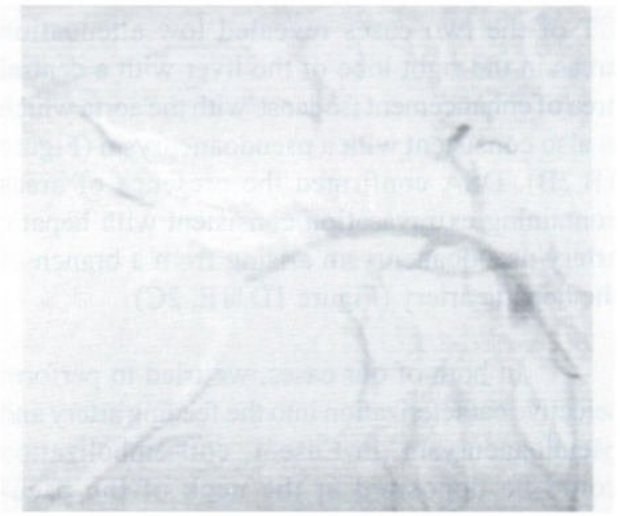

2D

Fig. 2D. Repeat contrast injection into the right hepatic artery demonstrates no further filling of the pseudoaneurysm.

DISCUSSION

Post-traumatic hepatic artery pseudoaneurysms are rare. Croce et al. presented a series of 482 patients with hepatic trauma and the incidence of hepatic pseudoaneurysms presenting with hemobilia was 1.2%.[5,6]

We had two cases of post-traumatic hepatic pseudoaneurysm causing hemobilia. These two cases occurred following blunt abdominal trauma and with accompanying multi-organ injury including hepatic laceration. We observed hepatic pseudoaneurysms in both cases using Doppler ultrasound, contrast enhanced CT and digital subtraction angiography (DSA). In each case, a Doppler sonogram demonstrated hypoechoeic areas in the right lobe of the liver, with a central jet flow consistent with a pseudoaneurysm (Figure 1C). Contrast enhanced CT of the two cases revealed low attenuation areas in the right lobe of the liver with a central area of enhancement isodense with the aorta which is also consistent with a pseudoaneurysm (Figure 1B,2B). DSA confirmed the presence of areas containing extravasation consistent with hepatic artery pseudoaneurysm arising from a branch of the hepatic artery (Figure 1D, 1E, 2C)

In both of our cases, we tried to perform selective catheterization into the feeding artery and pseudoaneurysm. In Case 1, coil embolization could be deposited at the neck of the pseudoaneurysm. Before depositing the coil, we put gelfoam into the pseudoaneurysm. In Case 2, we could not do selective catheterization into the neck of the aneurysm, therefore embolization coils were only deposited in the feeding artery proximal to the neck.

In general, angiography is the most sensitive technique for diagnosing and more accurately assessing hepatic pseudoaneurysms than ultrasonography and CT.[2,8]

Selective arterial transcatheter embolization is generally accepted for the treatment of hepatic vascular injury over operative repair because of its low mortality and morbidity.[1,3] A variety of embolic agents have been reported including silastic beads, detachable balloons, coils, gelfoam, polyvinyl alcohol, and a combination of coils and gelfoam.[1,2,7] Some investigators have suggested the use of both gelfoam and coil because the coils provide permanent occlusion and a structure on which to entrap gelfoam particles, while the gelfoam provides complete initial stasis.[4]

Embolization should be as selective as possible, to decrease the risk of ischemia (although the liver has excellent collateral circulation and a lower risk for ischemia than most organs), and to decrease the risk of collateral flow from branches distal to the point of embolization. In pseudoaneurysms, which arise from large, proximal branches of the hepatic artery, it is preferable to selectively embolize both distally and proximally to avoid retrograde collateral reconstitution of the pseudoaneurysm from the distal branches.[1,2]

In conclusion, transcatheter embolization is the treatment of choice for pseudoaneurysm. When technically possible, optimal treatment is superselective embolization both distally and proximally at the neck of aneurysm.

ACKNOWLEDGMENTS

Thanks to Mr. Bryan Roderick Hamman for assistance with the English-language presentation of the manscript.

REFERENCES

1. Schwart R, Teitelbaum G, Katz M, et al. Effectiveness of transcatheter embolization in the control of hepatic vascular injury. J Vasc interv Radiol.1993;4: 359-365.
2. Sidhu M, Shaw D, Daly D, et al. Post-traumatic hepatic pseudoaneurysm in children. Peddiatr Radiol. 1999;29: 46-52.
3. Knowdley D, Aggarwal A, Sachs P. Delayed hemorrhage after percutaneous liver biopsy: role of therapeutic angiography. J Clin Gastroenterol. 1994; 19:50-53.
4. Aboujaoude M, Noel B, Beaudoin M, et al. Pseudoaneurysm of proper hepatic artery with duodenal fistula appearing as a late complication of blunt abdominal trauma. J Trauma. 1996; 40: 123-125.
5. Gorich J, Rilinger N, Brado M, et al. Non-operative management of arterial liver hemorrhages. European Radiology 1999;9:85-88.
6. Croce M, Fabian T, Spiers J, et al. Traumatic hepatic artery pseudoaneurysm with hemobilia. Am J Surg. 1993; 168: 235-238.
7. Beningfield S, Bornman P, Krige E, et al. Control hemobilia by embolization of a false aneurym and arterioportobiliary fistula of hepatic artery. AJR 1991; 156: 1263-1265.
8. Tobben P, Zajko A, Sumkin J, et al. Pseudoaneuryms complicating organ transplantation: roles of CT, duplex sonography and angiography. Radiology. 1988; 169: 65-70.

SELECTIVE TRANSCATHETER COILS EMBOLIZATION FOR TREATMENT OF POST-TRAUMATIC DEEP FEMORAL PSEUDOANEURYSM

VALLOP LAOPAIBOON[1] JIRAPORN SRINAKARIN[1]
JITJROEN CHAIYACHUM[1] EIMORN MAIRIANG[1]
PIYAWAN CHATUPARISUTE[2]

ABSTRACT

Post-traumatic pseudoaneurysm of the deep femoral artery can be treated surgically. Alternative methods of abating peripheral aneurysm include: ultrasound-guided compression, percutaneous or transcatheter injection of bucrylate glue, thrombin, coils, detachable balloons or gelfoam. We report a successful transarterial coil embolization done on a patient with a post-traumatic deep femoral pseudoaneurysm at Srinagarind Hospital, Khon Kaen University, Thailand.

INTRODUCTION

Traditionally, treatment of peripheral pseudoaneurysms, such as a deep femoral artery pseudoaneurysm, is done surgically under direct vision. In recent years, utilization of angiographic and embolization techniques have allowed interventional radiologists an increasing role. Embolization was first considered an effective treatment of arterial bleeding and injury over 25 years ago.[1,2,3]

We report a case of post-traumatic deep femoral pseudoaneurysm treated using selective transcatheter embolization at Srinagarind Hospital, Khon Kaen University, Thailand.

CASE REPORT

A 69-year old man fell from the second floor of his house. Two weeks later, the patient was diagnosed with a neglected inter-trochanteric fracture of the left femur and was treated by closed reduction and a dynamic hip screw. Two weeks later, the patient still had painful swelling of the left thigh.

Digital subtraction angiography (DSA) demonstrated a pseudoaneurysm originating from the distal part of the left deep femoral artery (Figures 1A, B). Through a 4-French cobra curve catheter, the tip at neck of the pseudoaneurysm, three embolization coils (Cook, Bloomington) were deposited at the neck of the aneurysm (Figure 2A). Repeat contrast medium injection into the left deep femoral artery demonstrated no contrast filling of the pseudoaneurysm (Figure 2B). Within a week, the patient had improved and was discharged. At the five-month follow-up, the patient had no swelling or pain in the left thigh.

[1] Department of Radiology,Faculty of Medicine, Khon Kaen University, Khon Kaen, Thailand.
[2] Department of Orthopedics, Faculty of Medicine, Khon Kaen University, Khon Kaen, Thailand.

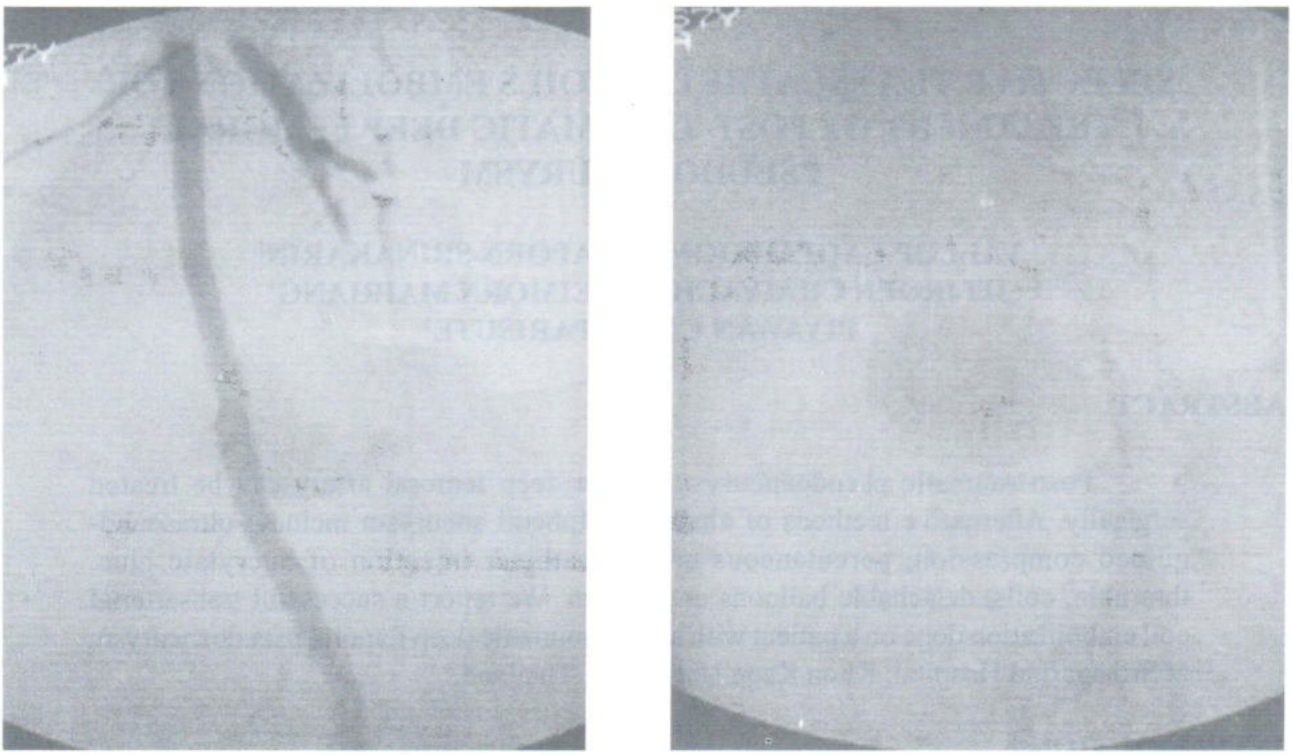

1A 1B

Fig. 1. DSA of femoral artery demonstate deep femoral artery Pseudoaneurysm.

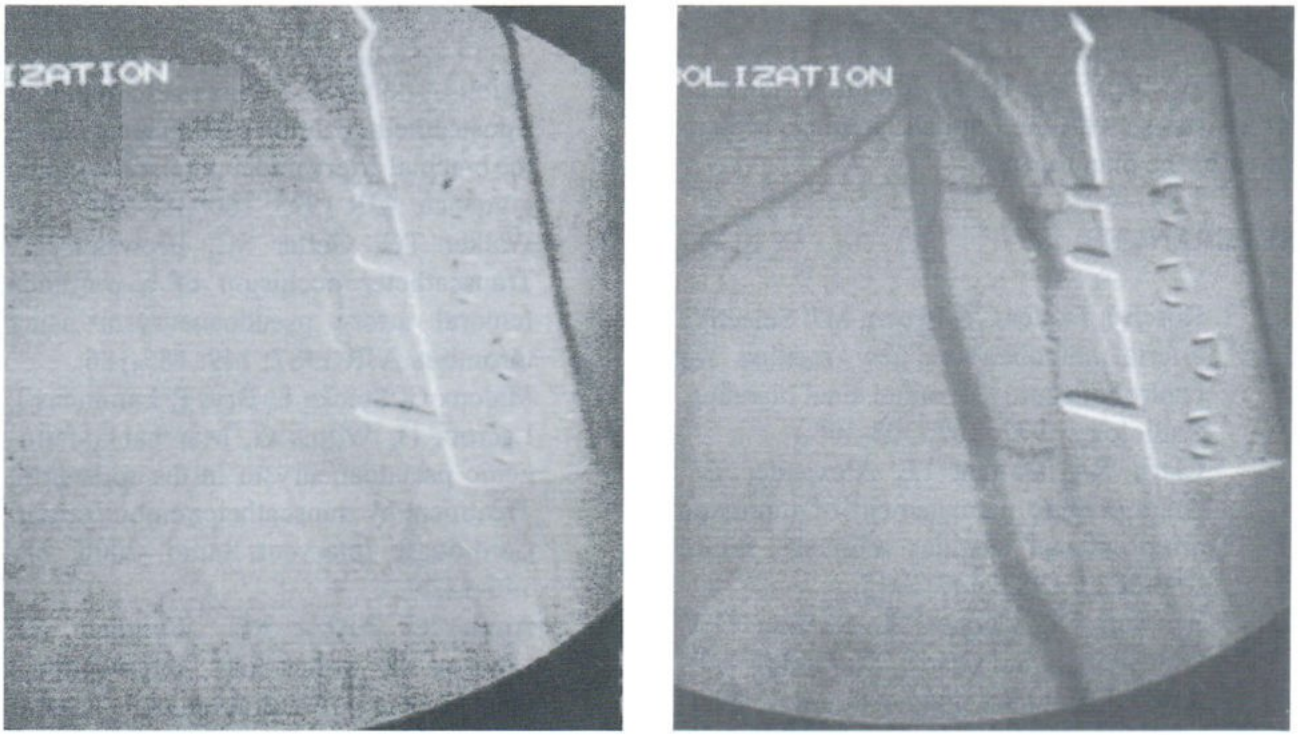

2A 2B

Fig. 2. After coils embolization (2A) and repeat contrast injection into femoral artery demonsrates no further filling of the pseudoaneurysm.

DISCUSSION

A femoral pseudoaneurysm can be managed definitively by a minimally-invasive or open surgical approach depending on its location, size, pathogenesis, and the patient's clinical status. When detected within a few hours of an invasive study, ultrasound-guided compression, is a highly successful procedure.

Ultrasound-guided compression was first introduced in 1991 and has become the treatment of choice.[4,5,6] If ultrasound-guided compression fails, surgical repair under direct vision is then the treatment of choice.

In recent years, utilization of angiographic and occlusive techniques have given interventional radiologists an increasing role in the management of pseudoaneurysms. Percutaneous or transcatheter injection of bucrylate glue, coils, thrombin detachable balloons and gelform are methods of abating peripheral aneurysms.[7,8,9,10,11,12] The most effective of these is probably coil embolization, which has been performed both transarterially and percutaneously. We reported a successful outcome for transarterial coil embolization, in a patient with a post-traumatic deep femoral aneurysm.

In conclusion, transcatheter coil embolization is safe and effective. This technique should be considered an option for treatment of peripheral arterial pseudoaneurysms as it has significant advantages over surgical repair.

ACKNOWLEDGMENTS

We thank Mr. Bryan Roderick Hamman for assistance with the English-language presentation of the manuscript.

REFERENCES

1. Rosch J, Dotter CT, Brown MJ. Selective arterial embolization: new method for control of acute gastrointestinal bleeding. Radiology 1972; 102: 303-306.
2. Clark RA, Gallant TE, Alexander ES. Angiographic management of traumatic arteriovenous fistula: clinical result. Radiologu 1983; 147: 9-13.
3. Scalfani SJ, Cooper R, Shaftan GW, Goldstein AS, Glanz S, Godon DH. Arterial trauma: diagnostic and therapeutic angiography. Radiology 1986; 161: 165-172.
4. Fellmeth BD, Roberts AC, Bookstein JJ, Freischlag JA, Forsythe JR, Buckner NK, Hye RJ. Postangiographic femoral artery injury: Non-surgical repair with US-guide compression. Radiology 1991; 178: 671-677.
5. Coley BD, Roborts AC, Fellmeth BD, Valji K, Bookstien JJ. Hye RJ. Postangiographic femoral artery pseudoaneurysm: Further experience with US-guide compression repaired. Radiology 1995; 307-311.
6. Skib0 L, Polak JF. Compression repair of a postcathetherization pseudoaneurysm of the brachial artery under untrasonographic guidance. AJR 1993; 160: 383-384.
7. Walker TG, Geller SC, Brewster SC. Transcatheter occlusion of a profunda femoral artery pseudoaneurysm using thrombin. AJR 1987; 149: 185-186.
8. Maleux G, Stockx L, Brys P, Lammens J, Lacroix H, Wilms G, Marchal G. Iatrogenic pseudoaneurysm in the upper arm: Treatment by transcatheter embolization. Cardiovase Intervent Radiol 2000; 23: 140-142.
9. Amin RJ, Fisher RG, Whigham CJ, Lindsey JI, Soltes GD. Interventional management of infrapopliteal arterial injury. Emergency Radiology 2000; 7: 276-283.
10. Fischer RG, Ben-Menachem Y. Interventional radiology in appendicular skeletal trauma. Radiol Clin North Am 1987; 25: 1203-1209.
11. Owen RJT, Haslam PJ, Elliott ST, Ross JDG, Loose HW. Percutaneous ablation of pseudoaneurysms using thrombin: a simple and effective solution. Cardiovase Intervent Radiology 2000; 23: 441-446.

GLUE EMBOLIZATION FOR TREATMENT OF RENAL INJURY

SILANATH PEUNGJESADA, M.D., ANCHALEE CHUROJANA, M.D.,
WALLAILAK CHAIYASOOT, M.D.

ABSTRACT

PURPOSE : To evaluate the outcome of glue embolization in two patients with renal AVF with and without pseudoaneurysm, one caused by percutaneous stone removal from the kidney and another one by trauma.

MATERIALS AND METHODS : History taking, physical examination and laboratory investigation were reviewed for patient evaluation. Then angiography of the pathologic kidneys were performed. It showed outpouching of contrast media and rapid draining vein which was connected to adjacent artery. Afterthat embolization was done with optimal mixture of glue and lipiodol.

RESULTS : Successful glue embolization of renal AVF and renal AVF with pseudoaneurysm of the kidneys with total occlusion of the affected vessels. Some degree of renal parenchyma infarction were seen without late complication.

CONCLUSION : Endovascular treatment is still useful in the treatment of renal AVF and pseudoaneurysm. Because it is a kidney-conservative therapy and provides less drastic,less invasive, less expenses and short hospitalization. Alternative embolized material is glue although coil is recommended to be the material of choice. The result of treatment is excellent when it is held in experienced hand.

INTRODUCTION

Vascular complications such as arteriovenous shunt (AVF) and pseudoaneurysm (PA) after surgical procedures and trauma can occurred especially post renal biopsy.[1-9] Biopsy is often performed in transplanted kidney to get a correct histological diagnosis of renal allograft rejection.[1-2] AVF has been reported in 0-15%[9] and most AVF remain asymptomatic and resolve spontaneously.[1-4] Although these two cases report of renal AVF with and without PA caused by previous stone removal from the kidney which is account for 0.5-1% complication and prior assult.

The treatment of choice is still endovascular procedures for both renal AVF and PA of the affected kidneys. Result of the treatment is excellent without late complication.

MATERIALS AND METHODS

History taking, physical examination and laboratory investigation were reviewed from the medical records. The 1st patient was a 56 year-old Thai man with a history of right RC came to Siriraj hospital to performed percutaneous nephrolithoplexy during August 2001. After the unevenful operation, he developed persistent gross hematuria for 12 days. So he went to the same hospital and for the initial impression for his hematuria, the provisional diagnosis was renal arteriovenous malformation (AVM). On physical examination, general appearance was moderately

DEPARTMENT OF RADIOLOGY, FACULTY OF MEDICINE SIRIRAJ HOSPITAL, MAHIDOL UNIVERSITY

pale and no juandice. Vital signs and other examination were normal. Laboratory studies disclosed the following value: hematocrit 21%, white blood count 15,000 cells/uL, platelets 755,000 cells/uL, blood urea nitrogen (BUN) 9 mg/dl (7-20) and creatinine 1.0 mg/dl (0.5-1.5). Cystoscopy was performed. Active bleeding from the right ureteric orifice was discovered. The foley's catheter was retained and bladder irrigation was initiated together with 4 units of blood transfusion in 2 days, but the last hematocrit was raised to only 25%. He was then sent to consult for embolization of the AVM of the kidney.

Selective renal angiography was performed with diagnostic subtraction angiographic unit (Advantax, GE Medical Systems, Milwaukee, USA) via an ipsilateral retrograde femoral approach using 5 Fr. Cobra catheter curve 2(Terumo, Tokyo, Japan). Right renal artery was selected. RA angiogram was done and it showed AVF which was diagnosed by rapid high flow connection between branch of renal artery and adjacent vein. (fig 1a and 1b) There were no evidence of nidus, abnormal dilation of an artery or extravasation of contrast medium into the renal pelvis.

Three Fr. SP catheter (Radiofocus, Tokyo, Japan) was used as superselective catherization by its coaxial system to confirm the diagnosis and search for optimal position for embolization. (fig 2)

Embolization was performed with appropriate proportion mixture of glue (Histoacryl, Braun, Melsungen, Germany) and ethiodized poppy-seed oil (Lipiodol, Guerbet, Paris, Franch)

The embolizing solution was infused via coaxial system into the optimal site of the right renal aretery (fig 3a) but accidental reflux of the solution into the other branches of RA was seen (fig 3b). So the procedure was discontinued.

The 2nd patient had a history of gross hematuria for 1 month after previous trauma. He obtained 6 units of blood transfusion but the hematocrit was not increased satisfactorily. Ultrasonography of the kidneys demonstrated normal left kidney and intrarenal collection of blood in the right kidney. Cystoscopy disclosed active bleeding per right ureteric orifice. He was, then, sent to the interventional radiology division to perform angiography for diagnosis and endovascular treatment.

Aortogram (fig 4 and 5) and selective right renal artery angiogram (fig 6 and7) showed a large rounded outpouching of contrast media from its branch with early draining vein. Superselection into optimal position was done with coaxial system to look for dynamic flow. This provided decision making in appropriate proportion and amount of mixture between glue and Lipiodol (fig 8 and 9).

RESULTS

After superselective angiogram via coaxial system was performed with infusion of glue mixture. It revealed 30% and 15% of renal parenchymal infarction in the 1st patient and 2nd patient respectively. Disapearance of renal AVF and PA were occurred (fig 10 and 11). Both patients had normal renal function in both pre and post embolization after 1 month follow up.

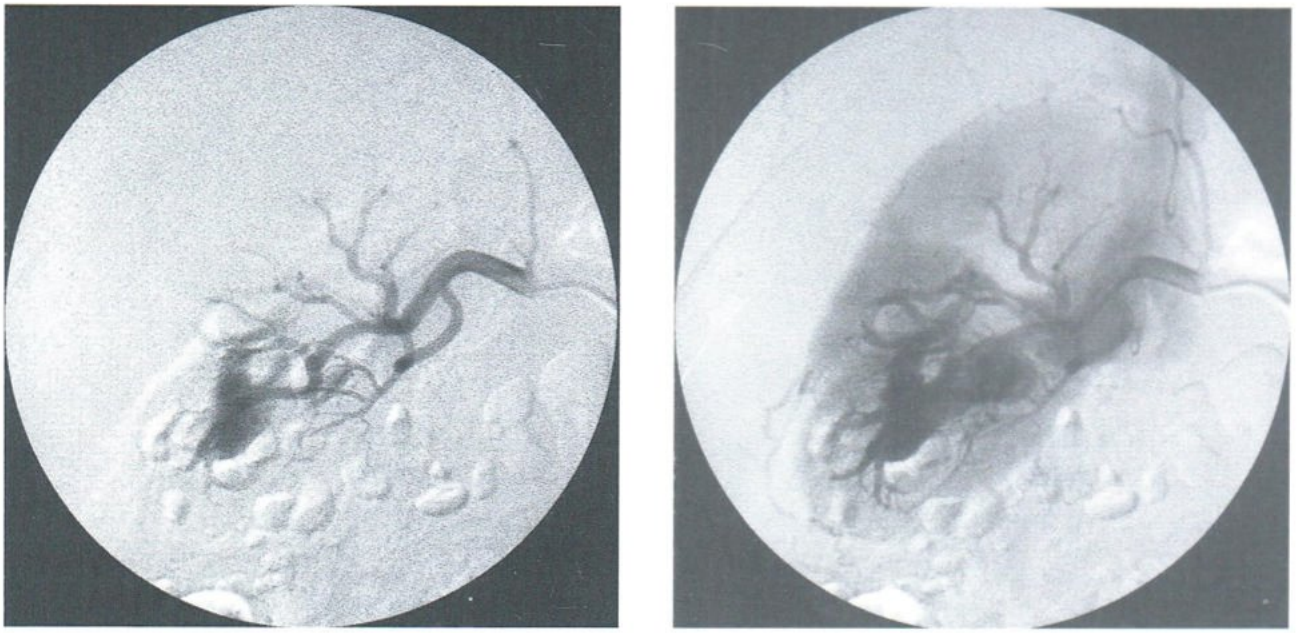

1a 1b

Fig. 1a and 1b. Selective renal angiogram in aterial phase showed rapid draining renal vein into IVC.

Fig. 2. Superselective angiogram by coaxial system was performed to find out the optimal position for embolization.

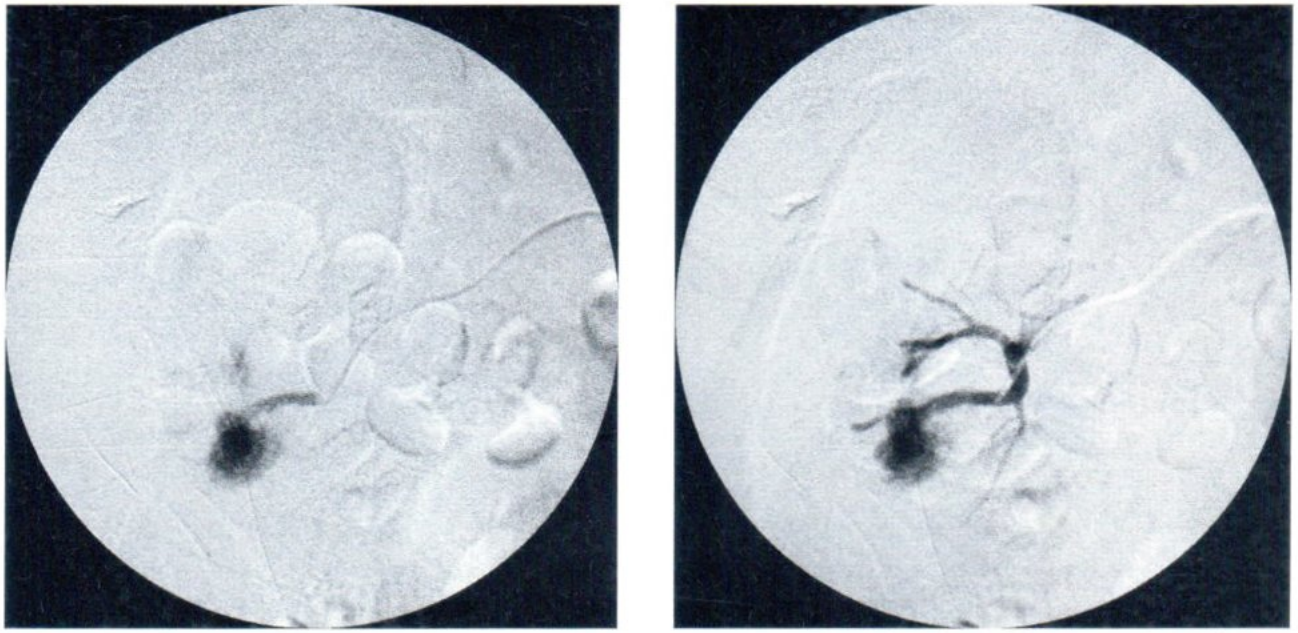

3a 3b

Fig 3a and 3b. During glue embolization, the glue mixture was reflux into another branches of renal artery so the procedure was discontinued.

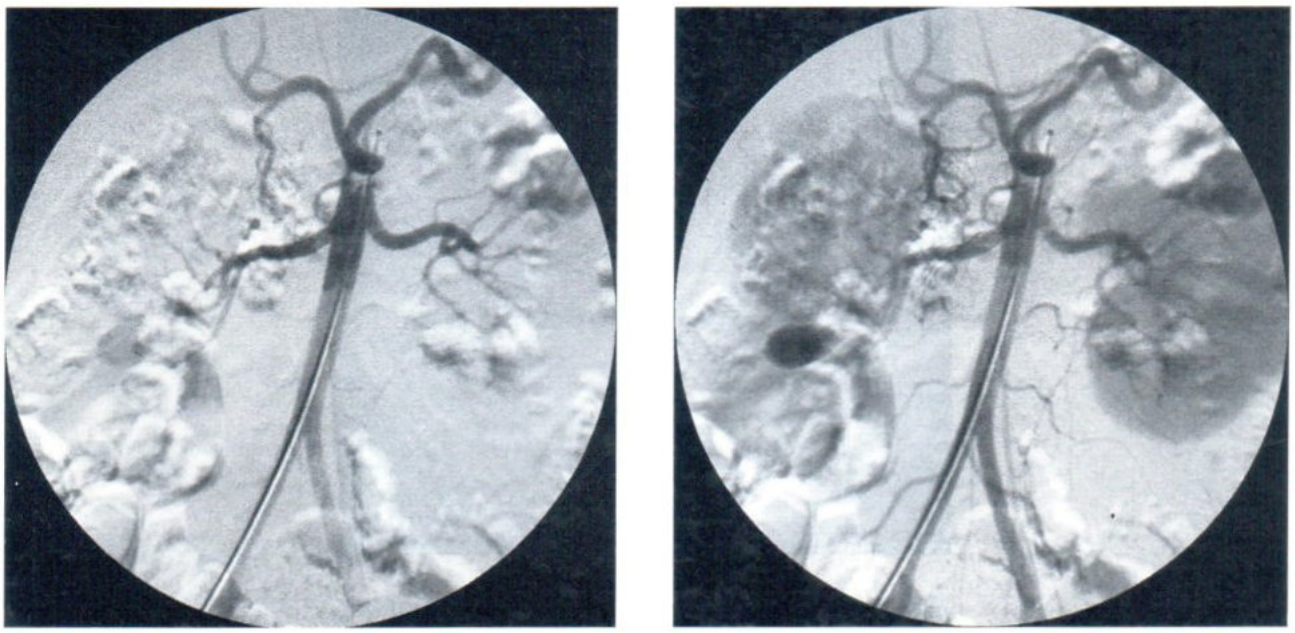

4 5

Fig. 4 and 5. Aortogram in early arterial and parenchymal phases demonstrated an oviod contrast collection of RK at the interpolar region.

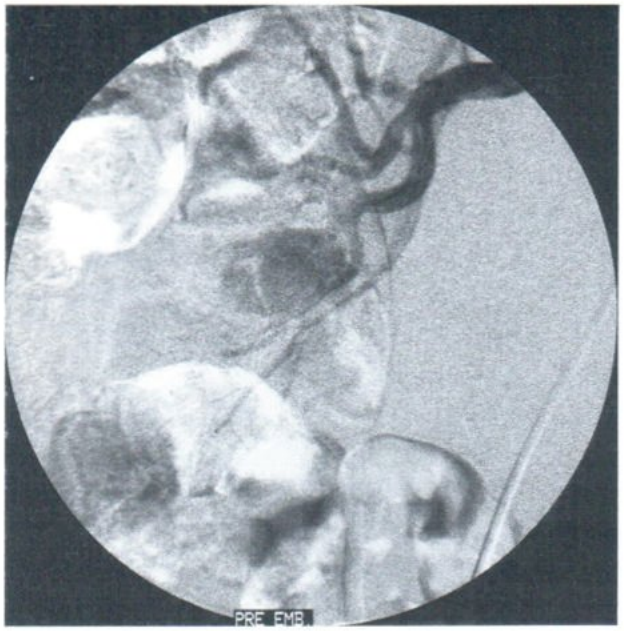

6

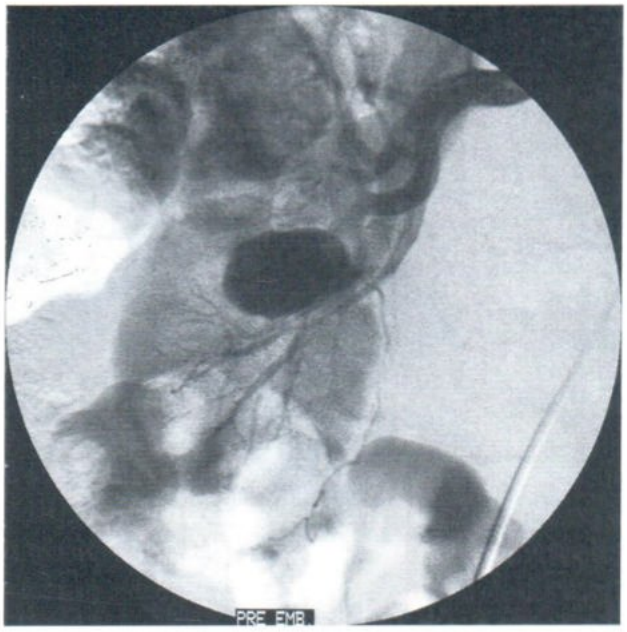

7

Fig. 6 and 7. Selective renal angiogram showed obvious pseudoaneurysm and additional rapid draining vein into IVC. So all findings were renal AVF with pseudoaneurysm. During glue embolization, the glue mixture was filled in the pseudoaneurysm.

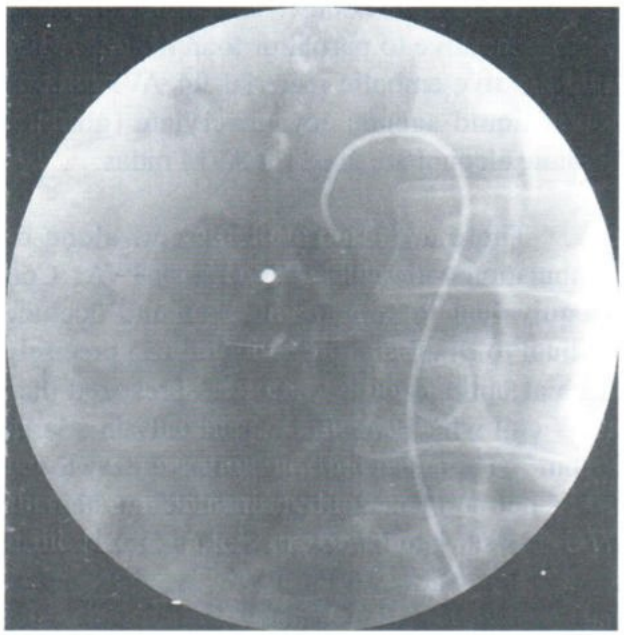

8

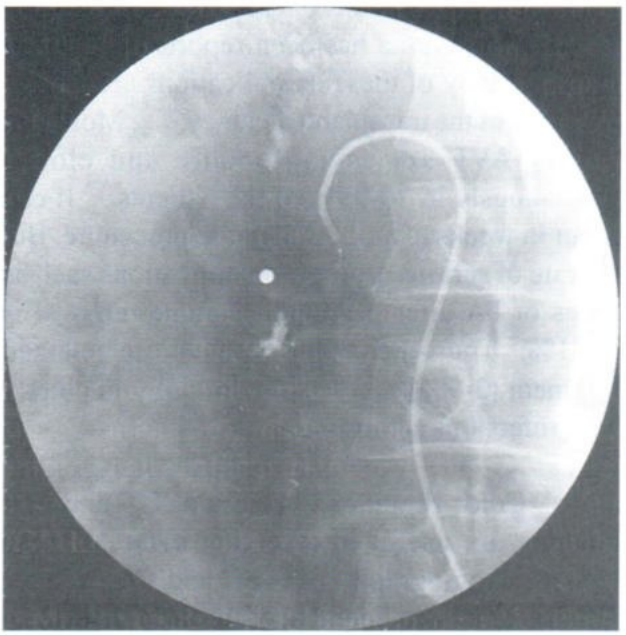

9

Fig. 8 and 9. The glue mixture is infused via coaxial system.

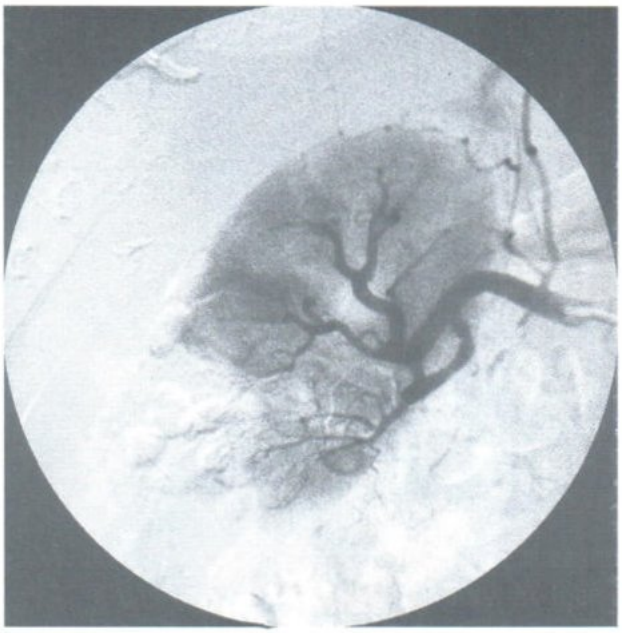

Fig. 10. Post embolization in the 1st patient revealed 30% renal infarction.

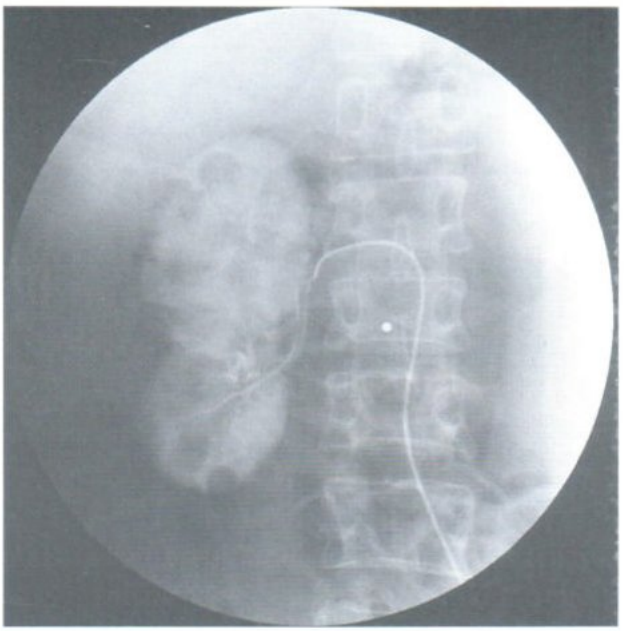

Fig. 11. Post embolization in the 2nd patient demonstrated 15% of renal infarction.

DISCUSSIONS

Incidence of AVF, PA and arteriocaliceal fistula after trauma has been reported to be 0.9-18%.[1,4] Many of these complications are related to biopsy of the transplanted kidney.[1,2,4,9] Most post biopsy AVF are asymptomatic and closed spontanously in 70-95% of the patients.[1-4] It can occur in weeks to months after the procedure. But the rate of serious urologic complications such as AVFs or PA after percutanous stone removal is 0.5-1%.[8] The other complications are retained fragment (3-9%) and sepsis especially in elderly with infectious stones.

Color droppler ultrasound, CT and MR imaging are useful in detecting some of these lesions.[5] Angiography of AVF and PA produce dilatation of the feeders with early filling of draining veins and outpouching of contrast media.

Transcatheter embolization is the best treatment for most lesions.[1-9] Because it can serve as an alternative to partial or total nephrectomy. The effective embolic material for AVF is coil. About liquid agents, acyanoacrylate (glue) or absolute alcohol are used for AVM nidus.

There are reports using coil alone or combination with gelfoam or glue or PVA.[1] Coil is equivalent to surgical ligation and occlude medium to small aretry. Microcoil can precisely place at optimal position so it is preferred than GAW coil which should be used only in a large lesion.[1,7] The advantage of gelfoam is easy to use and is not permanent. Glue occludes at ateriolar and capillary bed levels.[1,7] So it might be used only in high-flow AVFs. PVA also occludes at arteriolar and capillary bed levels. This makes the risk of tissue necrosis increased.[1,7]

The 1st patient developed renal AVF after the procedure. Hematuria treated by blood trans-

fusion with inappropiately increased hematocrit and persistent symptoms. All events also occurred in the 2nd patient. Angiography was done for embolization. AVF with and without PA were demonstrated. The embolic material of choice is still coil but the interventional radiologist is familiar with glue. After superselective angiography by coaxial system, the obvious position and dynamic flow of AVF and PA are precisely seen. So the optimal mixture of glue and lipiodol is used. Embolic solution is infused via microcatheter which is placed at optimal position. Post embolization demonstrates totally occlusion of AVF and PA. Some degree of renal infarction is noted. Followed up renal function is still normal.

Our results demonstrates that catheter embolization of AVF and PA can be performed successfully by glue. The several embolic materials can be used by preference of interventionists although the material of choice is coil. But this report includes only two patients, further study with various type of embolic materials in respect of single or combination with post embolization evaluation of the patients about renal function. Long term results should be followed up to find out the best embolic materials for treatment.

REFERENCES

1. Roland D, Siegfried T, Rupert P, et al: Embolization of iatrogenic vascular injuries of renal transplants:Immediate and follow-up results. Cardiovas Intervent Radiol (1998) 21:129-134
2. H. Shimmura, N. Ishikawa, K. Tanabe, et al : Angiographic embolization in patient with renal allograft arteriovenous fistula. Transplantation Preceedings (1998) 30: 2990-2992
3. Ahari et al: Arteriovenous fistula in a transplanted kidney. AJR (1999) 173:834-835
4. Karim V. Vascular and interventional radiology, 1 st ed. Philadelphia : W.B. Saunders Company, 1999 : 175-176
5. Saadoon K. Diagnostic angiography, Philadelphia : W.B. Saunders Company 1986:453-455
6. Michael A.B, Albert A.N, Jr, Robert L.V, Interventional radiology procedure manual, New York : Churchill Livingstone 1997:105-126
7. Fray F.M. Urologic complications, Chicago: Year Book Medical Publishers 1986:123,131-133,159-160
8. S. Ozdemir, S. Cekirge, A.Kara, et al: A rare complication of renal biopsy in a child with membranoproliferative glomerulonephritis. International Urology and Nephrology (1998) , 30 (6) : 689-692

CT FINDINGS OF PANCREATIC ADENOCARCINOMA

Laddawan VAJRAGUPTA, M.D., Busaba JIRAPPAPA, M.D[1]

ABSTRACT

The computed tomographic findings of 18 patients with pancreatic adenocarcinoma were reviewed between January 1993 to December 1999 in King Chulalongkorn Memorial Hospital. The diagnosis of pancreatic adenocarcinoma was confirmed by surgical exploration and biopsy in 16 patients (89%), and fine – needle aspiration (FNA) of peritoneal fluid in 2 patients (11%). CT criteria for unresectable included sign of involvement of the major peripancreatic vessels, signs of distant lymph node metastases, or liver metastases.

All patients fulfilled the criteria of unresectability, was found in our series. CT findings of pancreatic adenocarcinoma including, hypodense pancreatic mass with inhomogeneous enhancement (100%), most commonly at pancreatic head (72%), main pancreatic duct dilatation (50%), IHD and/or CBD dilatation (61%), vascular invasion (72%), contiguous organ invasion (22%), metastases (44%), and adenopathy (72%).

IHD = Intrahepatic duct
CBD = Common bile duct

INTRODUCTION

Computed tomography (CT) is the dominant imaging modality used for the diagnosis and staging of pancreatic adenocarcinoma, with an overall accuracy of more than 90% for dynamic CT.[1,2] This high accuracy is in part due to the advanced stage of most tumors at initial presentation.[3]

Despite advanced imaging in the diagnosis of pancreatic adenocarcinoma, 5-year survival rates following surgery continue to be less than 5% in most series, regardless of the type of resection employed (pancreaticoduodenectomy-Whipple resection or total pancreatectomy).[4,5,6] Patients with tumors that did not encase major vessels, and with tumors that have not metastasized to lymph nodes had 5-year survival of 36% and 57% respectively.[7] Thus, whereas it is crucial to avoid unneccessary operation and resection in patients whose tumors have spread beyond the margin of the gland and thus are unresectable for cure, it is equally important to attempt resection in the small group of patients with potentially curable tumors.

Radiologic staging of pancreatic carcinoma is based on evaluation of tumor extension beyond the margin of the gland and an identification of distant metastases, particular to the liver and regional lymph nodes. Spiral CT has been reported to provide high quality images of the pancreas during a single breath hold,[8,9] with excellent resolution of fine detail such as the pancreatic duct.[10]

[1] Department of Radiology, Faculty of Medicine, Chulalongkorn University, Bangkok 10330 Thailand.

The purpose of this paper is to report computed tomographic findings of pancreatic adenocarcinoma which can be used to identify resectable or unresectable cases.

MATERIALS AND METHODS

A retrospective series of 18 patients with pancreatic adenocarcinoma between January 1993 to December 1999 in King Chulalongkorn Memorial Hospital were reviewed. The diagnosis of pancreatic adenocarcinoma was confirmed by surgical exploration and biopsy in 16 patients (89%), and fine-needle aspiration (FNA) of peritoneal fluid in 2 patients (11%).

CT techniques

CT scan were performed with the CT Sytec 4000 (GE Medical Systems) in 17 cases and 1 case with the spiral CT (Siemen, Somatom Plus 4). All patients received 500 ml of 0.7% ionic water-soluble solution to opacify the stomach and small bowel. Noncontrast enhanced scans were obtained through the liver, pancreas and kidneys at 10 mm slice thickness in all patients. In 17 cases with conventional CT, intravenous contrast enhancement was achieved with 60% iodinated ionic or nonionic water-soluble contrast material administered by an injector at a rate of 1.5 ml/sec for a total of 100 ml. After complete contrast material injection, scans through liver, pancreas and kidney were performed at 10 mm contiguous slice thickness.

In 1 case with dual phase CT scan, intravenous contrast enhancement was performed with angiograffin administered by a rate for 1.5 ml/sec for a total of 100 ml. After intravenous contrast enhancement injection in 25 sec, a dynamic series of scans through the pancreas was performed at 5 mm slice thickness for arterial phase and a delayed for 85 sec after injection for venous phase.

CT scan interpretation

The 18 CT scans were reviewed retrospectively and the following 7 parameters were evaluated

1. Pancreatic mass (location, size, attenuation, enhancement)
2. Main pancreatic duct dilatation
3. Intrahepatic duct and common bile duct dilatation
4. Contiguous organ invasion (liver, stomach, root of the small bowel mesentery, duodenum)
5. Vascular invasion or tumor-vessel contiguity (tumor partially or completely surrounding a major extrapancreatic artery or vein ; tumor-vessels contiguity : tumor immediately contiguous with vessels with no intervening normal fat plane)
6. Metastasis (liver, lung, peritoneum)
7. Adenopathy

CT staging

The tumor was considered technically unresectable when CT revealed signs of involvement of the major peripancreatic vessels (superior mesenteric and splenic vessels, the portal vein, and the main hepatic artery), signs of distant lymph node metastases, or liver metastases.[11]

RESULT

Eighteen patients were evaluated by 17 conventional and 1 spiral thin-section contrast-enhanced CT, and all patients fulfilled the criteria for unresectability. The study population consisted of 10 women and 8 men, with a median age of 61 years (range : 51 to 72 years). The findings noted at histopathologic examination of the resected tumor specimens were adenocarcinoma. The tumor size was range from 2-17 cm. All pancreatic tumors were hypodensity lesion with inhomogeneous enhancement, located in the head of the gland in 13 tumors, the body in 4, the tail in 3, and the uncinate process in 4. (FIG. 1) Some

tumors were involved more than one location.

The most common findings was a pancreatic mass (100%), main pancreatic duct dilatation (50%), intrahepatic duct and/or common bile duct dilatation (61%) (FIG. 2) and extrapancreatic tumor extension. Extrapancreatic tumor extension encompassed the following findings : (1) tumor involvement of contiguous organs (22%), most commonly the stomach, mesentery, anterior abdominal wall, and duodenum. (FIG. 3) (2) vascular invasion or tumor–vessel contiguity, most often involving the superior mesenteric artery and vein, splenic vein, portal vein, inferior vena cava, common hepatic artery. (FIG. 4) Eight patients had metastases, most commonly in liver (33%) (FIG. 5), lung (11%), and the peritoneum (11%). Enlarged lymph nodes were identified on thirteen patients, including peripancreatic, periportal, celiac trunk, aortocaval, paraaortic, retrocaval, cardiophrenic lymph nodes. (FIG. 6) The results are summerized in Table I

TABLE I : CT FINDINGS

CT FINDINGS		No OF PATIENTS (%)
1.	TUMOR MASS	18 (100)
	- Hypodensiy lesion with inhomogenous enhancement	18 (100)
	- Location .... Head	13*
	Uncinate process	4*
	Body	4*
	Tail	3*
2.	MAIN PANCREATIC DUCT DILATATION	9 (50)
3.	IHD AND / OR CBD DILATATION	11 (61)
4.	CONTIGUOUS ORGAN INVASION**	4 (22)
5.	METASTASES	8 (44)
	- liver	6 (33)
	- lung	2 (11)
	- peritoneum	2 (11)
6.	VASCULAR INVASION / TUMOR-VESSEL CONTIGUITY	17 (94)
	- VASCULAR INVASION***	13 (72)
	- tumor - vessel contiguity	4 (22)
7.	ADENOPATHY****	13 (72)

* Number in location of the tumors which some of them had more than one location.

** stomach 2, mesentery 1, anterior abdominal wall 1, duodenum 1.

*** superior mesenteric artery 3, superior mesenteric vein 8, splenic vein 7, portal vein 1, inferior vena cava 1, common hepatic artery 1.

**** peripancreatic, periportal, celiac trunk, aortocaval, paraaortic, retrocaval, cardiophrenic lymph nodes.

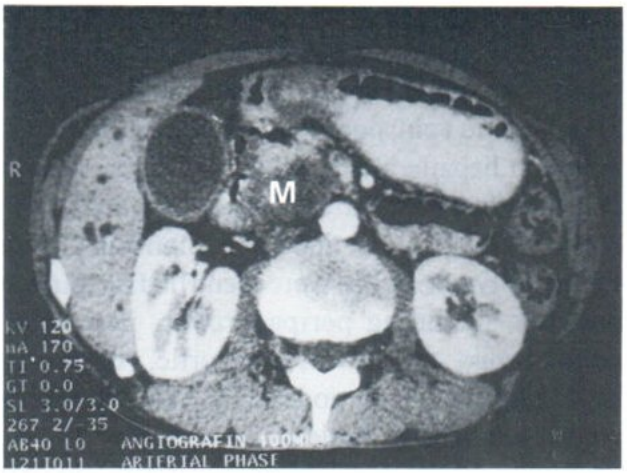

Fig. 1A. The arterial phase dynamic CT scan showed a 4 cm. low density lesion at pancreatic head. (M)

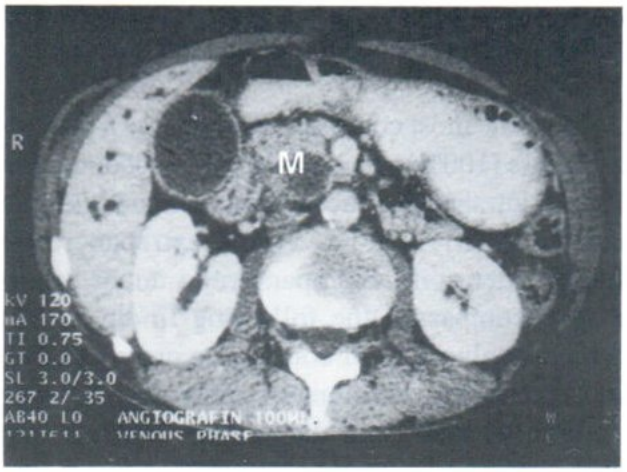

Fig. 1B. The venous phase dynamic CT scan revealed inhomogeneous enhancement of the pancreatic head mass. (M)

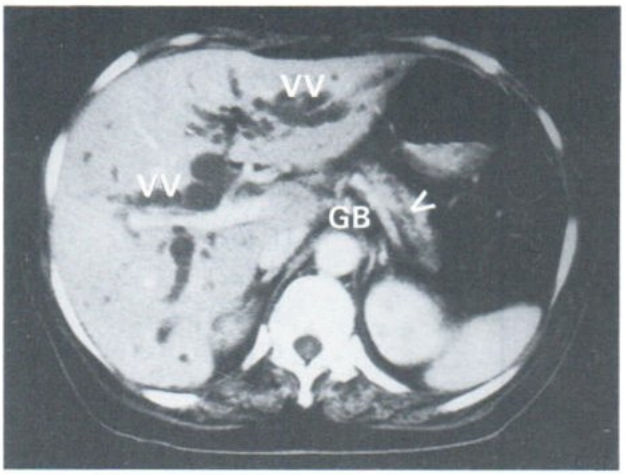

Fig. 2A. The CECT scan of the liver showed intrahepatic bile duct dilatation (VV) and main pancreatic duct dilatation (V) at the tail region. (Gb = gall bladder)

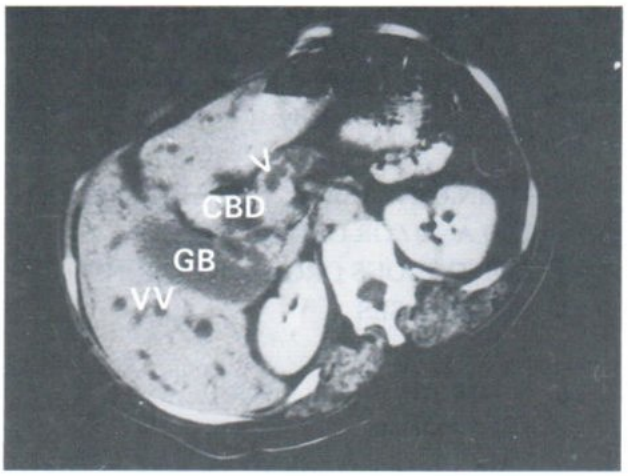

Fig. 2B. The CECT scan showed main pancreatic duc dilatation (V), dilated CBD and intrahepatic duct dilatation (VV) caused by pancreatic head adeno carcinoma which did not show in this figure.

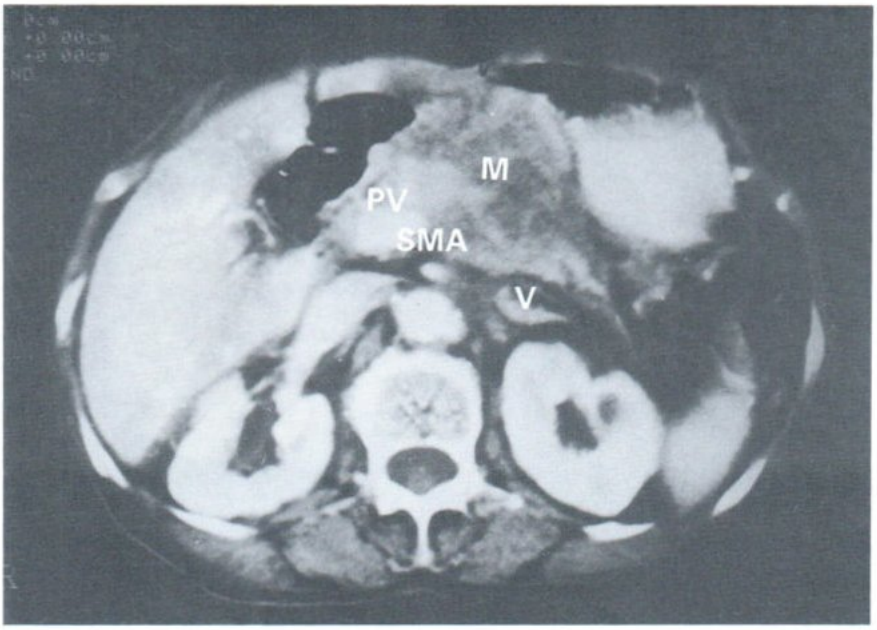

Fig. 3. The CECT scan showed a large inhomogeneous enhanced mass at body and tail of pancreas (M) encased SMA, portal vein (PV) and involved posterior wall of stomach (V).
SMA = Superior Mesenteric Artery

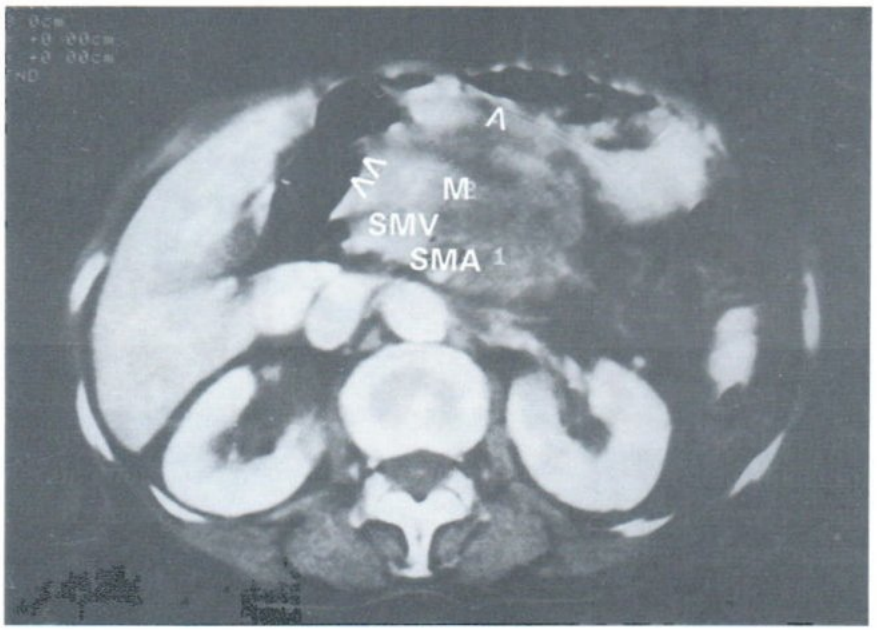

Fig. 4. The CECT scan showed a 6 cm. Inhomogeneous enhanced mass (M) at pancreatic body encased SMA, SMV and posterior wall of stomach (Λ) and medial wall of duodenum (ΛΛ) involvement due to loss of intervening fat plane.

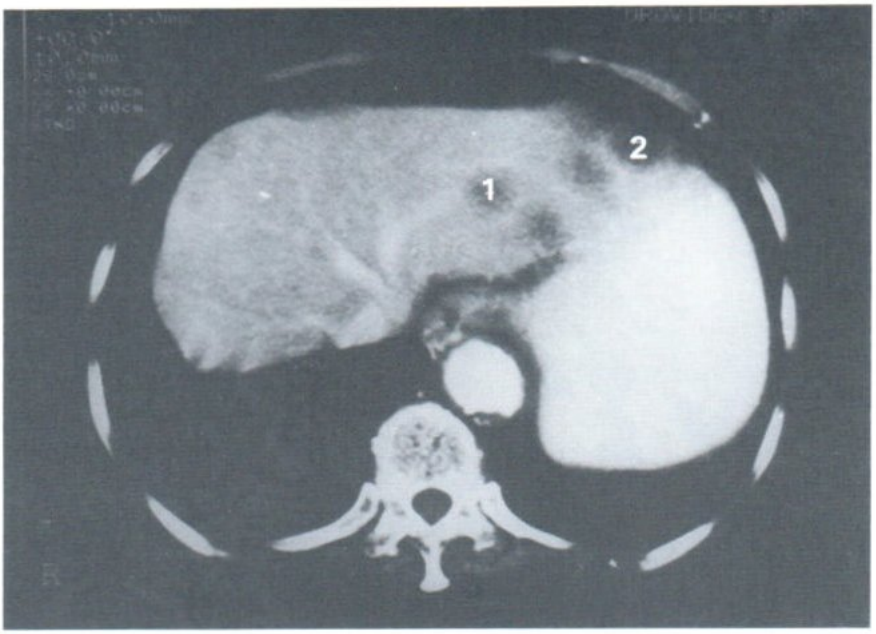

Fig. 5. The CECT scan revealed multiple low density lesions in both hepatic lobes, liver metastasis from pancreatic adenocarcinoma. (1, 2)

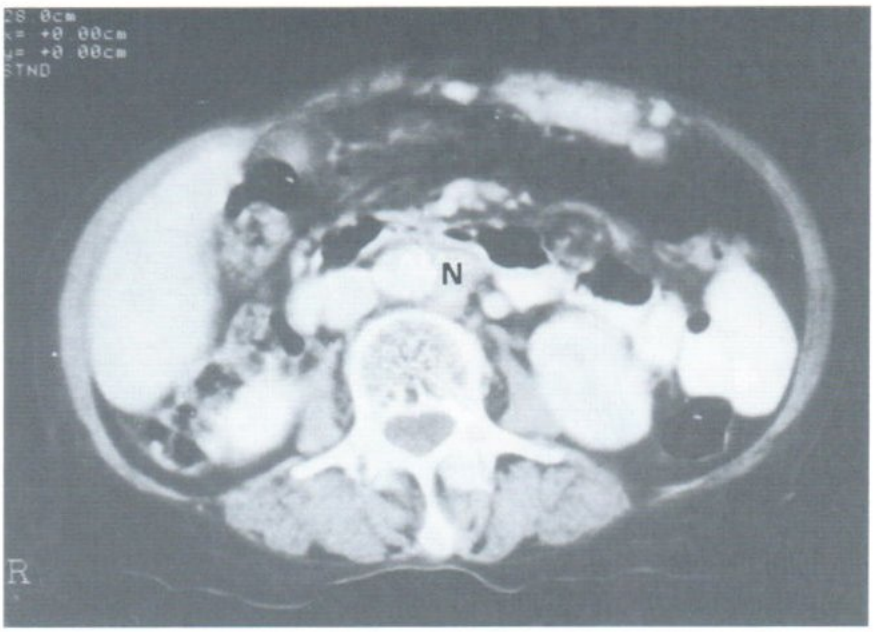

Fig. 6. The CECT scan showed a 2 cm. Left para aortic lymph node (N), lymphatic spreading of pancreatic adenocarcinoma.

DISCUSSION

Dynamic CT currently is the imaging modality of choice for diagnosis and staging of pancreatic carcinoma. It has an accuracy of 72% in predicting tumor resectability and an accuracy of virtually 100% in predicting tumor unresectability.[12] Many patients were found unresectable at laparotomy due to locally advanced diseases because of vascular encasement not well demonstrated by preoperative CT.[13] Most symptomatic patients with pancreatic carcinoma had unresectable tumors at the time of initial clinical presentation. 18 (100%) patients in this study had unresectable tumors by CT criteria and 44% of these patients had 3 to 5 CT criterias of unresectability, indicating widespread disease. It should be emphasized that the CT findings of a pancreatic mass are nonspecific, even when ancillary criteria of unresectability are present. Focal pancreatitis, other types of pancreatic neoplasms, particularly nonfunctioning islet cell carcinoma, metastases, and lymphoma, and variations in size and shape of the normal pancreas can mimic the CT appearance of pancreatic adenocarcinoma.[2]

In our 18 cases with radiologic findings, all (100%) tumors were hypoattenuating. This is not significantly different from the results reported previously by Freeney et al,[1] although their study population was primarily composed of patients with unresectable tumors (154 of 161 patients). In that series, 83% of tumors displayed focal area of hypoattenuation compared with the normal pancreas. The relative attenuation of the tumor to the pancreas is related to its vascularity compared with that of the surrounding pancreas. This relative attenuation is therefore a function of the presence of underlying parenchymal disease in the pancreas and changes as a function of time after intravenous contrast administration. Pancreatic adenocarcinoma also tends to incite a local fibrotic tissue response. Presumably, the blood supply to the tumor is frequently lesser than that to normal pancreas, and this difference accounts for relative tumor hypoattenuation. It seems likely that tumors that are isoattenuating to the pancreas at routine spiral scanning may become hypo-attenuating relative to the pancreas during the arterial phase and their conspicuity would subsequently be increased.[14] Secondary signs other than a focal mass are usually helpful in the diagnosis of pancreatic cancer. These signs include pancreatic and common bile duct dilatation and atrophy of the pancreas distal to the tumor. A high degree of suspicion for a malignant neoplasm must be present in the case of atypical pancreatic masses that may be isoattenuating and detected only as a bulge in the pancreatic contour, without evidence of pancreatic or bile duct dilatation.[3]

Spiral CT with overlapping reconstruction intervals every 4 mm has been shown to increase the detection of small lesions in the liver compared with that of contiguous 8 mm transaxial imaging.[15] However, in addition to lesion detection, it is necessary to characterize these focal abnormalities. Accurate assessment of tumor size was aided by obtaining overlapping axial reconstruction every 4 mm.

Because the pancreas is an extremely vascular organ and has a rich arterial supply, arterial phase scanning would likely have been more optimal for pancreatic tumor evaluation but less optimal for detection of liver metastases. Dual-phase arterial and portal phase scanning of the pancreas and liver, respectively, will likely prove advantageous for staging pancreatic neoplasm.[14] With arterial phase scanning of the pancreas, attenuation differences between tumor and the normal pancreas may be increased, rendering the tumor more conspicuous. In this study, 1 case of dual phase CT scan showed a 4 cm hypodense mass as compared to normal enhancing pancreatic parenchyma in arterial phase at pancreatic head and the uncinate process and inhomogeneous enhancement in portal venous phase.

Further progress in preoperative tumor staging for pancreatic ductal adenocarcinoma should be directed toward improving the detection of small pancreatic tumors and assessing early metastatic disease.

CONCLUSION

CT findings of pancreatic adenocarcinoma in our series included, hypodense pancreatic mass with inhomogeneous enhancement (100%), location most commonly at head (72%), main pancreatic duct dilatation (50%), IHD and/or CBD dilatation (61%), vascular invasion (72%), contiguous organ invasion (22%), metastases (44%), and adenopathy (72%). All of our cases are unresectable tumor. CT scan provides the preoperative information for appropriate surgical planning. Spiral CT scan is very helpful in detection small pancreatic tumors and detail of extension of disease.

REFERENCES

1. Freeny PC, Marks WM, Ryan JA, Traverso LW. Pancreatic ductal adenocarcinoma : Diagnosis and staging with dynamic CT. Radiology 1988;166:125-133.
2. Freeny PC, Traverso W, Ryan JA. Diagnosis and staging of pancreatic adenocarcinoma with dynamic CT. Am J Surg 1993;165:600-606.
3. Bluemke DA, Cameron JL, Hruban RH, et al ; Potentially resectable pancreatic adeno-carcinoma : Spiral CT assessment with surgical and pathologic correlation. Radiology 1995;197:381-385.
4. Cameron JL, Crist DW, Sitzman JV, et al ; Factors influencing survival after pancreatico-duodenectomy for pancreatic cancer. Am J Surg 1991;161:120-125.
5. Trede M, Schwall G, Saeger HD. Survival after pancreatoduodenectomy. Ann Surg 1990;211:447-458.
6. VanHeerden JA, Remine WH, Weiland LH, et al : Total pancreatectomy for ductal adeno-carcinoma of the pancreas. Am J Surg 1981;142:308-311.
7. Tsuchiya R, Noda T, Harada M, et al. Collective review of small carcinomas of the pancreas. Ann Surg 1986;203:77-81.
8. Dupuy DE, Costello P, Ecker CP. Spiral CT of the pancreas. Radiology 1992;183: 815-818.
9. Fishman EK, Wyatt SH, Ney DR, Kuhlman JE, Siegelman SS. Spiral CT of the Pancreas with multiplanar display. AJR 1992;159:1209-1215.
10. Zeman RK, Zeiberg AS, Davros WJ, et al. Routine helical CT of the abdomen : Image quality considerlations. Radiology 1993;189:395-400.
11. Andersen HB, Effersoe H, Tjalve E, Burcharth F. CT for assessment of pancreatic and periampullary cancer. Acta Radiologica 1993;34:569-572.
12. Nghiem HV, Freeny PC. Radiologic staging of pancreatic adenocarcinoma. Radiologic Clinic of North America 1994; 32:71-79.
13. Fuhrman GM, Chamsangavej C, Abbruzzese JL, Cleary KR, et al. Thin – Section contrast – enhanced CT accurately predicts the resectability of malignant pancreatic neoplasms. Am J Surg 1994; 167:104-113.
14. Hollett MD, Jorgensen MJ, Jeffrey RB Jr. Quantitative evaluation of pancreatic enhancement during dual phase helical CT. Radiology 1995;195:359-361.
15. Urban BA, Fishman EK, Kuhlman JE, Kawashima A, Hennessy JG, Siegeiman SS. Detection of focal hepatic lesions with spiral CT : comparison of 4 - and 8 - mm interscan spacing. AJR 1993;160:783-785.

GIANT CELL TUMOR OF THE RIB : A CASE REPORT

Petcharat SUANGKAEW, M.D.[1] Boonyaporn VASURATNA, M.D.[1]
Voranuch PUNYAVORAVUT, M.D.[1] P. SUANGKAEW, B. VASURATNA,[1]
V. PUNYAVORAVUT.[2]

ABSTRACT

A giant cell tumor involving the left anterior 4th rib was diagnosed in a 42-year-old female who presented with a large mass at left anterior chest wall. Plain radiographs demonstrated an expansile osteolytic lesion at anterior aspect of left 4th rib. CT scan revealed an expanding mass originating from anterior aspect of left 4th rib, suggestive of a benign bone lesion. On MRI, the appearance was non specific and the diagnosis was established by histological examination after removal of the tumor.

INTRODUCTION

Giant cell tumor of the rib is extremely rare and accounts for less than 0.6 % of all giant cell tumours.[1] We report a 42-year-old woman having a giant cell tumor of the rib with illustrations by plain radiographs, computed tomography and magnetic resonance imaging findings.

CASE REPORT

A 42-year-old woman without any underlying medical history presented with a 6-month history of non movable painless mass at left side of the chest wall which was thought to be a breast mass.

Physical examination revealed a non-tender, firm, fixed mass at left anterior chest wall measuring approximately 4x5 cms. The surface of the mass was smooth and the skin over it was stretched but not warm.

Ultrasonography was initially requested to rule out a breast mass. The ultrasonography of both breasts showed a lobulated-border lesion of inhomogeneous echogenicity with multiple internal septation in the region of left anterior rib which is suggestive of an expansile destruction of the rib. This mass was about 1.5x2.6 cm in size, abutted and displaced the overlying muscle and left breast anteriorly. No evidence of left breast invasion was seen Rt. Breast was normal.

PA and left lateral plain chest radiographs showed a markedly expansile osteolytic lesion at the anterior aspect of 4th rib left side near costosternal junction. No evidence of matrix mineralization was observed (Fig. 1).

Plain computed tomography scan showed an expanding mass originating from anterior aspect of left 4th rib. Irregular but complete calcific shell at its periphery was observed (Fig 2). The mass extended anteriorly displacing the chest wall muscle, and posteriorly with mild compression of the lung beneath.

MRI was performed with T1-weighted and T2-weighted sequences in the axial and coronal

[1] Department of radiology, Chulalongkorn University, Bangkok, Thailand
[2] Department of Pathology, Chulalongkorn University, Bangkok, Thailand

planes and GRE sequence in the axial plane. It demonstrated the mass arising from the left anterior 4th rib displacing the overlying muscle and left breast anteriorly. The tumor gave low signal intensity on T1-weighted images and heterogeneous signal intensity on T2-weighted images and GRE images (Fig.3), and was markedly enhanced with GdDTPA (Fig. 4). There were areas of dark signal intensity on GRE images, which were corresponded with foci of hemorrhage from the pathologic specimen.

A segmental resection of the tumor was performed. The specimen was submitted for pathological examination. The gross examination disclosed a portion of rib, measuring 8.0 cm in length. The expansile area with remaining peripheral bone was measured 5.0x5.0x4.0 cm. It revealed bright yellow anterior surface with scattered foci of hemorrhage (Fig. 5). Microscopic examination showed diffuse polygonal and spindle-shaped stromal cells with numerous multinucleated giant cell (Fig. 6 A,B).

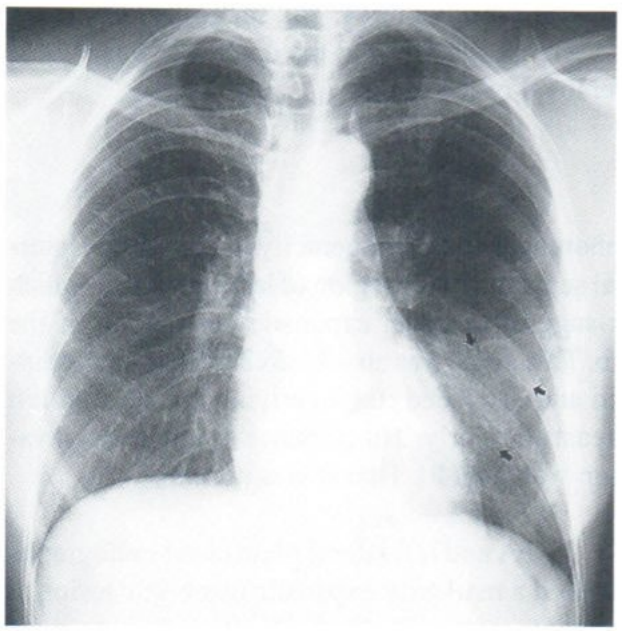

1A

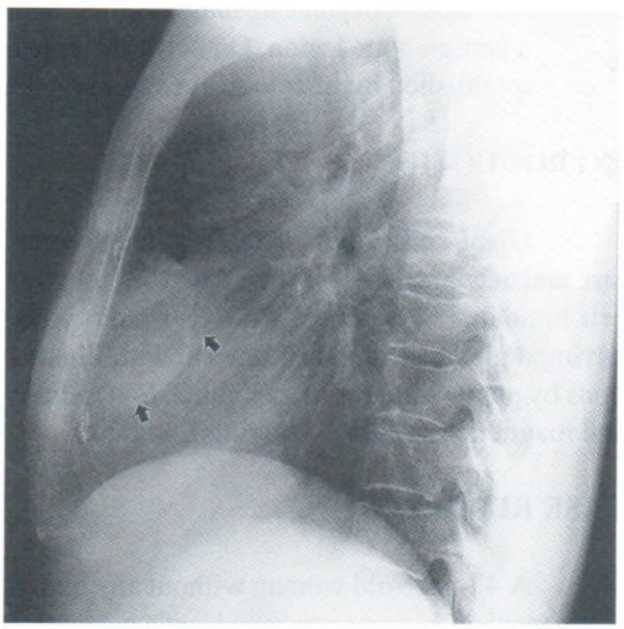

1B

Fig. 1. Posteroanterior (A) and left lateral (B) chest radiographs show an expansile, faintly trabeculated lytic lesion at anterior aspect of left 4th rib without matrix calcification. The cortex is thin but appears intact.

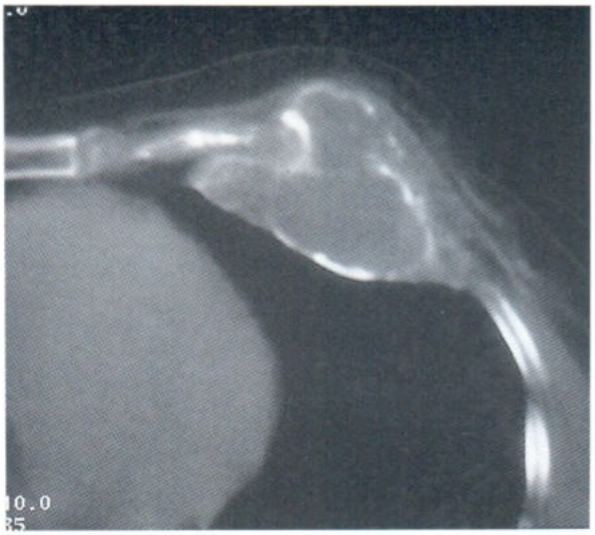

Fig. 2. A bone-windowed image of plain CT scan shows a large, expanding mass originating from the anterior aspect of the rib. A complete rim of bone surrounds the mass is seen.

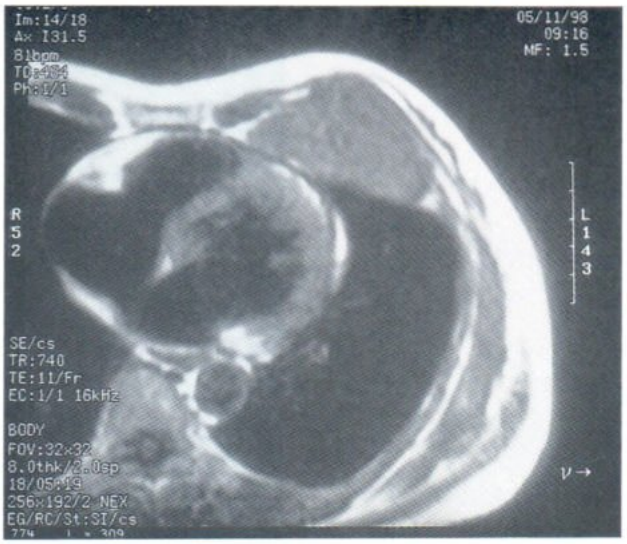

3A

Fig. 3A. Axial T1-weighted spin echo image shows a low signal intensity mass arising from the anterior aspect of left fourth rib.

3B

Fig. 3B. Axial T2-weighted spin echo MR image reveals a heterogeneous signal intensity of the mass.

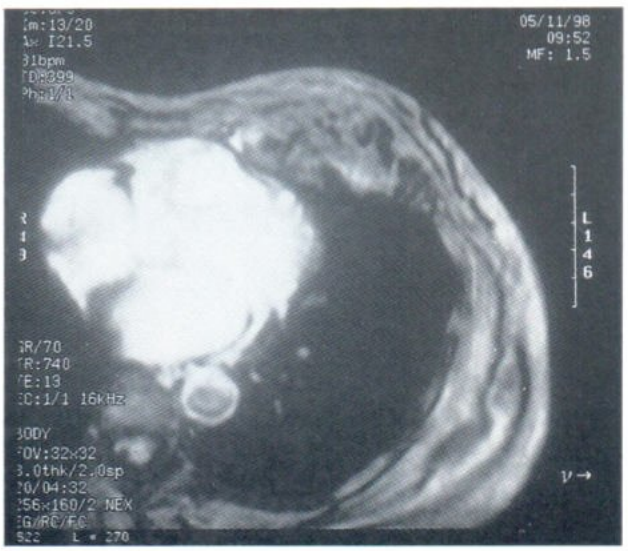

3C

Fig. 3C. Axial GRE image shows areas of dark signal intensity which are correlated with hemosiderin deposits.

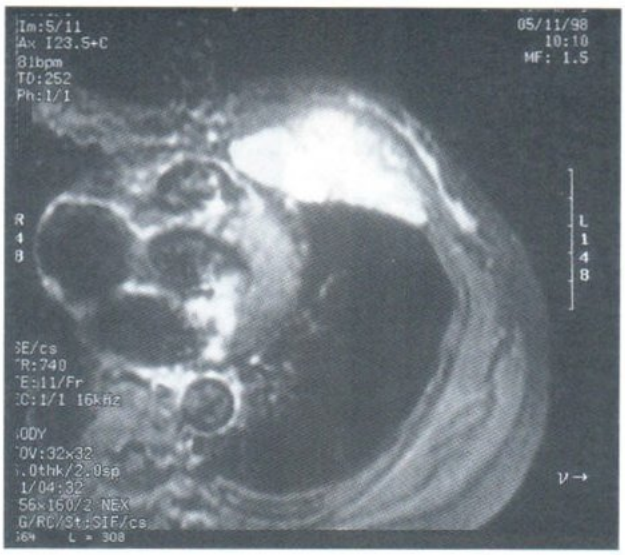

3D

Fig. 3D. Axial T1-weighted spin echo image with fat saturation obtained after intravenous GdDTPA administration shows intense enhancement of the tumor.

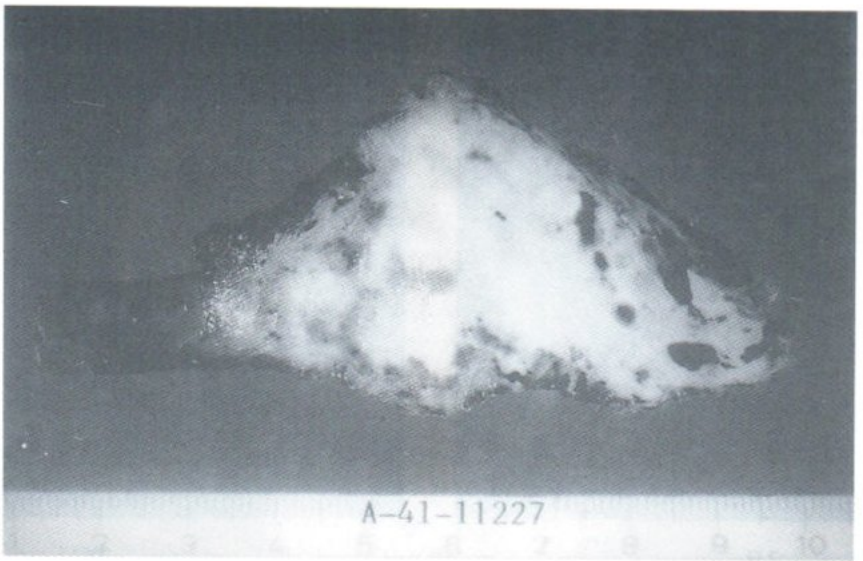

Fig. 4. A cross section of an expanded rib which was resected. The cortex is intact.

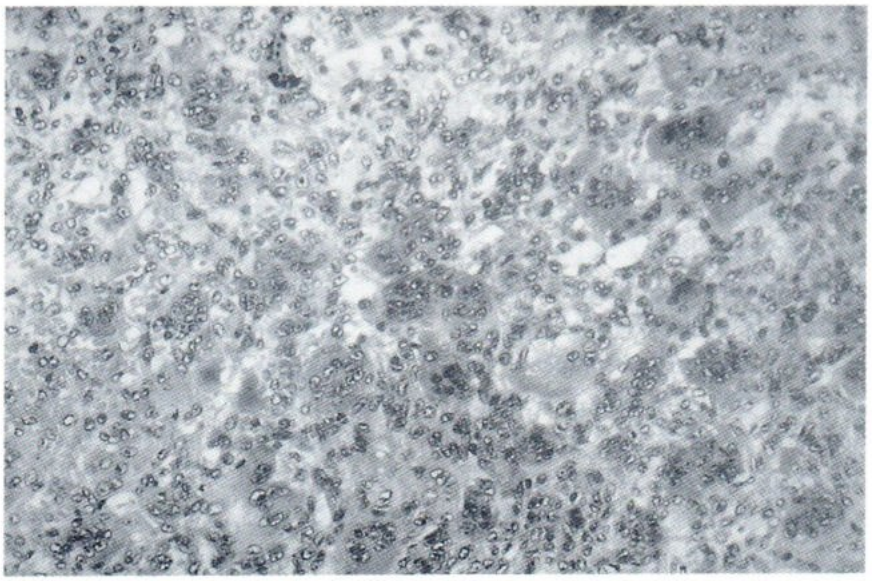

5A

Fig. 5A. This low-power microscopic field shows polygonal and spindleshaped stromal cells and mixed with multinucleated giant cell (x200).

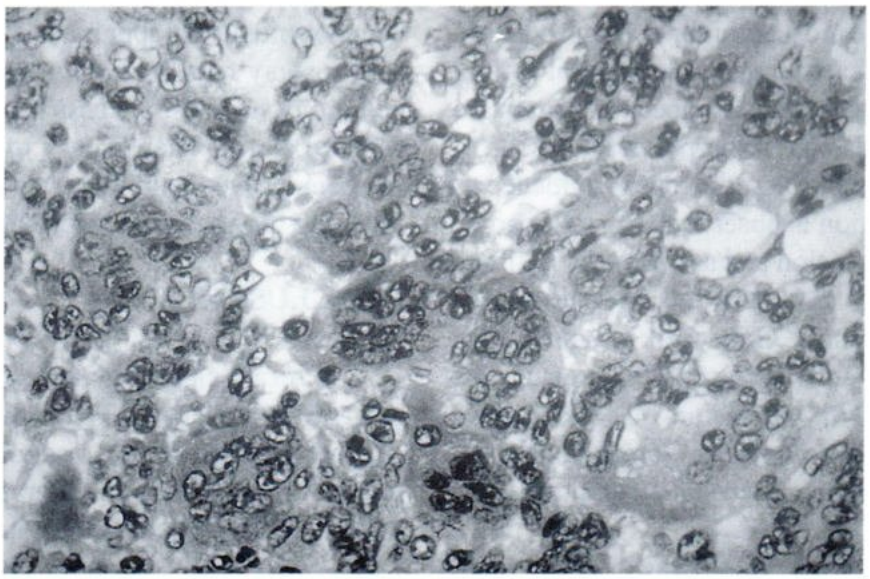

5B

Fig. 5B. The numerous giant cells with large number of nuclei are demonstrated (x400).

DISCUSSION

Giant cell tumor comprises about 5% of bone tumors and 90% of these involve the end of the long tubular bones such as the distal femur, proximal tibia and fibula, and distal radius and ulna, usually in patient with closed epiphyses.[2,3,4] Giant cell tumor most commonly occurs in third and fourth decades of life with a female preponderance.[5] They are histologically variable, but usually benign, although locally aggressive. Metastasis appears in 2 % of cases.[6] Giant cell tumor of the rib is extremely rare. In a review of 8 large series of giant cell tumors, each containing over 100 cases, Hanna et al found only 12 (0.6%) originated in the rib.[7] In a tabular summary of the Mayo Clinic experience, Dahlin and Unni list 88 benign tumors or tumor-like conditions of the rib. The most frequent of these, in descending order, was fibrous dysplasia, osteochondroma, aneurysmal bone cyst and chondroma.[8]

Radiographically, giant cell tumor of a long tubular bone most commonly is an eccentric osteolytic lesion extending to subchondral region. Bony expansion and delicate trabecular pattern are usually seen. It also has a sharply defined zone of transition that is not sclerotic and no evidence of new bone formation is observed.[5,9] In a flat bone, a large osteolytic lesion and associated soft tissue component may simulate the appearance of malignant neoplasm.[5] Giant cell tumour of the spine presents as a lytic appearance at the vertebral body with expansion of both cortices which may simulate an aneurysmal bone cyst, multiple myeloma and metastatic carcinoma.[10]

Radiological aggressiveness is not useful in distinguishing benign from malignant forms of giant cell tumor, as the benign forms may have cortical expansion and disruption with invasion of the soft tissue.[1,8] In our case, the presence of complete shell of bone around the tumor suggests benign character.

On MRI, the giant cell tumor has no specific appearance. MRI is useful to show the extension and displacement of the adjacent structures for planning complete resection. Both the excellent soft tissue contrast resolution and the multiplanar images make MRI superior to CT in demonstrating accurately the tumor extent both in the bone marrow and in the surrounding soft tissue.[11,12] However, CT is superior in demonstrating cortical thinning. In our case, the signal intensity of the tumor is non specific. Hyposignal intensity on T1-weighted images and heterogeneous signal intensity on T2-weighted images with areas of dark signal intensity on GRE images are observed. The dark signal intensities on GRE images are corresponded with areas of hemosiderin deposit secondary to hemorrhage on the pathologic specimen.

Optimal management of giant cell tumor is wide surgical excision. Local recurrence is a common problem in approximately 30 % of cases.[1,10] Controversy regarding the management of giant cell tumor persists. Success has been claimed for surgical alone.[2] The efficacy of radiotherapy has not been proved and it carries a potential risk of inducing malignant transformation.[2]

CONCLUSION

A rare case of giant cell tumor originated in a rib is presented. The radiological findings suggest a benign form, so segmental resection of the tumor was done. The literatures on giant cell tumors of the rib are reviewed.

REFERENCES

1. Huvos AG. Bone Tumors, Diagnosis, Treatment and Prognosis, 2nd ed. Philadelphia, W.B Saunders, 1991

2. Dahlin DC. Giant Cell Tumor of Bone : Highlights of 407 cases. AJR 1985;144: 955-960
3. Sung HW, Kuo DP, Sue WP, Chai YB, Liu CC, Li SM. Giant Cell Tumor of Bone: Analysis of two hundred and eight cases in Chinese patients. J. Bone Joint Surg (Am) 1982;64:755-761
4. Johnson J. Giant Cell Tumor of Bone : The role of giant cell in orthopedic pathology. Orthop Clin North Am 1975;8:751-770
5. Resnick D. Diagnosis of Bone and Joint, 3rd ed. Philadelphia, W.B. Saunders, 1995
6. Waldman HJ, Zerhouni EA, Franssica FJ. Recurrence of Giant Cell Tumor of Bone: The role of MRI in diagnosis. Orthopedics 1997 ; 20(1) : 67-69
7. Hanna RM, Kyriakos M, Quinn SF. Case report 757. Skeletal Radio 1992;21(2): 124-127
8. Dahlin DC, Unni KK. Bone tumors. General aspects and data on 8,542 Cases, 4th ed. Charles C. Thomas, Springfield, 1986
9. Larsson SE, Lorentzon R, Boquist L. Giant Cell Tumor of Bone: A demographic, clinical, and histopathological study of all cases recorded in the Swedish cancer registry for the years 1958 through 1968. J Bone Joint Surg (Am) 1975;57: 167-173
10. Goldenberg RR, Campbell CL, Bonfiglio M. Giant Cell Tumor of Bone : An analysis of two hundred and eighteen cases. J Bone Joint Surg (Am) 1970;52:619-664
11. Rimmelin A, Roth T, George B, Dias P, Cluet PL, Dietemann JL. Giant Cell Tumour of the Sphenoid Bone : case report. Neuroradiology 1996;38:650-653
12. Herman SD, Mesgarzadeh M, Bonakdarpour A. The Role of Magnetic Resonance Imaging in Giant Cell Tumor of Bone. Skeletal radio 1987;16(8):635-643

KEITHLEY

Model 6517 Electrometer/High Resistance Meter

* Measure resistance up to $10^{17}\ \Omega$
* Measure current with 100aA sensitivity
* Measure coulombs 10 fc – 2 mc
* Vottage Source f 1 kv

Nuclear Associates

WIPER™ SINGLE-WELL WIPE TEST COUNTER

* Meets all requirements for nuclear medicine wipe testing.
* Full-featured multichannel analyzer for high resolution detail.
* Automatic calibration for trouble-free compliance.

Model 35040

Advanced Therapy Dosimeter

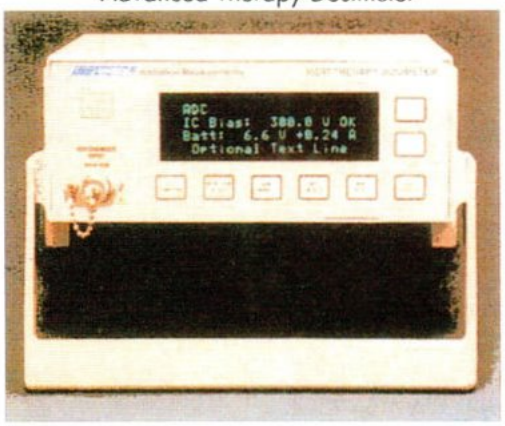

* Ultra long-term stability error of approximately 0.1% per five years
* Read out in C, A, R, Gy, Sv, Bq, and more
* Automatic reset and hold of measured values between exposures.
* Thirty-two (32) ion chamber calibration factors.

Victoreen Model 8000

NERO™mAx

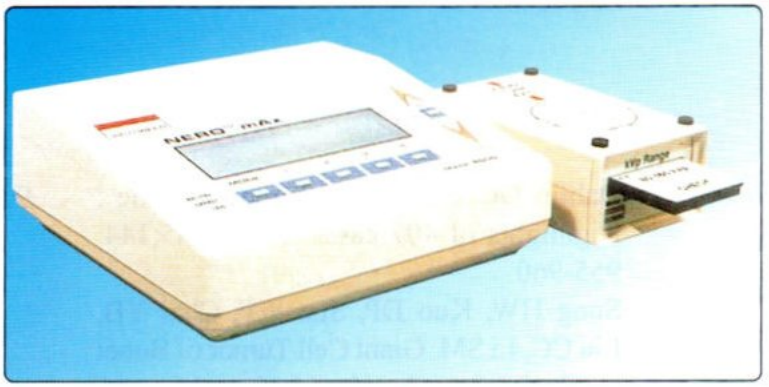

- 100 kHz sampling speed captures data from the most difficult machines
- 0.5 kV or 1% accuracy from 22 to 160 kV
- Measures kVp average, kV effective, kV peak, time, exposure or rate, mA or mAs, HVL, exposure/frame, and mAs/frame
- Displays R or Gy
- Convenient Excel Add-in with templates for Reproducibility, Accuracy, mAs Linearity, Beam Quality and Summary Reports
- RS-232 computer interface
- Enhanced dental capabilities

DDD DUAL-DIODE PATIENT DOSE MONITOR

* Provents the potential for misadministration.
* Provides instantaneous readings on the radiation dose being delivered to the patient.

Inovision Model 451P

Pressurized µR Ion Chamber Survey Meter

- High sensitivity µR measurements of exposure and exposure rate
- Available with dose equivalent energy response (SI units)
- Fast response to measure radiation from leakage, scatter beams and pinholes
- Ergonomic, anti-fatigue handle with replaceable grip and wrist strap
- Excel add-in for Windows® for data logging and selection of instrument operating parameters (optional)
- Low noise chamber bias supply for fast background reading
- Choice of bright, highly visible colors
- Easy touch keys

บริษัท เอช.วี.ที.ซัพพลาย จำกัด

82/31 หมู่ 2 ถนนกาญจนาภิเษก แขวงบางเชือกหนัง เขตตลิ่งชัน กรุงเทพมหานคร 10170

Tel. (662) 447-9111-3, 887-7037, 887-5602 Fax. (662) 447-9114

E-mail ; hvt@loxinfo.co.th

CASE REPORT TUBERCULOSIS OF THE BREAST

Patchrind KEOWCHUN, MD.[1] Darunee BOONYUNWETWAT, MD.[1]
Naruemon WISEDOPART, MD.[2]

Tuberculosis of the breast is rare and difficult to detect because clinical and radiological appearance are not specific. Isolation of the tubercle bacilli from the lesion is seldom possible[1]. Previously, there were many reports from both the west and the east countries. So far there has been no report of mammary tuberculosis in Thailand. We would like to describe the clinical presentation and imaging features including mammography and ultrasonography of a Thai woman proved to be a left mammary tuberculosis.[2-3]

CASE REPORT

A 56-year-old woman presented with painless swelling of the left breast 2 weeks prior to admission. The patient had underlying diabetes mellitus, hypertension, ischemic heart disease, chronic renal failure and gouty arthritis. She was on hemodialysis program 2-3 times a week.

Physical examination revealed BP 140/90 mmHg, pulse rate 80 beats/min and respiration rate 18 breaths/min. The patient was moderately pale, afebrile and not distressing. The left breast was diffusely swollen without palpable mass or tenderness. There was no ulcer on the overlying skin. A movable lump about 1 cm. in diameter was palpated at left axillary area, most likely to be an enlarged node. Mammography and ultrasonography of the breasts were performed.

Mammography showed diffusedly increased density of the left breast. Thickening of fibroglandular tissues and stroma was found. The skin was thickened, markedly at the areolar area. Three enlarged left axillary nodes contained pleomorphic microcalcifications were also detected.

Ultrasonography showed mark skin thickening of the left breast together with a large amount of subcutaneous low echoic networks, likely to be edema or lymphedema. There was no definite mass in the breast parenchyma. Three enlarged left axillary nodes were detected with increased vascularity.

Fine needle aspiration of a left axillary lymph node was carried out, the pathological result was inconclusive so that biopsy of the left axillary lymph node was performed. The microscopic examination revealed multiple necrotic foci surrounding with epitheloid cells and multinucleated giant cells, and also mixed with lymphoplasmacytic infiltration. The histopathological diagnosis was caseating granuloma within the lymph node. But no acid fast bacilli was detected. The short course regimen (2 IRZE/4 IR) of antituberculous drugs was administered. The patient got well after 6 months of treatment. The left breast swelling resolved without palpable lump.

[1] Department of Radiology, Faculty of Medicine, Chulalongkorn University, Bangkok, Thailand
[2] Department of Pathology, Faculty of Medicine, Chulalongkorn University, Bangkok, Thailand

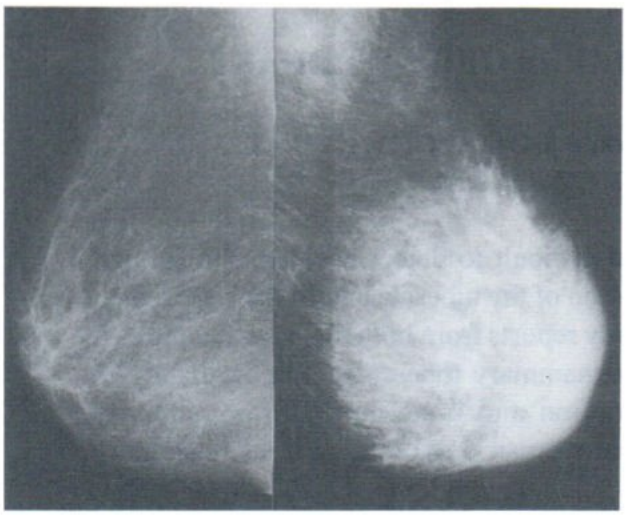

1A

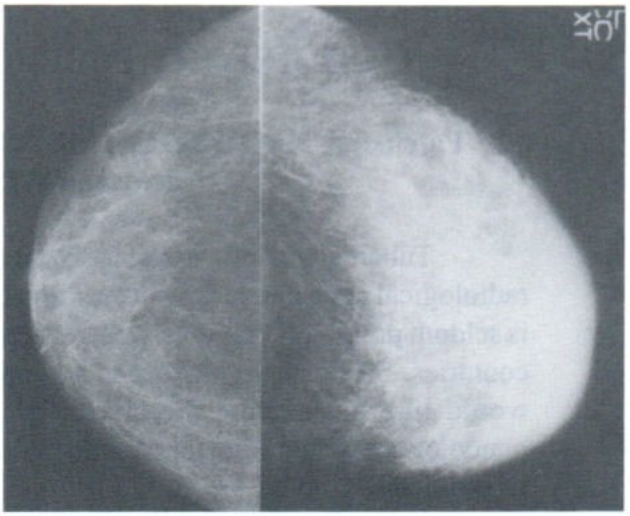

1B

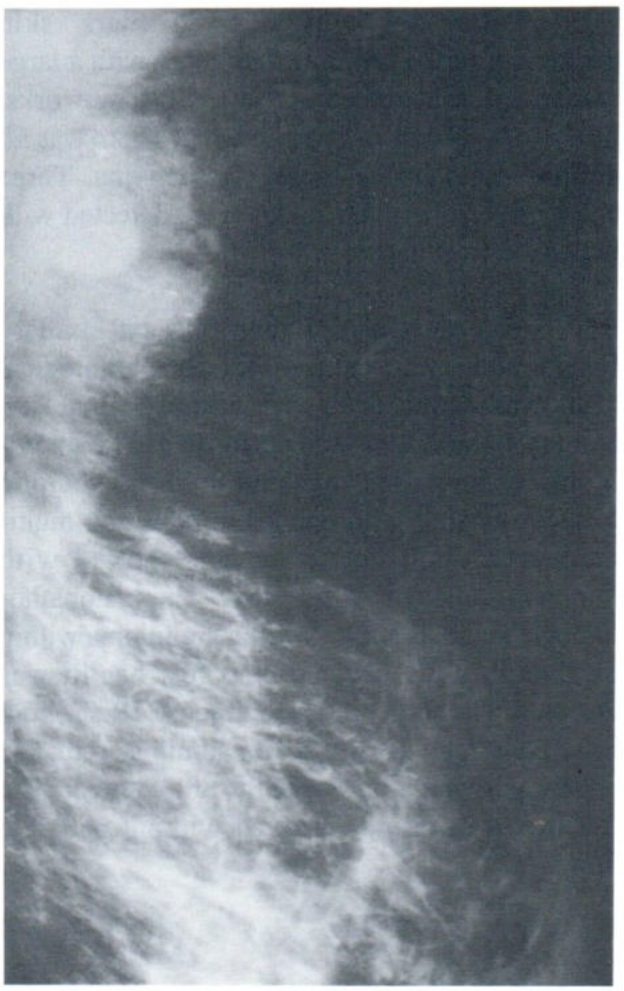

1C

Fig. 1A, B, C. Mammography of both breasts (A=MLO, B=CC, C=left axillary view) showed diffusedly increased density of the left breast. Diffuse skin thickening was seen markedly at areolar area. Three enlarged left axillary nodes contained clusters of microcalcifications were also detected.

2A

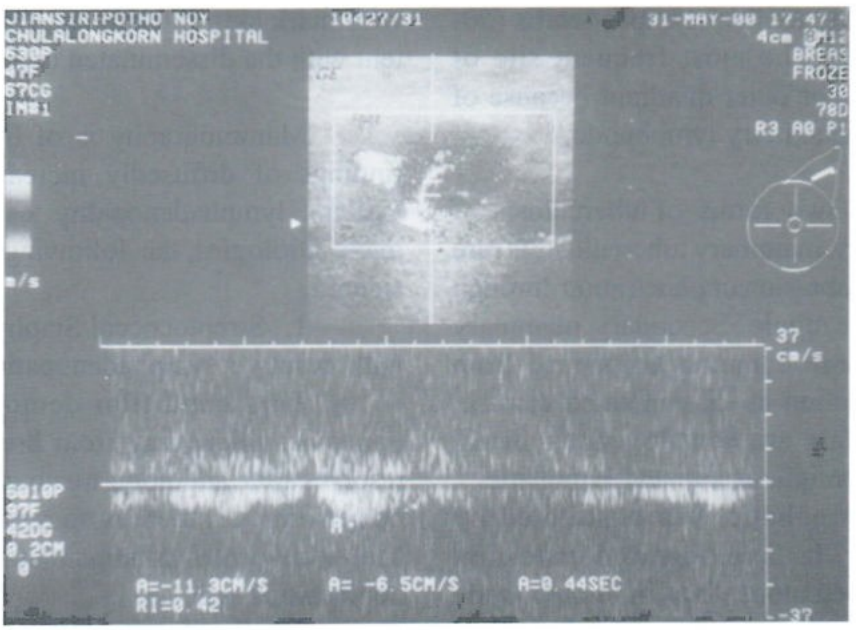

2B

Fig. 2A, B. Ultrasonography of left breast showed diffuse skin thickening markedly at areolar area with a large amount of subcutaneous low echoic networks, likely to be edema or lymphedema (Fig. A). Enlarged left axillary nodes were seen with hypervascularity (Fig. B).

DISCUSSION

Tuberculosis of the breast was first described by Sir Astley Copper in 1829, as "scrofulous swelling in the bosum of young woman".[4] Thereafter, there were previously about 700 cases reported later. This condition was rare in the west countries. The incidence was less than 0.1% of breast specimens that submitted to histological examination.[5] In the endemic area may found its incidence of up to 1.5%.[6] Mammary tuberculosis usually occurs in woman between the ages of 20 and 40, and is rarely bilateral.[7] It is rarely found in elderly man and prepubescent woman. The presenting signs of the breast are fluctuatant abscess, poorly defined firm mass with skin retraction, purulent discharge from nipple, painful or painless breast lump, ulceration and may be associated with lymphadenopathy, especially axillary lymphadenitis (50-75% of cases).[4,8-9] The most frequent site of involvement is upper outer quadrant because of its proximity to the axillary lymphnode.[10]

There are two forms of tuberculosis of the breast. Primary mammary tuberculosis is rare and resulted from abrasion or penetration through the opening of the nipple. Secondary mammary tuberculosis is more common and spread from other foci of infection as disseminated disease. Routes of spreading are hematogenous, direct extension from contiguous site and lymphatic.[7-8] Spreading via lymphatic was postulated by Cooper in 1829. It is retrograded extension from primary tuberculous foci in lymph node of mediastinum, axilla, parasternal and cervical region.[11] Our patient may be in this form of spreading because no other foci were found, except there was lypmphadenopathy.

The pathology of mammary tuberculosis was previously differentiated into 7 categories : acute, miliary, nodular, disseminated confluent, intraglandular cold abscess, sclerosing type and tuberculous mastitis obliterans.[5] However it is now generally accepted that mammary tuberculosis can be classified into three broader groups : nodular, dissiminated and sclerosing. This differentiation has been based on pathologic not radiologic findings. The findings from mammography in each pathological finding are 1) nodular type : the breast mass develops slowly and painlessly. This causes dense nodular opacity and commonly found draining sinus; 2) Disseminated type : there are multiple intercommunicating foci within the breast and associated with skin thickening; 3) Sclerosing type : the breast is uniformly dense fibrosis.[2-3] Our patient presented with painless swelling of left breast. The mammographic findings show thickening of the fibroglandular tissue and stroma with mark skin thickening. This may be consistent with the disseminated type.

Mammography is of limited value. The findings of diffusedly increased density with axillary lymphadenopathy can be caused by many etiologies, the followings should be considered.

1. Streptococcal/Staphylococcal mastitis with reactive lymphadenopathy.

This condition demonstrates diffuse trabecular thickening from breast edema which resolves after antibiotic treatment. Biopsy should be performed if there is no response to treatment trial or advocates prompt biopsy, particulary for nonlactating woman.

2. Inflammatory breast carcinoma causes diffusely increased parenchymal density and lymphadenopathy from metastasis. Sometimes microcalcification are found.

3. Lymphoma with breast involvement

4. Infectious granulomas such as parasites, fungus

5. Autoimmune diseases

Among these conditions may show different clinical presentations, histological and microbiological findings. However surgical excision is necessary because it can confirmed the diagnosis with sufficient certainty.[12-13]

Ultrasonography of the breast may be useful in guiding for FNA or biopsy and distinquishing between solid and fluid lesion.[2] Computer tomography is useful to evaluate the contiguity of the breast lesion and the pleural cavity.[2-9] The histological diagnosis is important for differentiation. The diagnostic criteria are the presence of granulomatous inflammatory infiltration and / or tubercles, with central caseation. Interestingly, acid fast bacilli were present in only 25% of the cases. The mammary tuberculosis responds well to antituberculosis drugs and conservative surgery.[14]

In conclusion, mammary tuberculosis is rare. The significant point is that its clinical signs and mammography cannot be differentiated from the breast carcinoma. Histological diagnosis must be done to distinguish these two conditions.

REFERENCE

1. Guillet JL, Salmon RJ, Pilleron JP. Mammary tuberculosis. Lancet 1982;17: 166
2. Ertugrul G, Mete D, Vedut D, Nesrin V. Tuberculosis of the breast. Eur J Surg 1995;161:471-3
3. Peter S, Dorothea S, Marieke K, Maximilian FR. Tuberculosis of the breast : US, Mammographic, and CT findings. J Comput Assist Tomogr 1994;18(6):970-1
4. Cooper A : Illustrations of Diseases of the breast. London, Longmans Rees, 1829
5. Domingo CH, Ruiz J, Roig J, Texido A, Aguila X, Morera J. Tuberculosis of the breast : a rare modern disease. Tubercle 1990; 71 : 221-3
6. Morgen M. Tuberculosis of the breast. Surg Gynecol Obstet 1931; 53 : 593-60
7. Hamit HF, Ragsdale TH, Mammary Tuberculosis J Roy Soc Med 1982;75:764-5
8. Hale JA, Peters GN, Cheek JH. Tuberculosis of the breast : rare but still extant. Am J Surg 1985; 150 : 620-4
9. Alagaratuam TT, Ong GB. Tuberculosis of the breast. Br J Surg 1980; 67 : 125-6
10. Gilbert AI, Mc Gough EC, Farell JJ. Tuberculosis of the breast. Am J Surg 1962;103:424-7
11. Jo PW, Stanley WC. Tuberculous mastitis. Chest 1990;98:1505-9
12. Laurence WB. Diagnosis of disease of the breast. Los Angeles; Califonia : WB Saunders, 1997 : 203-208
13. Sylvia H. Diagnostic Radiology. Germany : Thieme,1997 : 382-385
14. Morris H,Howard LL. Tuberculosis of the Breast as a Presenting Manifestation of AIDS. CID 1992; 15 : 692-3

PERFORMANCE OF BONE MINERAL DENSITY AT ULTRADISTAL RADIUS IN DIAGNOSIS OF OSTEOPOROSIS AT AXIAL SKELETAL SITES

Charoonsak SOMBOONPORN, M.D.[1], Suppasin SOONTRAPA, M.D.[2], Sukree SOONTRAPA, M.D.[3], Woraluk SOMBOONPORN, M.D.[3]

ABSTRACT

Background: Bone mineral density (BMD) measurement at the forearm has some advantages over at the axial skeletal sites due to lower radiation dose, lower cost, more patient's comfort, faster scan time and not interfered by abnormal calcification or degenerative change of the spines. Performance of the forearm BMD in the diagnosis of osteoporosis at the axial skeleton in the northeastern Thai women has not been reported.

Objective: The study was aimed to determine the performance of the ultradistal radial BMD in the diagnosis of osteoporosis at the lumbar spines and proximal femur in terms of sensitivity, specificity, positive predictive value (PPV), negative predictive value (NPV) and likelihood ratio for positive and negative test.

Design: Retrospective, descriptive study

Setting: Srinagarind Hospital, Faculty of Medicine, Khon Kaen University

Study methods: Results of 592 BMD measurements simultaneously performed at all three skeletal sites including lumbar spines, proximal femur and ultradistal radius from May 1998 to August 2000 of all consecutive women were retrospectively reviewed and classified as non-osteoporosis and osteoporosis according to WHO cirteria. The BMD of the lumbar spines and proximal femur was used to be the standard to determine the diagnostic performance of BMD at the ultradistal radius.

Results: High sensitivity of the ultradistal radial BMD for the diagnosis of osteoporosis at the femoral neck and trochanteric regions, 82.9% and 82.5% respectively, was found but the sensitivity for L_{2-4} was only 37.5%. Specificity and NPV for the lumbar spines and proximal femoral regions were very high, whereas the likelihood ratio for the positive test for the proximal femoral region was better than that for the lumbar spine region.

Conclusion: The ultradistal radial BMD measurement is a promising method as a screening for the diagnosis of osteoporosis at the proximal femur but it is of limitation when applied for the lumbar spines.

Key words: BMD, Ultradistal radius, Osteoporosis, Diagnostic performance

[1] Department of Radiology,
[2] Department of Orthopaedics
[3] Department of Obstetrics and Gynecology, Faculty of Medicine, Khon Kaen University, Khon Kaen 40002, Thailand

For correspondence: Associate Professor Charoonsak Somboonporn, M.D. Division of Nuclear Medicine, Department of Radiology, Faculty of Medicine, Khon Kaen University, Khon Kaen 40002, Thailand e-mail address: chasom@kku.ac.th

INTRODUCTION

Over the past decade, osteoporotic fractures have come to be recognized as one of the most serious problems in public health.[1,2] The growing awareness of the impact of osteoporosis on the elderly and postmenopausal population and the development of new treatment modalities have led to a rapid increase in the demand for bone densitometry services.[3] It has been accepted that dual-energy X-ray absorptiometry (DEXA) is the most appropriate technique for bone mineral density (BMD) measurement because of its high accuracy, high precision and low radiation exposure.[4-6] The common sites of BMD measurement are those at high risk of fracture including lumbar spines, hip and forearm. However, the study at the forearm has some advantages over at the axial skeletal sites, such as lower radiation dose, lower cost, more patient's comfort and faster scan time. Moreover, it is not affected by abnormal calcification or degenerative change as in the antero-posterior spinal BMD measurement.[7] Although high correlation between the forearm BMD and the axial BMD, both lumbar spines and proximal femur, have been reported,[8-9] few studies regarding performance of the forearm BMD in the diagnosis of osteoporosis at the axial skeleton have been reported. [10-12]

One of the forearm regions commonly measured for BMD is the ultradistal radius. It is located approximately between 10-mm to 25-mm proximal to the level of the tip of ulnar styloid process[13] and is the area that has high trabecular to cortical bone ratio, of about 60%: 40%, comparable to the vertebral body and has been recognized a sensitive area in the detection of alteration of bone mass.[14]

We, therefore, conduct this study to determine the performance of the ultradistal radial BMD in the diagnosis of osteoporosis at the lumbar spines and proximal femur according to the World Health Organization (WHO) criteria in terms of sensitivity, specificity, positive predictive value (PPV), negative predictive value (NPV) and likelihood ratio for positive and negative test.

MATERIALS AND METHODS

The studied population was women who were referred for BMD measurement at the Division of Nuclear Medicine, Department of Radiology, Srinagarind Hospital, Faculty of Medicine, Khon Kaen University from May 1998 to August 2000. Their medical records and results of BMD measurement were retrospectively reviewed. The inclusion criterion was women who had the BMD measurement at all three parts of the skeleton-lumbar spines, proximal femur and ultradistal radius. The exclusion criterion was those who had the history of fracture.

The recorded data included age, weight, height, body mass index (BMI) and BMD with T-score at these various sites including antero-posterior lumbar spines (L_1, L_2, L_3, L_4, L_{2-4}), femoral neck, Ward's triangle, trochanteric region, total proximal part of the non-dominant femur and ultradistal part of the non-dominant radius.

The BMD was measured using DEXA technique of EXPERT-XL bone densitometer of Lunar Corp, USA, by the standardized well-trained technician. Quality control of the instrument was undertaken daily, using the standard phantom with automatic software program by technicians under the supervision of an experienced nuclear medicine physician. Precision error of each site of measurement was about 1-2%. The BMD of all sites was classified as non-osteoporosis or osteoporosis for further analysis. T-score of the studied subject was calculated using the BMD database from the

normal Japanese population. The T-score > –2.5, as normal or osteopenia according to WHO criteria, was classified as non-osteoporosis, whereas the T-score ≤ –2.5 was classified as osteoporosis. BMD of the axial skeletal sites, as non-osteoporosis or osteoporosis, was then used to be the standard to determine the diagnostic performance of BMD of the ultradistal radius.

The tabulated data were edited and analyzed using SPSS program for Windows, version 9.0. Sensitivity, specificity, PPV, NPV, likelihood ratio for positive and negative test of the axial BMD determined by the ultradistal radial BMD were shown. The continuous data including age, weight, height, BMI and BMD were reported as mean ± standard deviation (SD). The prevalence of osteoporosis and all diagnostic performance parameters were shown as percentage or ratio. This study was approved by the Ethics Committee of Faculty of Medicine, Khon Kaen University.

RESULTS

Of all subjects referred for BMD measurement during the studied period, 477 cases meeting our criteria were recruited. Almost all subjects were from the northeast of Thailand. Two hundred and sixty cases (55.5%) were sent from the Menopause Clinic, Srinagarind Hospital, for baseline BMD measurement, to find evidence of low bone mass or osteoporosis, or to follow-up BMD after a period of hormone replacement therapy, and 217 cases (45.5%) were sent from various other units in order to find the evidence of osteopenia or osteoporosis. From all 477 cases, 71 were studied for 2 times and 22 were studied for 3 times, resulting in overall 592 studies enrolled for analysis.

Baseline characteristics of subjects were shown in Table 1. Using T-score ≤ –2.5, the prevalence of osteoporosis for each skeletal site was demonstrated (Table 2). The prevalence of osteoporosis at the ultradistal radius was higher than that of various regions of the proximal femur and the lumbar spines except at L_1. It was also noted that the prevalence of osteoporosis at the femoral and trochanteric region was very low, 2.2% and 1.4% respectively,

The diagnostic performance parameters in the diagnosis of osteoporosis at various regions of the lumbar spines and proximal femur determined by the ultradistal radial BMD were shown in Table 3 and 4 respectively. Very high specificity and NPV of the ultradistal radial BMD in the diagnosis of osteoporosis at the lumbar spines and proximal femoral regions were observed. Sensitivity of the ultradistal radial BMD in the diagnosis of osteoporosis at the proximal femoral regions was high, while sensitivity for the diagnosis at the lumbar regions was relatively compromised. Low PPV for the diagnosis at the lumbar spines and proximal femur was observed, more prominent at the femoral neck, trochanteric region and total proximal femur. The likelihood ratio for the positive test was highest at the trochanteric region and was lowest at the L_{2-4} spines.

Table 1. Baseline characteristics of the subjects (N=477 cases, 592 studies).

Characteristics	Value
Age (y)	
mean ± SD	52.1 ± 8.5
range	28 - 88
Weight (g)	
mean ± SD	57.4 ± 8.4
range	37 - 85
Height (cm)	
mean ± SD	154.9 ±+ 5.6
range	133 - 175
BMI (kg/m^2)	
mean ± SD	23.9 ± 3.4
range	16.2 - 38.4
BMD (g/cm^2)	
mean ± SD	
L_1	0.908 ± 0.178
L_2	1.004 ± 0.184
L_3	1.086 ± 0.183
L_4	1.091 ± 0.182
L_{2-4}	1.063 ± 0.171
Femoral neck	0.874 ± 0.136
Ward's triangle	0.721 ± 0.153
Trochanteric region	0.749 ± 0.125
Total proximal femur	0.945 ± 0.136
Ultradistal radius	0.319 ± 0.059

Table 2. Prevalence of osteoporosis in each skeletal site diagnosed by using T-score ≤ -2.5 SD criteria (N=592 studies)

Skeletal sites	Prevalence	
	N	(%)
L_1	125	21.1
L_2	89	15.0
L_3	40	6.8
L_4	45	7.6
L_{2-4}	64	10.8
Femoral neck	13	2.2
Ward's triangle	80	13.5
Trochanteric region	8	1.4
Total proximal femur	10	1.7
Ultradistal radius	108	18.2

Table 3. Performance of ultradistal radial BMD in the diagnosis of osteoporosis at various regions of the lumbar spines.

	Lumbar spines				
	L_1	L_2	L_3	L_4	L_{2-4}
Ultradistal radius					
Sensitivity (%)	42.4	50.6	55.0	55.6	37.5
Specificity (%)	88.0	87.3	84.2	84.6	83.9
PPV (%)	48.6	41.3	20.2	22.9	22.0
NPV (%)	85.1	90.9	96.3	95.9	91.7
Likelihood ratio +	3.5	4.0	3.5	3.6	2.3
Likelihood ratio -	0.7	0.6	0.5	0.5	0.7

Table 4. Performance of ultradistal radial BMD in the diagnosis of osteoporosis at various regions of the proximal femur.

	Proximal femur			
	Neck	Ward's	Trochanter	Total
Ultradistal radius				
Sensitivity (%)	76.9	58.8	87.5	80.0
Specificity (%)	82.9	87.9	82.5	82.6
PPV (%)	9.2	43.1	6.4	7.3
NPV (%)	99.4	93.2	99.8	99.6
Likelihood ratio +	4.5	4.9	5.0	4.6
Likelihood ratio -	0.3	0.5	0.2	0.2

DISCUSSION

Although osteoporosis is described conceptually as a systemic skeletal disease characterized by low bone mass and microarchitectural deterioration of bone tissue with a consequent increase in bone fragility and susceptibility to fracture,[15] it may not occur at all skeletal sites at the same time, of the same severity and in the same individual. Using WHO criteria as a T-score of $\leq$ -2.5, we found a wide variety of prevalence of osteoporosis in the three skeletal sites studied, varying from 1.4% at the trochanteric region to 21.1% at L_1. These findings corresponded to those of a recent large study from Japan, which reported a fivefold difference among the prevalence of osteoporosis at different skeletal sites with lower prevalence at the hip as compared with that at the lumbar spines and distal one-third of the radius.[16] Variations in the prevalence of osteoporosis with skeletal sites of BMD measurement have been reported in the literature.[17-18] This showed that using a unique T-score of $\leq$ -2.5 might not be appropriate to be applied to different sites in the diagnosis of osteoporosis. Recently, the WHO diagnostic guidelines were updated and were clearly stated that the diagnosis of osteoporosis by T-score $\leq$ -2.5 was applicable only to measurements at the hip and possibly the spine.[19]

From our findings regarding the diagnostic performance of the ultradistal radial BMD, because of high sensitivity for the femoral neck and trochanteric regions, 76.9% and 87.5% respectively, the ultradistal radial BMD measurement could be the method in the screening for evidence of osteoporosis at these two common sites of fracture. Moreover, it also provided very low false positive rate owing to high specificity in these two regions. Very low PPV for the diagnosis of osteoporosis at the femoral neck and trochanteric regions was observed, 9.2% for the femoral neck and 6.4% for the trochanteric region and could be resulted from very low incidence of osteoporosis in these regions, 2.2% and 1.4% respectively. Thus if we apply this in the higher prevalence population such as in the elderly or high risk individuals, the PPV would be higher than that in this study. The likelihood ratio of positive test for the femoral neck was 4.5 which is fair and for the trochanteric region was 5.0 which was rather good. It means that the ratio of probability between those being osteoporotic and those being non-osteoporotic in the positive-test individuals is acceptable.

For the diagnosis at the lumbar spines, although providing very high specificity and NPV, the ultradistal radial BMD seemed too compromised to be used as a screening test because of too low sensitivity, especially at the L_{2-4}. In addition, the likelihood ratio for positive test for the lumbar spines was not good as that at the proximal femoral regions.

Regarding other previous study in Thai population, Trivitayaratana W et al.[10] reported the accuracy of BMD at distal 1/10 of radii in the identification of non-forearm osteoporosis in Thais and found high NPV, varying from 71.43% to 96.88%, in the diagnosis of osteoporosis at the lumbar spines, hip, femoral neck and Ward's triangle.[19] These figures were comparable to those in our study. However, sensitivity and PPV from their study were clearly higher than those in our study, whereas specificity was somewhat lower. The difference in PPV could be attributed to the prevalence of osteoporosis in the studied population. Since their studied population was recruited from the elderly club which certainly had a higher prevalence of the disease than that in our studied population, which was mostly from the Menopausal Clinic. Moreover, they used the distal 1/10 radius region, not the ultradistal radius, in identifying non-forearm osteoporosis, whereas we chose the ultradistal radius because of, unlike the distal 1/10, its availability in the software of our instrument. Although these two regions are close proximity, they have different onsets and rates of trabecular and cortical bone losses. Diagnostic discrepancies between these two closely related forearm sites of BMD measurement, distal and ultradistal, were recently reported in Bulgarian population by Boyanov M and were found to be more pronounced after the age of 60.[18]

However, our study had some drawbacks. T-scores used in the study were calculated from the Japanese BMD database, which might not be suitable for the diagnosis of osteoporosis in the northeastern Thai women. In addition, since most of our studied population came from the Menopause Clinic, the prevalence or pretest probability of osteoporosis therefore might not be the same as that in the general population. Accordingly, the diagnostic performance obtained might not be the same.

In conclusion, the ultradistal radial BMD measurement is a promising method as a screening for the diagnosis of osteoporosis at the proximal femur but it is of limitation when applied for the lumbar spines. Further studies should be carried out on the basis of population-based, especially focussing at the proximal femoral region and it will be better if the northeast Thai BMD database or Thai BMD database was used in stead of the Japanese database.

REFERENCES

1. Kanis JA, Delmas P, Burckhardt P, Cooper C, Torgerson D. Guidelines for diagnosis and treatment of osteoporosis. Osteoporos Int 1997;7:390-406.
2. Cooper C, Campion G, Melton LJ. Hip fractures in the elderly: A world-wide projection. Osteoporos Int 1992;2:285-9.
3. Baran DT, Faulkner KG, Genant HK, Miller PD, Pacifici R. Diagnosis and management of osteoporosis: guidelines for the utilization of bone densitometry. Calcif Tissue Int 1997;61:433-40.
4. Cullum ID, Ell PJ, Ryder JP. X-ray dual-photon absorptiometry: a new method for the measurement of bone density. Br J Radiol 1989;62:587-92.
5. Mazess R, Collick B, Trempe J, Barden H, Hanson J. Performance evaluation of a dual-energy x-ray bone densitometer. Calcif Tissue Int 1989;44:228-32.

6. Lang T, Takada M, Gee R, et al. A preliminary evaluation of the lunar expert-XL for bone densitometry and vertebral morphometry. J Bone Miner Res 1997;12: 136-43.
7. Mole PA, McMurdo ME, Paterson CR. Evaluation of peripheral dual energy X-ray absorptiometry: comparison with single photon absorptiometry of the forearm and dual energy X-ray absorptiometry of the spine or femur. Br J Radiol 1998; 71: 427-32.
8. Limpaphayom K, Bunyaveichevin S, Taechakraichana N. Similarity of bone mass measurement among hip, spines and distal forearm. J Med Assoc Thai 1998; 81: 94-7.
9. Trivitayaratana W, Trivitayaratana P, Kongkiatikul S. Prediction of bone mineral density of lumbar spine, hip, femoral neck and Ward's triangle by forearm bone mineral densiy. J Med Assoc Thai 2001; 84: 390-6.
10. Trivitayaratana W, Trivitayaratana P. The accuracy of bone mineral density at distal radius on non-forearm osteoporosis identification. J Med Assoc Thai 2001; 84: 566-71.
11. Pouilles JM, Tremollieres FA, Martinez S, Delsol M, Ribot C. Ability of peripheral DXA measurements of the forearm to predict low axial bone mineral density at menopause. Osteoporos Int 2001;12:71-6.
12. Gnudi S, Malavolta N, Lisi L, Ripamonti C. Bone mineral density and bone loss measured at the radius to predict the risk of nonspinal osteoporotic fracture. J Bone Miner Res 2001;16:1130-5.
13. Blake GM, Washner HW, Fogelman I. The evaluation of osteoporosis: dual energy X-ray absorptiometry and ultrasound in clinical practice. 2nd ed. London: Matin Dunitz Ltd, 1999: 303-4.
14. Leboff MS, Fuleihan GE, Angell JE, Chung S, Curtis K. Dual-energy x-ray absorptiometry of the forearm: reproducibility and correlation with single-photon absorptiometry. J Bone Miner Res 1992; 7:841-6.
15. Consensus development conference: diagnosis, prophylaxis and treatment of osteoporosis. Am J Med 1993;94:646-50.
16. Iki M, Kagamimori S, Kagawa Y, Matsuzaki T, Yoneshima H, Marumo F. Bone mineral density of the spine, hip and distal forearm in representative samples of the Japanese female population: Japanese Population-Based Osteoporosis (JPOS) Study. Osteoporosis Int 2001;12:529-37.
17. Frost ML, Blake GM, Fogelman I. Can the WHO criteria for diagnosing osteoporosis be applied to calcaneal quantitative ultrasound? Osteoporos Int 2000;11:321-30.
18. Boyanov M. Diagnostic discrepancies between two closely related forearm bone density measurement sites. J Clin Densitom 2001; 4: 63-71.
19. Kanis JA, Gluer CC. An update on the diagnosis and assessment of osteoporosis with densitometry. Osteoporos Int 2000; 11:192-202.

MALIGNANT SCHWANNOMA IN NEUROFIBROMATOSIS 1

PEUNGJESADA S.[1], CHUROJANA A.[1], CHIEWVIT P.[1],
BENAJARASSAMEROTe S.[2] and ASAVAMONGKOLKUL A.[3]

ABSTRACT

Malignant peripheral nerve sheath neoplasms are serious complications of Neurofibromatosis. The incidence of which reported in literatures is between 2% and 29%. Once it occurs, the prognosis is poor. We reviewed 2 cases of malignant schwannoma in the vicinity of Neurofibromatosis-1 at Siriraj Hospital in the points of view of radiographic findings with histopathological correlations. One had lesion at chest wall and the other at sacral area. Both CT and MRI provided good structural delineation and tumor extension but malignant or benign lesions can not be distinguished with certainty. Because of its aggressiveness, biopsy with histological diagnosis should be performed in those Neurofibromatosis patients who have peripheral nerve sheath tumors before surgical planning.

Malignant degeneration of peripheral nerve sheath tumors is problematic in NF-1 patients. Its incidence has been estimated to be 2-29 %.[1] or 10 to 10,000 times more than general population.[2] Spontaneous sarcomatous change in patients without von Recklinghausen 's disease is very rare.[3] It has poor prognosis[1,4-9] and causes high morbidity and mortality. Early recognition of this change brings about early treatment and greater awareness. But they are difficult to be differentiated from benign neoplasm.[10] Because they can produce no symptom, either, mild or aggressive symptoms.[3,10]

There is no imaging criteria for differentiation malignant from benign tumor.[10] This study was performed retrospectively to determine if CT scans and MR imaging would be any useful for distinguishing malignant from benign neoplasms. Pathological findings and correlation between pathology and radiology were also analyzed.

MATERIALS AND METHODS

Retrospective medical records of 2 patients at Siriraj Hospital from the period of 1998-1999 who had been diagnosed to be NF-1 according to diagnostic criteria were reviewed. They had sarcomatous degeneration which had been proved by histology. CT scan and MR imaging were reviewed by 1 experienced radiologist. After surgical resections were performed, the histologic sections were reviewed by 1 experienced pathologist. Radiographic findings from CT scan and

[1] Department of Radiology, Faculty of Medicine, Siriraj Hospital, Mahidol University, Thailand.
[2] Department of Pathology, Faculty of Medicine, Siriraj Hospital, Mahidol University, Thailand.
[3] Department of Orthopaedic surgery, Faculty of Medicine, Siriraj Hospital, Mahidol University, Thailand.

MR imaging were analyzed from the following point of views :

1. size
2. homogeneity
3. margins
4. pattern of enhancement and
5. extension .

CT scans of the lesions at the chest and pelvis were performed with 10 mm. interval slice thickness in both pre and post contrast enhancement. One hundred millilitres of Angiografin was given intravenously. All images were filmed at suitable window widths and level for demonstrating both soft tissue and bone detail. Multisection turbo spin-echo (TSE) imaging was done with a superconducting magnet (ASC II, Phillips Medical System, Best, Netherland) operated at 1.5 T. A body coil with a 50 cm field of view was used routinely. Data were acquired with a 152-203x256 matrix and were displayed with 256x256 matrix. The pixel size was about 1.5x1.5 mm for body coil. TSE pulse sequence was used with T1weighted (TR = 500-729 ms. TE = 12-15ms.) and T2 weighted (TR = 2400 ms. TE = 120-150 ms.) images. T1 weighted with Gd enhancement was also performed. Continuous 8-10 mm. sections were obtained and seperated by 0.8-1.2 mm. gaps.

Pathologic findings were also analyzed about gross pathology , diagnostic histologic criterias of schwannoma and sarcomatous changes and correlation between histology and radiology.

RESULTS

The first patient was 33 years old, a single female who presented with progressively enlarged mass at Rt. anterior chest wall for 4 months. Physical examination revealed a large mass at Rt. Anterior chest wall which was measured about 12x10 cm. It had hard consistency and was fixed to the chest wall with slight tenderness and smooth surface. She also had cafe- au- lait spots more than 6 lesions which each one was larger than 5mm. in diameter. Axillary region freckling was seen. Immediate CXR- PA and CT scans of the chest were performed.

The CXR-PA revealed a large soft tissue mass at Rt. anterior chest wall with rib destruction (fig 1).

CT scans showed heterogeneous density of soft tissue mass. It had smooth border and located at Rt. anterior chest wall. Its size was about 4.53x4.50 cm. This mass destroyed Rt. 6th to 9th ribs and extended into thoracic cavity with invasion of the lung. It has peripheral enhancement (fig 2).

Incisional biopsy was done about 2 weeks later and histologic section was malignant peripheral nerve sheath tumor. Then the patient received a wide excision with RML segmentectomy. The operative findings discovered compression of the liver from the tumor mass without invasion. It extended through the diaphragm and also invaded the Rt. Middle lobe. Serosanguinous pleural effusion about 300 ml. was seen.

Gross pathologic examination showed a lobulated mass with rib and lung involvement (fig 3). Microscopic examination demonstrated spindle cell tumor which has hypercellularity, increased N/C ratio, hyperchromatic nucleus, abundant mitosis, pleomorphism and necrosis. The special staining was performed with S-100 protein that was positive in this specimen which confirmed MPNST (fig 4). Heterogeneous density in the mass was necrotic area.

MPNST = Malignant peipheral nerve sheath tumor

The patient was free of disease for 2 months. Local recurrence of tumor had occurred with multiple varying in sizes of soft tissue masses adjacent to old surgical scar at Rt. Anterior chest wall. So MR imaging of the chest was done. It showed heterogeneous hyposignal intensity in T1WI (fig 5), heterogeneous hypersignal intensity in T2WI , irregular border with invasion to the lung and liver moderate enhancement (fig 6). The patient obtained symptomatic treatment and external radiation because surgery and chemotherapy played no roles.The patient expired about 3 months later.

The second patient was 34 years old and single female who presented with Rt. Sciatica pain for 4 months. Physical examination revealed loss of sensation at L5 to S2 nerve root levels of Rt. leg. Motor power of Rt. EHL was grade 3 and SLRT was positive about 45° of Rt. leg. She had cafe-au-lait spots more than 6 lesions. Each one had more than 5mm. in diameter. Axillary flecklings were also seen.Prompt plain film pelvis - AP and CT scans of lower abdomen were done. MR imaging of LS spines was accomplished in 3 weeks.

Plain film pelvis- AP revealed soft tissue mass at Rt. side of pelvic cavity with sacral erosion (fig 7).

CT findings showed a large heterogeneous density of soft tissue mass located at Rt. side of pelvic cavity (fig 8). It had smooth margin, lobulated shape, well-defined capsule, protrusion via greater sciatic notch and hrterogeneous enhancement (fig 9). Sacral erosion was noted in bone window (fig 10).

MR imaging demonstrated heterorogeneous signal intensity in T1WI, heterogeneous hypersignal intensity with peripheral hypersignal intensity in T2WI and peripheral enhancement (fig 11 and 12). Afterthat intrapelvic biopsy was performed and histologic section was malignant peripheral nerve sheath tumor. The patient underwent Rt. hemisacrectomy with tumor resection and partial resection of iliac crest about 3 weeks later. Operative findings revealed sacral nerve root involvement at S2 to S4 levels. The mass also compressed and blended to sciatic nerve. Tumor extended beyond sciatic notch. Mass was removed by blunt dissection. Sciatic nerve which attached to the mass was resected. Post operative infection had occured but finally it could be got rid off.

Gross pathologic examination showed lobulated mass covered with capsule (fig. 13).

Microscopic examination demonstrated the ame histologic findings as the first case (fig. 14). But there was a larger area of necrosis. Capsule of the mass on imaging findings consisted of compact surrounding fibrous tissue. Hence it was pseudocapsule. Heterogeneous density in the mass were necrotic areas.

The patient lost follow up and expired 15 months later from lung metastasis.

EHL = Extensor Hallucis Longus
SLRT = Straight Leg Raising Test

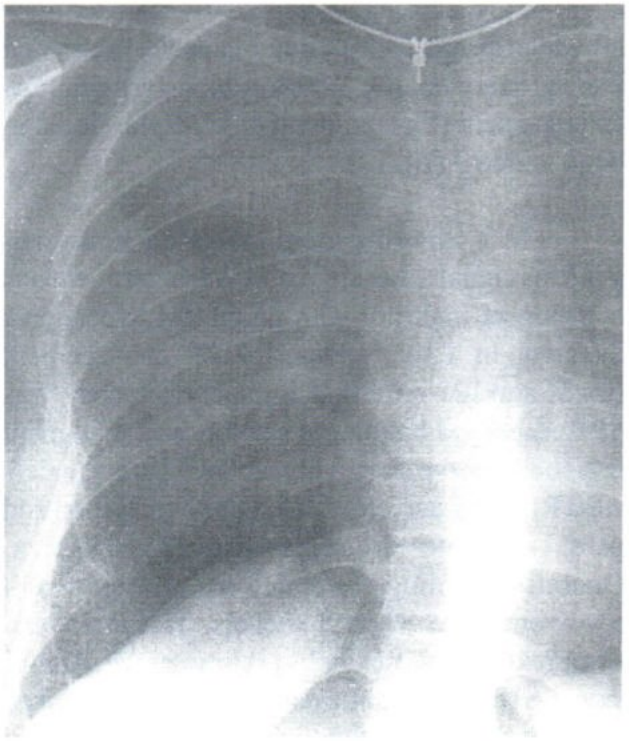

Fig. 1. CXR-PA demonstrated soft tissue mass at right chest wall with adjacent multiple rib destruction.

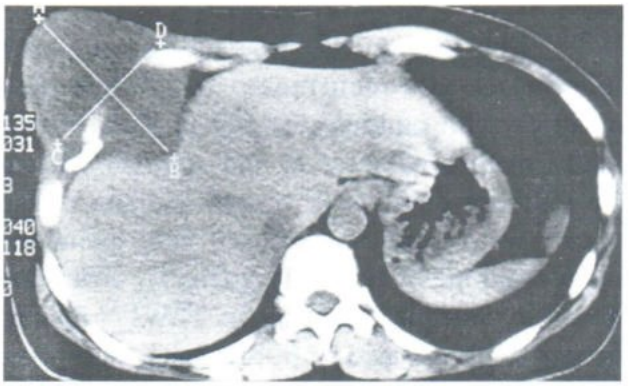

Fig. 2. NECT of the chest included upper abdomen reveals heterogenous hypo-density soft tissue mass at right anterior chest wall with multiple rib destruction.

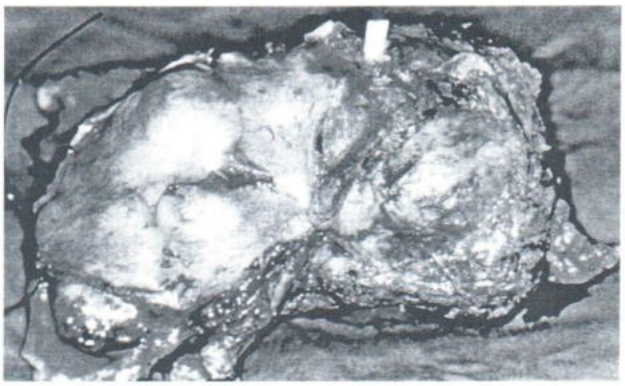

Fig. 3. Gross features of the resected tumor showed the attachment of diaphragm and some ribs.

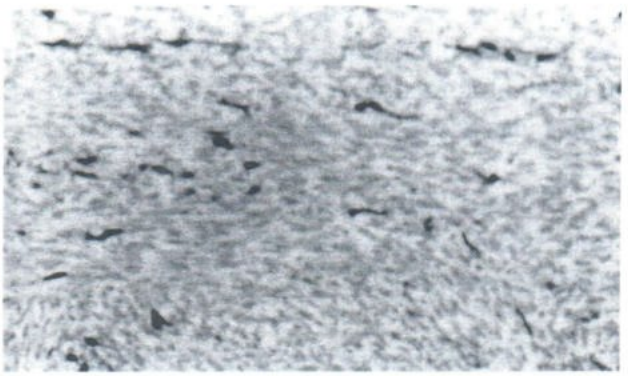

Fig. 4. Special stain by S-100 protein discovered MPNST.

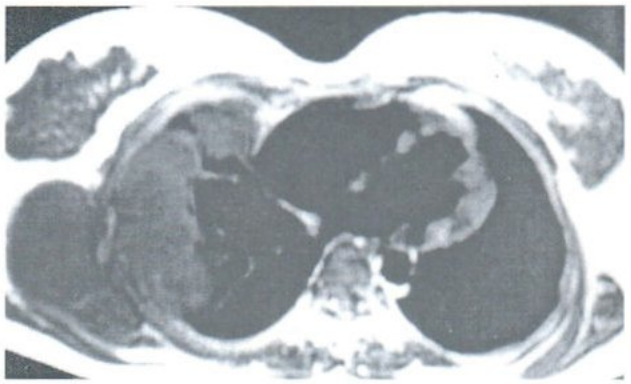

Fig. 5. Axial MRI of the chest in T1W revealed hyposignal intensity soft tissue mass at right anterior chest wall with irregular border and invasion into thoracic cages.

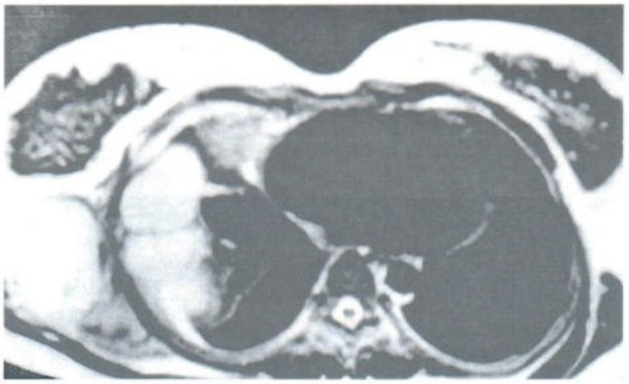

Fig. 6. Axial MRI of the chest in T1W with Gd enhancement disclosed markedly homogenous enhanced mass.

Fig. 7. Plain film pelvis AP showed soft tissue mass at right side of pelvis and erosion of sacrum.

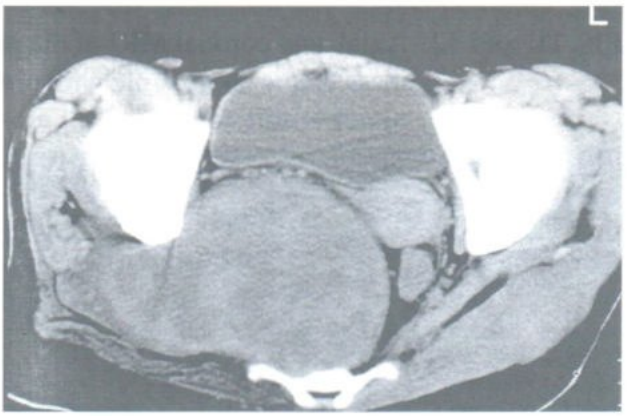

Fig. 8. NECT of the pelvis showed a large heterogenous soft tissue mass extended via greater sciatic notch which is typically seen in nerve sheath tumor.

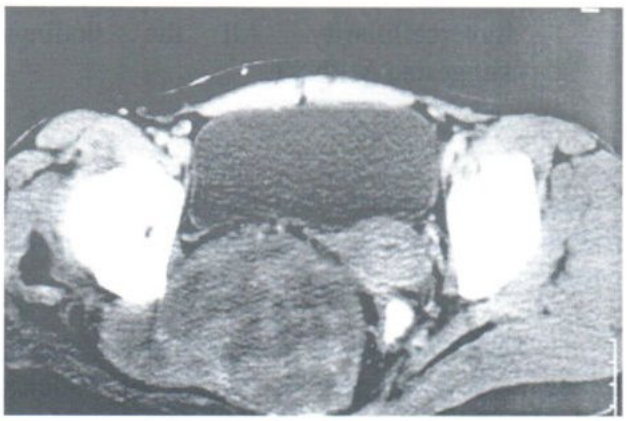

Fig. 9. CECT of the pelvis reveals heterogenous enhanced mass at the same level

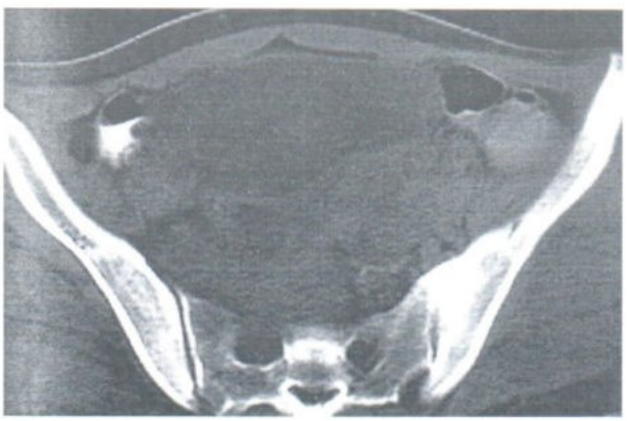

Fig. 10. Bone window of the pelvis demonstrated widening and erosion of the foramen.

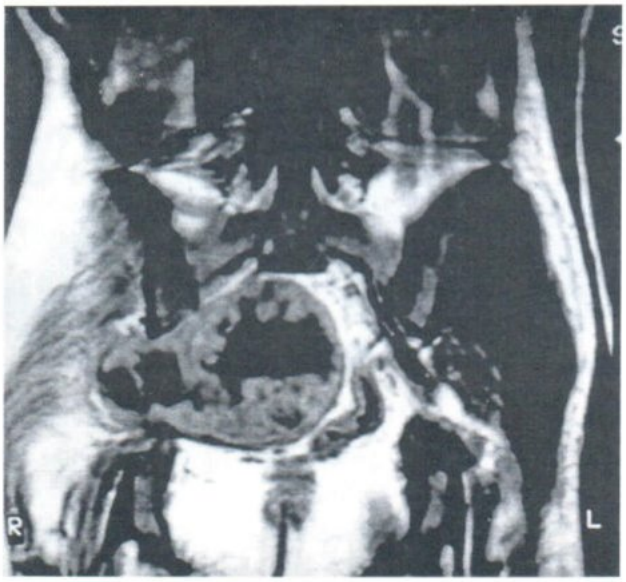

Fig. 11. and 12. Axial and coronal MRI of the pelvis showed heterogenous signal intensity soft tissue mass that is compatible with previous CT scan. The characteristic of the nerve sheath tumor is still noted.

Fig. 13. Gross specimen revealed smooth round encapsulated mass with some part of resected pelvic bone.

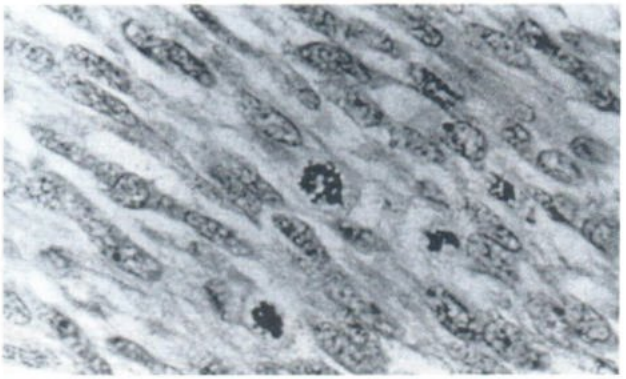

Fig. 14. Microscopic examination disclosed abundant mitosis, pleomorphism and hypercellularity. All the findings suggested MPNST.

DISCUSSION

Neurofibromatosis is neurocutaneous syndrome that is inherited as an autosomal dominant that which virtually 100% penetrance.[11] Mainly sarcomatous degeneration complicated neurofibromatosis are of nerve trunk origin and uniform composition. The other type of sarcoma which is lessly occured attributed to multipotentiated neurilemmal cells. They can produce fat, striated muscle, cartilage and osteoid by metaplasia and finally they will be rhabdomyosarcoma, liposarcoma or osteosarcoma.[1,11]

About malignant peripheral nerve sheath tumor, it is developed in 2-29% of patients with NF-1.[1] The latent period is vary from weeks to 18 years.[12] The causes are still unknown and the hypothesis that trauma and surgery

predispose to sarcomatous degeneration remains unsubstantiated.[1,13] They usually arise in deep structures[10] so early detection can not be performed until symptoms are appeared. The disease has poor prognosis.[1,2,4,5,7-9] Location and histology do not seem to affect the prognosis.[12] But some studies comment that deep location do.[14] Several diagnostic tools are established, CT scan, MR imaging and Ga-67 scanning for examples, but histologic section is still necessary for definite diagnosis. These lesions have tendency to grow slowly, local recurrence after excision and metastasis via blood stream especially to the lungs.[4]

Either CT scans or MR imaging were analyzed about size, homogeneity, margin, pattern of enhancement and extension of the masses. Both patients had a huge mass at Rt. anterior chest wall and pelvic cavity respectively but the size did not give an indication of the likelihood of malignancy.[10] Neoplasm inhomogeneities on CT scan and MR imaging were seen in both patients. Low density component usually resulted from hemorrhage or necrosis[10,13,14,16,17] Benign neoplasms also mimic malignancy by inhomogeneity. Both patients have smooth border of masses, One had rib destruction and RML involvement. The other had sacral bone erosion. But MR imaging of the chest showed irregular border of recurrent tumor. So malignant tumors had either aggressive behavior such as an irregular, infiltrative border, bone destruction and RML involvement or non aggressive behavior such as smooth edge without surrounding extension. Benign tumor also had the former feature but it is less obvious.

Malignant tumors demonstrated peripheral and moderate enhancement. Extension could not predict malignant potential because one looked well capsulated without breaking through its margin. It showed extension from pelvic cavity to outside via greater sciatic notch which was suggestive of nerve sheath tumor. The other extended outward from its margin and invaded surrounding structures. RML involvement and rib erosion were occured. In conclusion, there are no definite imaging criterias suggesting malignancy by CT scans or MR imaging. Although inhomogeneity, infiltrative margin or irregular bone destruction are more common in malignant neural neoplasm.[10] Finally they are still overlapped. But CT scans and MR imaging provide better structural delineation of the mass and its relationship to adjacent structures for surgical planning. The gross pathology of Rt. anterior chest wall mass is lobulated mass with invasion to Rt. hemidiaphragm, RML and rib. Pelvic mass is characteristic by lobulation with pseudocapsule.

Neurofibroma in general population rarely changes into malignant schwannoma. NF-1 patients who have neurofibroma tend to occur sarcomatous degeneration so histologic diagnosis of MPNST is related to clinical manifestation such as NF-1 patient and mass that arise in close contact with a peripheral nerve. Microscopic appearance of MPNST is hypercellularity, increased nuclear cytoplasmic ratio, hyperchromatic nucleus, abundant mitosis, pleomorphism and necrosis of spindle cells. Malignant spindle cell tumors include MPNST, fibrosarcoma, leiomyosarcoma and synovial sarcoma which can be differentiated from each other by immunohistochemical stains such as S-100 protein. S-100 protein is an antigen that present in the cytoplasm of schwann cells. So this comfirmation is MPNST. Both patients have spindle cell tumors with positive staining for S-100 protein and microscopic appearance of MPNST as mentioned. Well capsulated pelvic mass is surrounding fibrous tissue which is looked like capsule from compression. Hence it is pseudocapsule. Heterogeneous areas in both mases are resulted from necrosis which are more obviously seen in the pelvic mass.

The treatment of choice is surgical removal of the tumors but local recurrence and distant metastasis are still presented.

REFERENCES

1. Donald Resnick. Diagnosis of bone and joint disorder, vol. 6 Philadelphia: W.B. Saunders company,1995:4370-4377
2. Ricardo Salazar, Enrico B. Robotti, Douglas H.L. Chin and John A.I. Grossman. Giant neurofibromatosis of the chest wall: two patient reports. Ann Plast Surg 1988;41:211-214
3. K. Mortele, M. Lemmerling, L. Defreyne, F. Speleman, C. De potter, S. Van belle and M. Kunnen. Ossified retroperitoneal malignant schwannom with spinal leptomengeal metastasis. Neuroradiology 1998; 40:48 -50
4. Preston F.W., Walsh W.S. and Clake, T.H. Cutaneous neurofibromatosis (von Recklinghausen's disease) : clinical manifestations and incidence of sarcoma in 61male patients. A.M.A. Arch Surg 1952;64:813-82
5. Aguiar - Vitacca S, Sarrazin D, Henry - Amar N, et al. Neurosarcoma associated with von Recklinghausen disease: apropos of 25 cases observed at the Gustave Roussy Institute from1967 to 1990. Bull cancer Paris 1992;79:101-102
6. von Gumppenberg S, Karpf PM, Prokscha GW, et al. Neurofibroma and neurofibrosarcoma in Recklinghausen's neurofibromatosis. Fortschr Med 1978;96:1563-1568
7. Riccardi VM, Powell PP. neurofibrosarcoma as a complication of von Recklinghausen neurofibromatosis. Neurofibromatosis 1989; 2:152-165
8. Gucccion JG, Enzinger FM. Malignant schwannoma associated with von Recklinghausen neurofibromatosis. Neurofibromatosis. Virch Arch Pathol Anat 1979; 383:43-57
9. Storm FK, Eilber FR, Mirra J, Morton DL. Neurofibrosarcoma. Cancer 1981;45:126-129
10. Errol Levine, Manop Huntrakoon and Louis H. Wetzel. Malignant nerve sheath neoplasms in neurofibromatosis : distinction from benign tumors by using imaging techniques. AJR 1987:149:1059-0-1064
11. William A. Knight, Willium K. Murphy and Jeffrey A. Gottleb. Neurofibromatosis associated with malignant neurofibromas. Arch Dermat 1973;107:747-750
12. Antony N.D, Agostino, Edward H. Soule and Ross H. Miller. Sarcomas of the peripheral nerves and somatic soft tissues associated with multiple neurofibromatosis (von Recklinghausen's disease). Cancer 1963;23:1015-1027
13. Beverly G. Coleman, Peter H. Arger, Murray K. Dalinka, Angela C. Obringer, Beverly R. Raney and Anna T. Meadows. CT of sarcomatous degeneration in neurofibromatosis. AJR 1983;140:383-387
14. Enzinger FM, Weiss SW. Soft tisue tumors. St, Louis: Mosby, 1983:580-656
15. Simon MA, Kirchner PT. Scintigraphic evaluation of primary bone tumor. J Bone Joint Surg(Am) 1980;62:758-764
16. Kumar AJ, Kuhajda FP, Martinez CR, Fishman EK, Jezic DV, Siegelman SS. Computeed tomography of extracranial neve sheath tumors with pathological correlation. J Comput Assist Tomogr 1983; 7:857-865
17. Woodruff JM, Horten BC, Erlandson RA. Pathology of peripheral nerves and paragangliomas. In, Silverberg SG, ed. Principles and practice of surgical pathology, vol. 2. New York: Wiley, 1983:1503-1520

IMAGING OF EXTRASPINAL TUBERCULOUS OSTEOMYELITIS

Jariya THIRASAK,[1] Anchalee CHUROJANA,[1] Pipat CHIEWVIT,[1] Apichart ASAVAMONGKOLKUL,[2] Suchart BENJARASSAMEROTE.[3]

Purpose: To describe the radiographic patterns of tuberculous osteomyelitis whereas extraspinal location was uncommon.

Materials and methods: Five of twenty-two patients with pathological diagnosis of skeletal tuberculosis who had extraspinal lesions were retrospectively reviewed. All imaging techniques including routine plain radiographs, CT scan or MR imaging were evaluated.

Results: Four patients had solitary lesion with different sites in phalanx, metacarpal bone, capitulum and ilium respectively. The other one had two lesions in bony pelvis. All had similar patterns of osteolysis with irregular borders and cortical violations. None had sclerosis or periosteal reaction. CT and MRI exhibited one sequestrum and one abscess extension into soft tissue.

Conclusion: On the basis of radiologic appearance, the extraspinal tuberculous osteomyelitis is difficult to be differentiated from tumor and tumor-like conditions. CT or MRI can provide more information of sequestrum and abscess that is helpful for diagnosis and evaluation of extent of the lesion.

Tuberculous infection of musculoskeletal system is the least common manifestation of TB infection with reported frequency about 1-2%.[1] The patient of all ages can be affected without predilection for either sex. Musculoskeletal tuberculosis (TB) may be divided into tuberculous infection of bone, joints, or soft tissue.[2] The osseous TB can be further subdivided into more common spinal tuberculosis and uncommon extraspinal tuberculous osteomyelitis.

There have been many reports of the imaging patterns of spinal tuberculosis with its classical or atypical features,[2-6] but only few that mentioned to those in appendicular skeleton and flat bone. So we reviewed the imaging appearances of these unusual site to assess whether they had any characteristics.

MATERIAL AND METHODS

In this retrospective study, the cases of tuberculous osteomyelitis were identified from revision of pathological reports in Siriraj Hospital over a two years period (January 1998 to December 1999). The positive diagnosis of tuberculous osteomyelitis was based on a presence of caseous granuloma with or without positive AFB from surgical biopsy or removal specimens.

[1,2,3] Department of Radiology, Orthopedics and Pathology, Faculty of Medicine, Siriraj Hospital, Mahidol University

Table 1. Skeletal TB in Siriraj hospital

Site	No. of lesions
Spinal TB	17 (77%)
Extraspinal TB	5 (23%)
Total	22 (100%)

A total of 22 patients (11 women, 11 men) were identified (Table 1). Seventeen patients (77%) with spinal tuberculosis were excluded from the study. So five patients with extraspinal involvement of bone were analyzed. Of these, positive AFB was established for the diagnosis in 2 cases. All patients had available imaging studies of involved bone as followings: plain radiographs in all cases, CT scan in 2 cases and MR imaging in 2 cases. The chest film was taken in all patients.

RESULTS

The 5 patients with extraspinal tuberculous osteomyelitis were encountered in 23% of skeletal TB cases, which were 1 man and 4 women (Table 2).

Table 2. Patients with extraspinal tuberculous osteomyelitis

Case	Sex	Age (years)	Site of lesions	No. of Lesions	Pulmonary TB
1	M	10	Prox. phalanx	1	-
2	F	46	Capitulum	1	-
3	F	20	Metacarpal	1	-
4	F	23	Iliac bone	1	-
5	F	51	pelvis	2	+

The patients' ages were range from 10-51 years with an average of 28 years. Four of the five patients had solitary lesion with different sites in the phalanx, metacarpal bone, capitulum and iliac bone, respectively. The other patient had two lesions in the bony pelvis. The chest film revealed pulmonary TB only in this case, which was occurred for 20%.

In the first case with the lesion at proximal phalanx of 5th finger, it was not difficult to diagnose because of the classic spina ventosa in appearance including expansion and thinning of cortex with surrounding soft tissue swelling.[2-7]

In the case of capitulum lesion, a 47-year-old patient had 9 months of a tender swelling at the right elbow. The well-defined border geographic bony destruction was seen radiographically at the medial epicondyle of right humerus without joint involvement (Fig. 1). Neither sclerosis nor periosteal reaction was evidenced. The diagnosis of bone tumor was the first impression. Subsequent CT scan showed sequestrum that was not seen on plain film. So the infective process was included in differential diagnosis and finally proved pathologically.

About metacarpal lesion, the third patient

presented with painful swelling at the dorsum of right hand for I week. The plain radiograph demonstrated poorly marginated non-sclerotic, expansile geographic destruction at base of right 2nd metacarpal bone with adjacent soft tissue swelling (Fig. 2). No sclerosis or periosteal reaction was seen. The adjacent MCP joint was not involved. Due to failure of medical treatment as inflammatory condition, CT scan was requested showing irregular border of osteolysis that was expansile causing very thinning and disruption of cortex. No periosteal reaction was revealed. After that, the open curettage was done and pathologically proved to be positive for AFB.

The forth case was a 23-year-old man with right groin pain on movement for 6 months and palpable groin mass for 2 months. The plain radiograph revealed a well-defined large geographic bony destruction at right iliac bone with irregular border and without sclerosis (Fig. 3). There was soft tissue mass at RLQ causing medial displacement of bowel gas. The malignant bone tumor was most likely provisional diagnosis, so the MRI was obtained later for surgical planning. The study showed huge multiloculated soft tissue mass originated from right iliac bone with enhancing of its thicken wall and solid portion. The mass extended superiorly into the pelvic cavity displacing pelvic organs and psoas muscle, and inferiorly into groin region. The diagnosis of malignant bone tumor was now changed because of the appearance of that mass which was most likely to be an abscess. So an infective process was become the first in the differential diagnosis. Finally, the incisional biopsy was performed and obtained a large amount of draining pus. The pieces of bone and soft tissue were sent for cytology and the tuberculous bacilli were discovered.

The last case was a 51-year-old female, who had 2 months of tenderness on movement of right hip. Plain film of pelvis exhibited geographic bony destruction at the right superior pubic ramus with ill-defined border, expanding and breaking cortex without sclerosis or periosteal reaction. Another suspected lesion was at the inferior right acetabulum appearing ill-defined osteolysis. The MRI was requested to define their extension and number of lesions, which showed 2 lesions with broken cortex and no associated soft tissue mass. Due to patient's history of pulmonary TB with positive sputum and chest film, so the diagnosis was most likely to be osseous TB.

In all cases, the plain radiographs showed that the lesions were geographic lytic destruction with irregular border and no sclerosis or periosteal reaction (Table 3). Three of the five lesions were expanding and breaking cortex resulting to pathological fracture. All solitary lesions had associated soft tissue swelling.

CT scan or MRI was performed in 4 patients. Sequestrum was demonstrated from CT scan of the capitulum lesion, and large abscess was identified from MR imaging of the iliac wing lesion.

Table 3. Imaging findings

Case	Type of destruction in plain film	Marginal sclerosis	Periosteal reaction	Cortical violation	Soft tissue swelling	CT/ MRI	Additional findings
1	geographic	-	-	-	+	-	-
2	geographic	-	-	-	+	CT	Sequestrum
3	geographic	-	-	+	+	CT	-
4	geographic	-	-	+	+	MRI	Abscess
5	geographic	-	-	+	-	MRI	-

1A

Fig. 1A. Plain film of right elbow shows geographic bony destruction at medial epicondyle of right humerus. (Black arrow heads)

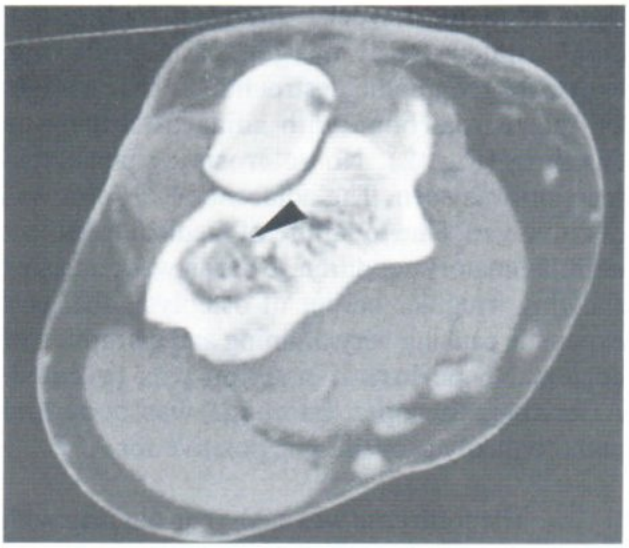

1B

Fig. 1B. Axial non-enhanced CT scan reveals sequestrum not seen on plain film. (Black arrow head)

2A

Fig. 2A. Plain film of right hand shows poorly marginated non-sclerotic, expansile geographic destruction at base of right 2nd metacarpal bone. (Black arrow head)

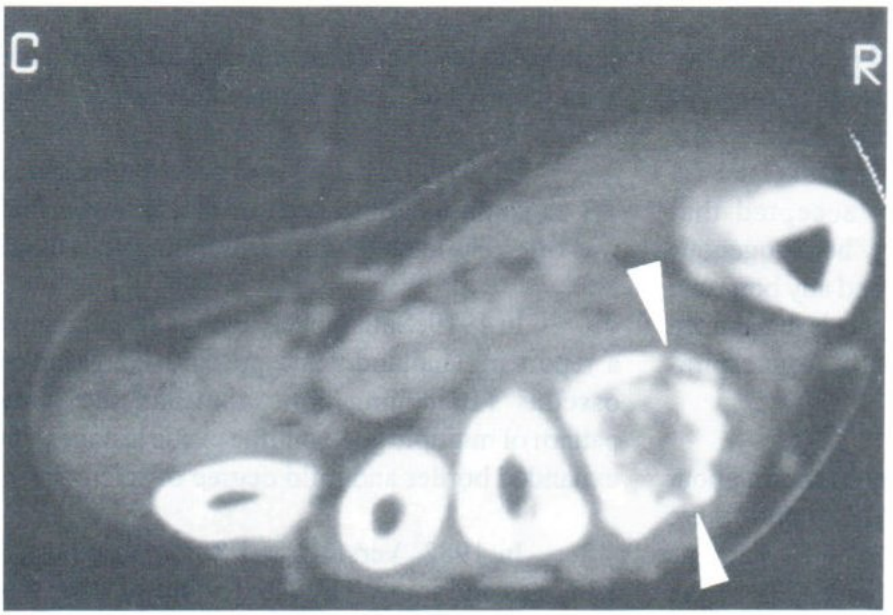

2B

Fig. 2B. Axial non-enhanced CT scan shows irregular border, expansile osteolytic lesion causing very thinning and disruption of the cortex. (White arrow heads)

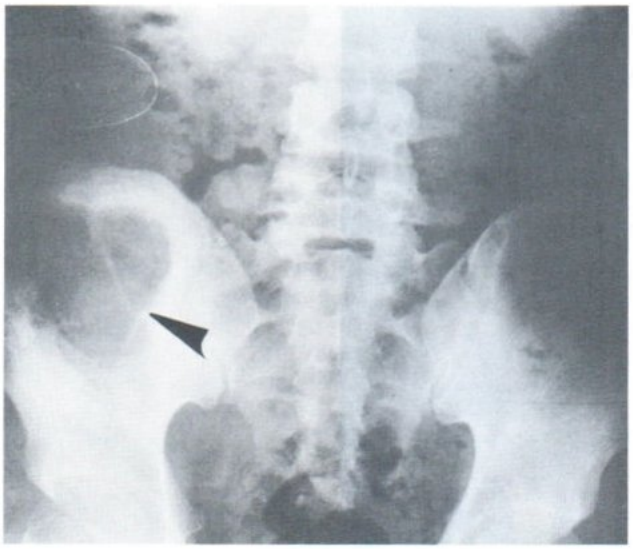

3A

Fig. 3A. Plain film of the pelvis shows well -defined large geographic bony destruction at right lilac bonr with irregular border and no sclerosis. There is soft tissue mass at RLQ causing medial displacement of bowel gas. (Black arrow head)

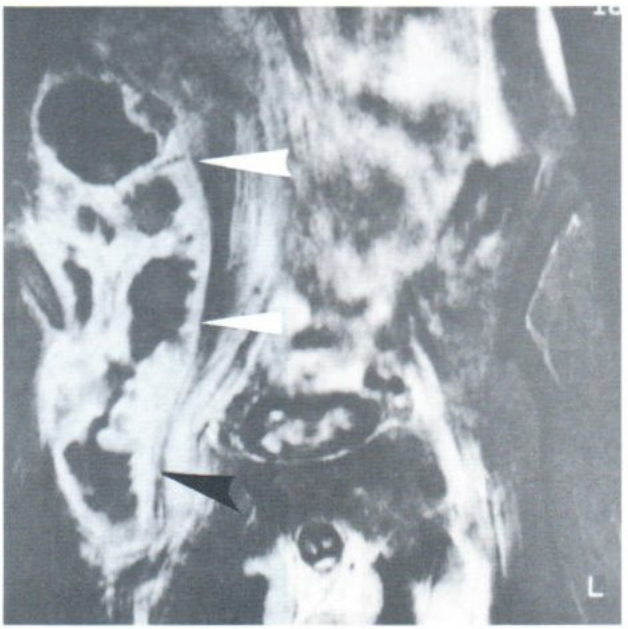

3B

Fig. 3B. T1-weight MRI post gadolinium shows huge multilobulated mass originates from right iliac bone with enhancement of thicken wall and solid component. The mass is also extending superiorly into pelvic cavity and inferiorly into groin region. (Two white arrow heads, One black arrow head)

DISCUSSION

TB was often overlooked as a possibility in the differential diagnosis of skeletal lesions. An average delay of 16 to 19 months between the initial symptoms and the diagnosis of skeletal TB was reported.[3] It is generally accepted that skeletal involvement is caused by hematogenous dissemination of tubercle bacilli and any bone can be affected. The definitive diagnosis is made from a positive culture of tubercle bacilli from aspiration fluid or bone biopsy.

In TB patients, there were reports about 1-2% to be skeletal TB and 50-70% of these were spinal lesions.[1] In our study 11 of 22 patients (77%) are spinal TB and 5/22 patients (23%) have extraspinal lesions. These unusual locations have been reported as a part of rare skeletal TB.

In 1970, Davidson et al described osseous TB as small-localized area of osteoporosis that was often associated with surrounding sclerosis.[8]

In 1979, Sathaphatayavongs B. published a report in Thailand.[7] She presented 2 cases of osseous TB in long bone, that had the same pattern of multiple good outline cystic lesions with expanded border and mild degree of sclerosis.[7]

In 1982, Versfeld and Solomon reported 17 bones and joints TB. The feature of bony TB

included poorly defined round edge cyst-like lesion with minimal surrounding sclerosis.[9]

In 1990, Abdelwahab et al reported 3 osseous TB that showed tumor-like lesion with sclerotic changes, periosteal reaction and sequestrum.[10]

In 1995, Yao and Sartoris claimed that tuberculous osteomyelitis of the extremities typically affected the metaphyses with radiographic findings of osteopenia, osteolytic foci with poorly defined edges, and minimal surrounding sclerosis.[3]

The largest series had been of Hugosson et al in 1996 reported 10 patients with osseous TB.[1] All were irregular border lytic lesions with surrounding bone. Trabecular bone still present and no or little reactive bone formation. Minor periosteal reaction was present.

Recent publications were reviewed by Ridley et al in 1998. The lesion of appendicular skeleton was lytic with little or no sclerosis and no periosteal reaction.[2]

All reports since 1970 until recently had shown similar pattern of osteolytic destruction with minimal or no sclerosis. The border may be poorly defined or good outline. Sequestrum may be associated. The periosteal reaction is minimum or absent and pathological fracture is rare.

This is in agreement with our study, in which the appearances of extraspinal tuberculous osteomyelitis are osteolytic destruction causing bony expansion with or without cortical violation. Minimal or no sclerosis can be encountered but no periosteal reaction. These radiographic appearances are non-specific and cannot be distinguished from other conditions. So, when this lesion is evident on plain film, the differential diagnoses of tumor and tumor-like diseases, osteolytic metastasis, multiple myeloma, hyperparathyroidism and fungal infection should be included.

The supplemental diagnostic hallmarks are including the present of abscess, sequestrum or pulmonary TB. The first two findings are generally accepted that represent the infective processes which are clearly demonstrated from CT scan and MRI. The presence of pulmonary TB. has been reported to occur in approximately 12-50% of skeletal TB patients.[1] In this study we found that the frequency of pulmonary TB was 20%. However, a normal chest film does not exclude skeletal TB and a history of tuberculous infection or exposure may or may not be present.

CONCLUSION

The conventional radiography remains the best initial diagnostic test and the most useful and least expensive modality for imaging of skeletal lesion. However, on the basis of radiographic appearance alone, the extraspinal tuberculous osteomyelitis has its own characteristics but not specific and difficult to be differentiated from other conditions. We highlight that CT and MRI can provide more information of sequestrum and abscess that is helpful for diagnosis and evaluation of the extent of this unusual lesion and also facilitating guided biopsy.

REFERENCES

1. Hugosson C, Nyman RS, Brismars J, Larsson SG, Lindahl S, Lundstedt C. Imaging of tuberculosis V peripheral osteoarticular and soft tissue tuberculosis. Acta Radiologica 1996; 37:512-6.
2. Ridley N, Shkikh MI, Remedios D, Mitchell R. Radiology of skeletal tuberculosis. Orthopedics 1998;21:1213-20.

3. Yao DC, Sartoris DJ. Musculoskeletal tuberculosis. Radiol Clin North Am 1995; 33:679-89.
4. Ahmadi J, Bajaj A, Destian S, Segall HD, Zee CS. Spinal tuberculosis: atypical observation at MR imaging. Radiology 1993;189:489-93.
5. Watts HG, Lifeso RM. Tuberculosis of bones and joints. J Bone Joint Surg (Am) 1996;78:288-98.
6. Resnick D, Diagnosis of bone and joint disorders. 3rd ed. Philadelphia: WB Saunders, 1995.
7. Sathaphatayavong B. Peripheral bone and joint tuberculosis. Thai J Radiol 1979; 16: 38-47.
8. Davidson PT, Horowitz I. Skeletal tuberculosis. Am J Med 1970; 48:77-84.
9. Versfeld GA, Solomon A. A diagnostic approach to tuberculosis of bones and joints. J Bone Joint Surg 1982; 64:446-9.
10. Abdelwahab I, Norman A, Herman G, Santini L, Klein MJ. Atypical radiographic appearance of tuberculous granulomas of bone. J Can Assoc Radiol 1990; 41:72-5.

THE COUCH TURNTABLE TECHNIQUE IN LATERAL HEAD AND NECK IRRADIATION : A HOMOGENEITY OF DOSE DISTRIBUTION AND DOSE DELIVERED TO ADJACENT NORMAL TISSUES

Lalida TUNTIPUMIAMORN, MSc. (Radiation Scince)
Vinai POLWATSATIAN, BSc.(Radiological Technology)
Udomsak KARNJANATHITIWORN BSc.. (Radiological Technology)

ABSTRACT

The objective of this study was to investigate for the uniformity of dose distribution and also the dose delivered to adjacent normal tissues compared between the Straight Field and the Couch Turntable technique in Cobalt-60 lateral head and neck irradiation. Doses were measured in an anthropomorphic wax phantom with TLD-100 dosimeters. Measurements were performed three times in each technique and the analysis was done by normalizing doses at each measuring point as a percentage of dose at the reference point. From the study, the doses distribution homogeneities are satisfied in both techniques. The average doses were 95.38+7.41 in the technique of Straight Field and 95.07+8.15 in the technique of Couch Turntable. In the matter of doses to adjacent normal organs, it is likely that the use of Couch Turntable provided higher doses than the technique of Straight Field. Measured doses at brain tissue (under shielding blocks) in the technique of Couch Turntable was 45.74+11.83, at buccal mucosa was 65.18+5.24 and at lens was 5.05+14.8 respectively. Compared to the technique of straight field, the average measured dose were 30.39+5.39 at brain, 56.10+6.56 at buccal mucosa, and 4.88+16.7 at lens. It is clearly shown that uses of the Couch Turntable to solve for the beam divergence do not affect on the dose distribution homogeneity when compared to the technique of Straight Field. But higher doses at adjacent normal tissues, especially at brain should be aware of.

INTRODUCTION

In the treatment of most head and neck tumors, irradiation of the regional lymph nodes is always necessary in order to complete irradiation of the diseases to prevent local recurrent. This is mostly accomplished by two lateral opposing fields including the primary tumor site and cervical lymph nodes. The third anterior split field that covers the lower neck and bilateral supraclavicular lymph nodes may also be used.[1-3] Whenever, head and neck lateral fields are used together with the third anterior split field, the potential of overlapping doses at the junction of the fields are increased. Several methods have been used to eliminate the problem including the technique of couch turntable with the purpose of reduction of the overlapping doses from the diverging lateral fields. In this technique, the foot of the couch is rotated so that the caudal end of the two lateral fields parallel and cross the patient's neck as a straight line. Study of Tuntipumiamorn L. and Polwatsatian V.[4] had presented that the technique of Couch Turntable in the head and neck irradia-

Division of Radiation Oncology, Department of Radiology, Faculty of Medicine, Siriraj Hospital, Mahidol University, BANGKOK-10700, THAILAND

tion was able to improve the dose uniformity at the junction plane between the two lateral opposing fields and the third anterior split field from 112.56% to 103.69%. However, because of an uncommon beam geometry, this technique may affect on the dose distribution homogeneity and the dose delivered to surrounding organs.

In this study we intended to investigate for the effect of couch turntable in the lateral head and neck irradiation on the dose distribution and also to access for the dose delivered to the brain, lens and buccal mucosa from this technique in comparison with those delivered by the Straight Field technique with our Cobalt-60 teletherapy machine.

MATERIALS AND METHODS

Studying the homogeneity of dose distribution and the doses to specific organs in this study required a phantom that provided for both the suitable measuring positions and also an adequate number of positions. An anthropomorphic head and neck phantom was newly made from paraffin wax and the accuracy in dose measurement between the two phantoms (old and new) were verified prior taking to be used in this study. After that, our routine lateral treatment fields were defined on the phantom with the simulator. (Fig 1) Fifty-eight holes, 2.5 mm in diameter were drilled around different positions in different levels of the phantom for giving the spaces for the TLD-100 dosimeters (1x1x6 mm, rod shaped, Harshaw Company) to be put in. Thirty-nine points in 3 slices of the phantom representing for the upper, central and lower slices of the lateral treatment fields were filled with the TLD-100 dosimeters to investigate for the dose uniformity (Fig 2). Fourteen measuring points at three different levels of the lateral superior beam edge was also chosen to access for the effect of the tilting beam geometry from the couch turntable to the dose that may deliver to the brain from the lateral fields (Fig 3). For buccal mucosa and lens, there were five and two measuring points respectively.

After having placed the TLD-100 into different positions in the phantom, it was irradiated at 80 cm SSD with Cobalt-60 teletherapy machine. Measurements of doses were performed by the Straight Field technique and Couch Turntable technique.

In the Straight Field technique, the angle of a collimator and a treatment couch was at zero, while in the technique of Couch Turntable, the collimator angle was in the same position but the couch was turned to an angle of 5^0 in the direction to make the lower border of the divergence beam of radiation to be in the same straight line as the lower lateral neck field across the phantom's neck.[5]

Measurements were performed in each technique three times. To analyze the data, doses at each point will be normalized as a percentage to the dose at the reference point. The reference point here was set at the midline of head and neck phantom at the level of field center and dose delivered to this point was 100 cGy from each port.

Fig. 1. Anthropomorphic head and neck paraffin wax phantom

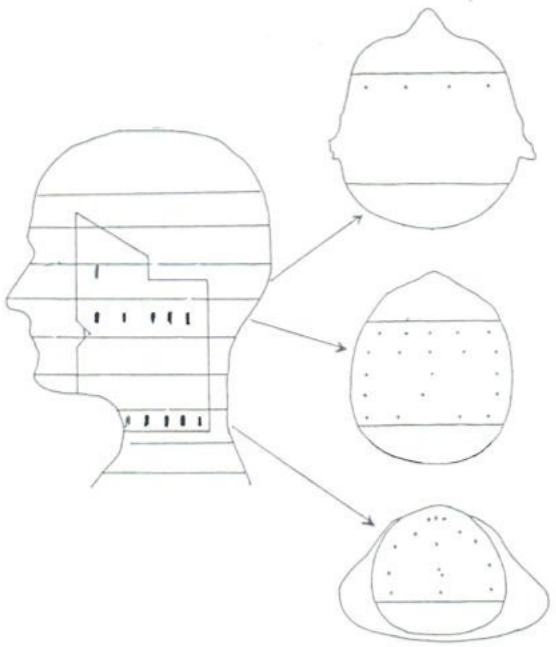

Fig. 2. Diagram shows the TLD positions in the three different levels of lateral head and neck treatment field to investigate for the dose homogeneity. The total number of measuring points was thirty-nine.

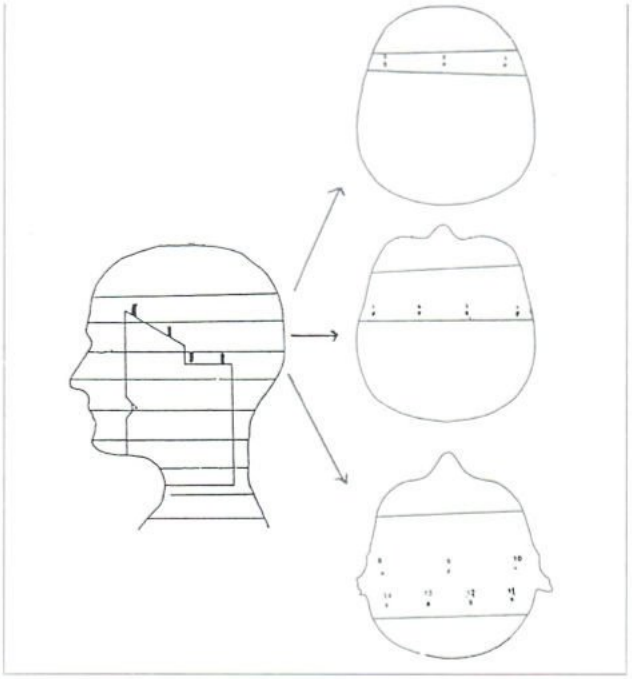

Fig. 3. Diagram shows fourteen measuring positions in three different levels of the lateral superior beam edge to access for the dose delivered to brain tissue (under shielding blocks)

RESULTS

The anthropomorphic wax phantom used in this study do not represent for the tissue inhomogeneity as in the Alderson rando phantom. Therefore, verification in the accuracy of dose measured in our paraffin wax phantom was necessary. We found that the accuracy of doses measured in our wax phantom was acceptable. The doses measurements in both phantoms were shown to be different within $\pm$ 5%.

The results for the investigation of dose distribution homogeneity, no difference of the results in both techniques of Straight Field and Couch Turntable was detectable. Measured doses at point by point in both techniques were much closely the same.

The average measured doses in the Straight Field technique was 95.83 ± 7.41 and 95.07 ± 8.15 in the technique of Couch Turntable. Data of measured doses in three different slices were presented in Table I.

Table I. The measured doses in three different levels of the lateral head and neck treatment field compared between the technique of Straight Field and Couch Turntable.

Site	Number of Measuring Points	% Averaged Dose	
		Straight Field	Couch Turntable
Upper slice	4	84.99±1.88	84.46±2.45
Central slice	20	95.36±5.19	96.21±4.75
Lower slice	15	92.39±8.67	95.78±6.50
Mean± SD	39	**95.38±7.41**	**95.07±8.15**

Table II-IV presented data for dose measured at the adjacent organs. We found that the doses delivered to brain and buccal mucosa was higher in the technique of Couch Turntable than in the technique of Straight Field. While the doses scattered to lens from both techniques were quite equal.

It was noted that, the data of the measured doses at different points recorded in Table II were higher in the Couch turntable technique than the Straight Field technique, especially at the 6 measuring points (# 2, 5, 6, 9, 12,13) are remarkably high. All these 6 points previously mentioned were located near the sagittal midplane of the phantom.

Table II. Doses measured at brain compared between the technique of Straight Field and Couch Turntable

Measuring Points	% Averaged Dose	
	Straight Field	Couch Turntable
1	22.25±4075	32.03±8.64
2*	37.31±26.36	66.89±5.49
3	29.65±11.80	39.09±17.45
4	36.08±59.62	36.53±30.01
5*	39.40±30.47	64.81±8.75
6*	32.83±22.27	65.18±3.75
7	27.26±13.11	35.43±8.91
8	34.56±8.07	37.54±19.51
9*	35.07±42.45	54.49+31.45
10	25.59+42.65	39.05±29.26
11	24.71±31.86	35.86±8.42
12*	27.85±46.05	47.10±12.32
13*	25.67±61.21	47.92±21.26
14	27.28±74.81	38.37±27.04
Mean±SD	**30.39±17.7**	**45.74±26.8**

*** Measuring points that presented remarkbly higher dose.**

Table III. Doses measured at lens compared between the technique of Straight Field and Couch Turntable

Site	% Averaged Dose	
	Straight Field	Couch Turntable
Left lens	4.30±7.54	4.52±2.10
Right lens	5.45±5.27	5.58±0.99
Mean±SD	**4.88±16.7**	**5.05±14.80**

Table IV. Doses measured at buccal mucosa compared between the technique of Straight field and Couch turntable

Measuring Point	% Averaged Dose	
	Straight Field	Couch Turntable
1	61.02+10.52	60.92+10.13
2	65.00+10.52	71.42+10.52
3	53.61+16.86	65.92+13.22
4	54.99+18.31	68.68+15.55
5	45.88+22.85	58.95+19.16
Mean±SD	**56.10±6.56**	**65.18±5.24**

DISCUSSION

The use of couch turntable in the lateral head and neck irradiation was proved to be an effective method to solve for a problem of lateral beam divergence. It is interesting that this technique is simple, easy to be used, no need of extra accessory and applicable to all kinds of teletherapy machines,

Anyhow, the tilting beam geometry raised a question of whether the dosage distribution in the treatment volume is still be uniform or not. And also the doses to the normal surrounding structures obtained by this technique are still acceptable or not.

For the results obtained in this paper, we found that by turning the treatment couch 5^0 to make the inferior border of the lateral treatment field to match with the superior border of the anterior supraclavicular field do not affect on the dose homogeneity of the area to be treated.

The overlapping field between the right and the left superior beam edge at the midline of the head may be the hot spot of the Couch Turntable technique. Thereby, the 6 measuring

points located near the midplane of the phantom had shown significantly higher doses in the technique of Couch Turntable than in the technique of Straight Field. The highest dose point in this region from the measurements, was about 2/3 of the dose at the reference point.

CONCLUSION

In the institute that Cobalt-60 machine are being used for lateral head and neck irradiation, the Couch Turntable technique may be considered to be used as an alternative to other techniques in solving the problem of beam divergence. It provided a dose homogeneity both at the junction plane between the upper and lower cervical fields and also the treatment volume to be irradiated. But the surrounding normal tissues, especially the brain, should be well aware of if this technique are being applied.

REFERENCE

1. Bentel GC. Treatment planning – head and neck region. In: Radiation therapy planning. Second edition. New York: McGraw-Hill, USA, 1996: 268-330
2. Griffiths SE, Short CA, Jackson C, Ash D. Head and neck techniques. In: Radiotherapy principles to practice a manual for quality in treatment delivery. London: Churchchill Livingstone, UK, 1994:189-197
3. Marks JE. Cancers of the head and neck. In: Khan FM, Potish R. Treatment planing in Radiation oncology. Williams& Wilkins : Baltimore, USA: 425-448
4. Tuntipumiamorn L, Polwatsatian V. Junction plane dosimetry in different techniques of Cobalt-60 head and neck irradiation. The Asian Journal of Radiology, 2001:
5. Bentel GC. Treatment planning – head and neck region. In: Radiation therapy planning. Second edition. New York: McGraw-Hill, USA, 1996: 139

DETECTION OF ACUTE CEREBRAL ISCHEMIA WITH Tc-99m APCITIDE SCINTIGRAPHY

Supatporn TEPMONGKOL, M.D.

ABSTRACT

The established indication of Tc-99m apcitide scintigraphy is to detect deep venous thrombosis. However, due to its mechanism of binding to GP IIb/IIIa receptor on activated platelet, imaging of acute cerebral thrombosis is possible. This is a case report of acute ischemic stroke patient with right leg swelling who was referred to have Tc-99m apcitide scintigraphy for diagnosis of deep venous thrombosis. The scan showed no abnormal uptake in both legs but, interestingly, uptake in the left parieto-occipital region. This corresponds to clinical and the computer tomographic finding of acute ischemic stroke in the same area. With the use of Tc-99m apcitide scintigraphy, the area of acute cerebral ischemia and its causes can be synchronously identified. Various causes of progressing stroke may also be differentiated at the same time as well.

Key Words : stroke, platelet membrane glycoprotein (complex IIB-IIIA), radionuclide imaging

INTRODUCTION

P280 is a synthetic peptide containing an arg-gly-asp (RGD) sequence, which enables the binding to the GP IIb/IIIa receptor expressed on the activated platelets.[1,2] It has been successfully used for the detection of acute deep venous thrombosis[3,4,5,6,7] for many years by mean of Tc-99m apcitide scintigraphy. There has not been any case report of application in acute cerebral ischemia.

CASE REPORT

A 64-year-old female patient with underlying diabetes mellitus and old cerebral infarction presented to the hospital with drowsiness and dysarthria for 2 days. Her general physical examination was unremarkable. The neurologic examination revealed sensory aphasia and jargon speech. Others were unremarkable. CT scan (Fig. 1) revealed very low density area involving gray and white matter at right temporo-occipital lobe adjacent to the occipital horn of the right lateral ventricle with adjacent volume loss consistent with old infarction. There was also a wedge shaped low-density lesion occupying the left parieto-occipital area. This was interpreted as a recent infarction. Then low molecular weight heparin 0.4 mL. was given subcutaneously every 12 hours. Two days afterward, the patient developed upper gastrointestinal hemorrhage. Gastroscopy revealed erosive gastritis. Low molecular weight heparin was withdrawn. One day later, the patient developed right leg edema. The patient was sent to nuclear medicine division to perform scintigraphy for diagnosis of deep venous thrombosis.

Nuclear Medicine Division, Department of Radiology, Faculty of Medicine, Chulalongkorn University, Bangkok, Thailand
Tel. 02-2564283-4, Fax. 02-2564162, Email : supatporn@hotmail.com

For correspondence : contact Supatporn Tepmongkol, M.D

MATERIAL AND METHOD

After informed consent was obtained from the patient, the whole body scintigraphy was done at 1 hour and 3 hours after 740 MBq (20 mCi) Tc-99m apcitide (Acutect – Diatide, Inc.) intravenous injection. The gamma camera used was a single-headed GE-CAMSTAR equipped with a low-energy, high resolution parallel hole collimator. Data were collected using 20% energy window centered at 140 keV in a 128x128 matrix. Static left lateral view was acquired using preset count of 300,000 counts. Then right lateral view using the same time required for left lateral view was acquired.

RESULT

The result of Tc-99m apcitide scintigraphy was negative for acute thrombosis at both lower extremities but, strikingly, an area of abnormal uptake was seen at the left parieto -occipital region on 1 and 3 hours images (Fig. 2) which was the same area as the recent infarction revealed on CT scan.

Fig. 1. Brain CT of the patient 2 days after stroke onset showing a wedge-shaped low density lesion occupying the left parieto -occipital area which was acute ischemic infarction and a very low density area involving gray and white matter at right temporo-occipital lobe with adjacent volume loss, consistent with an old infarction.

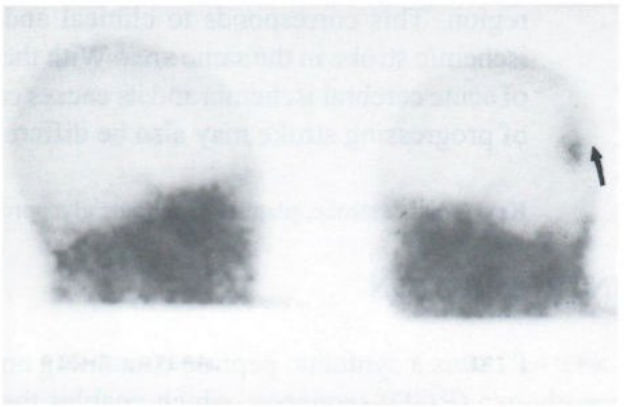

Fig. 2. Static right and left lateral views of the skull revealed a focus of abnormal uptake at the left parieto-occipital region (arrow).

DISCUSSION

Tc-99m apcitide is indicated for scintigraphic imaging of acute deep venous thrombosis due to its preferential binding to glycoprotein (GP) IIb/IIIa receptors found on activated platelets.[1,2,8] Though, this is a functional rather than morphologic imaging which theoretically could detect acute thrombosis anywhere in the body. For stroke, there were some studies using this agent to identify intra-arterial thrombi associated with carotid atherosclerosis.[9] There has not been any study reporting the clinical relevance of this agent for intracerebral stroke. The question arose whether this agent passes blood-brain-barrier or not. Imaging of the whole body did not show any uptake in the normal brain. There were some reports of brain tumor Tc-99m apcitide uptake.[10,11] Binding was proven to be due to receptor -mediated mechanism not the non-specific trappping or blood-brain-barrier leakage.

In this patient the diagnosis was Wernicke's aphasia. The CT scan showed a new infarcted area at the left parieto-occipital region and an old infarction at right temporo-occipital lobe. The Tc-99m apcitide scintigraphy which was performed 5 days after stroke onset showed uptake only at the area of recent infarction, not the old infarcted area. This can be explained by the fact that platelet aggregation increases significantly within 10 days after ischemic stroke or TIA but then returns to normal.[12] So that if the uptake is really due to binding to the receptor on activated platelets, like in brain tumors, identification of early (within 24 hours) acute ischemic stroke is possible. This may be the advantage over CT scan in this period. We may also pick up the patients with TIAs and differentiate it from other causes of acute focal neurologic deficits such as seizures or migraine. Thus it needs to be proven whether Tc-99m apcitide scan were positive or not in early stroke and TIA. Furthermore, we might be able to early differentiate progressive thrombosis[13] from progressive cerebral edema,[14] or hemorrhagic infarction,[15] all of which are causes of progressing stroke in cerebral ischemia. Simultaneously, carotid atherosclerosis[9] or mural thrombus[16] in myocardial infarction which are causes of ischemic stroke may be identified by imaging activated platelet as well.

Thus, scintigraphic imaging with ^{99m}Tc-apcitide should be a promising mean to evaluate patient with cerebrovascular disease in terms of diagnosis, not only for identifying the area of involvement but may also for exploring the causes. However, mechanism of uptake and time interval of optimal uptake in acute ischemic stroke needs to be clarified.

TIA = Transient Ischemic Attack

ACKNOWLEDGEMENT

Tc-99m Apcitide was supported in part by Syncor International (Thailand), Inc.

This is one of the patients in a research, granted by Rachadapiseksompoch Grant, Faculty of Medicine, Chulalongkorn University.

REFERENCES

1. AcutectTM Prescribing Information
2. Becker RC (1996). Antiplatelet therapy. Science&Medicine July/August: 12-21
3. Muto P, Lastoria S, Varella P, Vergara E, Salvatore M, Morgano G, Lister-James J, Bernardy JD, Dean RT, Wencker D, Borer JS (1995) Detecting deep venous thrombosis with Technetium-99m labeled synthetic peptide P280. J Nucl Med 36(8): 1384-1391

4. Lister-James J, Knight LC, Maurer AH, Bush Lr, Moyer BR, Dean RT (1996) Thrombus imaging with a technetium-99m-labeled, activated platelet receptor-binding peptide. J Nucl Med 37(5): 775-781
5. Dodd LR, Krishnamurthy GT, Kreis JM, Walsh TK , Shah JH (1996) Detection of acute deep venous thrombosis (DVT) by scintigraphy with Tc-99m P280, a synthetic peptide that binds to glycoprotein IIb/IIIa receptors on activated platelets. J Nucl Med 37(5S):95P-96P. Abstract
6. Weiland FL, Obranovich GT, Vande Streek PR, Carretta RF (1996) Technetium-99m P280 labeled peptide in the detection and localization of deep vein thrombosis: a prospective study in 32 cases. J Nucl Med 37(5S):294P. Abstract
7. Taillefer R, Therasse E, Turpin S, Lambert R, Robillard P, Soulez G (1999) Comparison of early and delayed scintigraphy with 99mTc-Apcitide and correlation with contrast-enhanced venography in detection of acute deep vein thrombosis. J Nucl Med 40:2029-2035
8. Pearson DA, Lister-James, McBride WJ, Wilson DM, Martel LJ, Civitello ER, Dean RT (1996) Thrombus imaging using technetium-99m-labeled high potency GPIIb/IIIa receptor antagonists. Chemistry and initial biologic studies. J Med Chem 39(7):1372-1382
9. Vallabhajosula S, Weinberger J, Machac J, Lister-James J, Dean RT, Lipszye H, Patel SL, Harrington E, Harrington M (1996) Technetium-99m P280, activated platelet specific techtideTM. Phase II clinical studies in patients with carotid atherosclerosis. J Nucl Med 37:272P. Abstract
10. Muto P. Lastoria S, Varella P, Acampa W, Vergara E, Mainolfi C, Spaziante R, Ferone D, Bernardy JD, Salvatore M (1994) Brain tumors imaging with Tc-99m labeled synthetic peptide P280. Eur J Nucl Med 21:S198. Abstract
11. Lastoria S, Muto P, Varella P, Vergara E, Mainolfi C, Spaziante R, Bernardy JD, Goldsmith SJ, Salvatore M (1994) Localization of human brain tumors by Tc-99m labelled P-280 synthetic peptide. J Nucl Med 35:97P. Abstract
12. Dougherty JH, Jr, Levy DE, Weksler BB (1977) Platelet activation in acute cerebral ischemia. Lancet 1:821-824
13. Millikan CH, McDowell FH (1981) Treatment of progressing stroke. Stroke 12:397-409
14. Katzman R, Clasen R, Klatzo I, Meyer JS, Pappius HM, Waltz AG (1977) Report of joint committee for stroke resources IV. Brain edema in stroke. Stroke 8:512-540
15. Hachinski V, Norris JW (1985) The deteriorating stroke. In: Hachinski V, Norris JW (eds) The acute stroke. F.A. Davis F.A. Davis, Philadelphia, pp 123-140
16. Tsuda T, Kubota M, Iwakubo A, Akiba H, Shido M, Takahashi T, Nakata T, Noto T, Tanaka S, Iimura O (1989) Availability of 111In-labeled platelet scintigraphy in patients with postinfarction left ventricular aneurysm. Ann Nucl Med 3(1): 15-24.

ROLES OF NUCLEAR MEDICINE IMAGINGS IN DIAGNOSIS MULTIPLE ENDOCRINE NEOPLASIA TYPE 2a : A CASE REPORT

Kanaungnit KINGPETCH [1] ,M.D. , Makumkrong POSHYACHINDA [1] ,M.D. , Sasitorn SIRISALIPOCH [1], M.D.

ABSTRACT

Multiple endocrine neoplasia type 2a (MEN 2a) is rare, with complex disorders. MEN 2a is characterized by medullary thyroid carcinoma in combination with pheochromocytoma and hyperparathyroidism. We report a case of 48-year-old woman who had a severe hypertension. Physical examination revealed a painless enlarged thyroid gland and palpable abdominal mass. Hyperparathyroidism was diagnosed by elevated serum calcium level and parathyroid hormone level. ^{99m}Tc-pertechnetate thyroid scinitigraphy showed 2 hypofunctioning nodules at both thyroid lobes but both nodules were hot on ^{131}I MIBG imaging. ^{131}I MIBG imaging also revealed intense uptake at both enlarged adrenal glands. Medullary thyroid carcinoma and pheochromocytomas were subsequently proved by pathologic sections. Double phase ^{99m} Tc sestamibi parathyroid scintigraphy showed intense uptake at the right side of lower neck, suggesting parathyroid adenoma or hyperplasia. In conclusion,nuclear medicine imaging is very useful in the diagnosis of MEN 2a.

Key Words : multiple endocrine neoplasia , MEN 2a , nuclear medicine imaging, ^{131}I -MIBG

INTRODUCTION

The multiple endocrine neo-plasia (MEN) is a rare disease. It is divided into two categories: MEN type 1 and MEN type 2. The MEN type 2 is further divided into MEN 2a and MEN 2b. The association of medullary thyroid carcinoma with unilateral or bilateral pheochromocytomas and less common with parathyroid hyperplasia or adenomatosis is termed MEN 2a.[1,2]

We report a woman with MEN 2a. The presented case illustrates the important role of nuclear medicine in the diagnosis of endocrine neoplasms associated with MEN 2a.

CASE REPORT

A 42-year-old-woman was refered to Chulalongkorn Memorial hospital because of a severe hypertension. She had loss of weight (approximately 11 kg. in 2 months), palpitation, sweating, headache, tremor of hands and exhaustion for 7 months. One month prior to admission, her headache and palpitation became more severe with high blood pressure. On admission, her BP was 230/150 mm Hg, heart rate was 108/min and she looked chronically ill. On physical examination, thyroid gland was enlarged with nodular surface, firm consistency. A mass at left side of abdomen was found by bi-manual palpation.

[1] Division of Nuclear Medicine . Department of Radiology. Faculty of Medicine. Chulalongkorn University

Laboratory findings showed increased levels of serum calcium (12.1 mg/dl), CEA (202 ng/ml), PTH (79.47 pg/dl), calcitonin (2511.77 pg/ml) and urine VMA (22.54 microgram/24 hrs). Thyroid function test was within normal limit. Ultrasonography of thyroid gland showed multinodular goiter with a few propable degenerated nodules. ^{99m}Tc-pertechnetate thyroid scintigraphy revealed enlargement of thyroid gland with two hypofunctioning thyroid nodules (figure 1). Double-phase ^{99m}Tc-sestamibi parathyroid scintigraphy suggested an adenoma or hyperplastic parathyroid gland (figure 2).^{99m} Tc-MDP bone scintigraphy revealed no metabolic bony disease but demonstrated abnormal radiotracer uptake at thyroid gland (figure 3). MRI of whole abdomen showed well-marginated mixed solid and partly cystic bilateral adrenal masses with heterogenous enhancement. Whole body imaging with ^{131}I-metaiodoben-zylgaunidine (MIBG) showed two focal areas of high activity at thyroid gland and enlargement of both adrenal glands (figure 4).

Bilateral adrenalectomy was done, the tumor in the left and right adrenal glands weighed 265 gm. and 70 gm. respectively. The histopathologic finding was bilateral pheochromocytomas. Total thyroidectomy and subtotal parathyroidectomy with implantation of the parathyroid glands into the left forearm were subsequently performed. Pathological section revealed medullary carcinoma of thyroid gland with foci of calcification. Surgical finding of parathyroidectomy shows enlargement of the right upper parathyroid gland but the right lower parathyroid gland cannot be identified. The other parathyroid glands on the left side are normal.

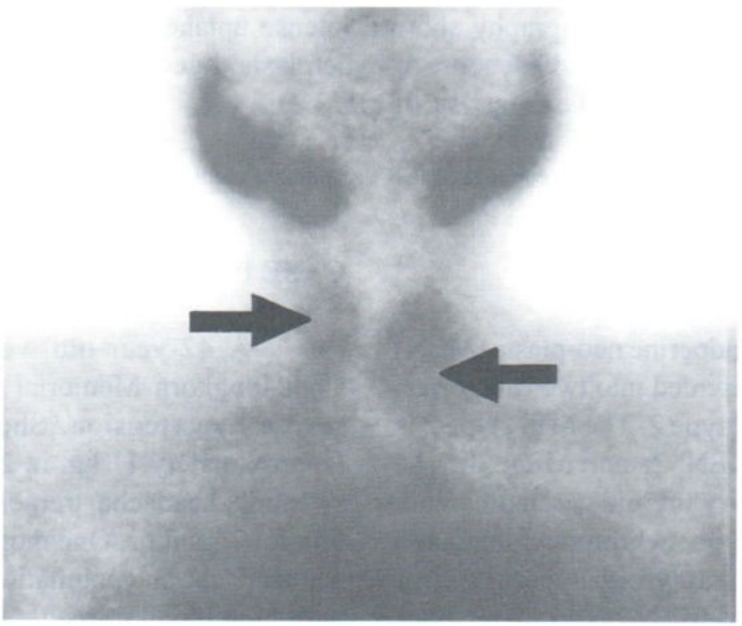

Fig. 1. ^{99m}Tc-pertechnetate thyroid scintigraphy shows 2 hypofunctioning thyroid nodules (arrows) at both thyroid lobes.

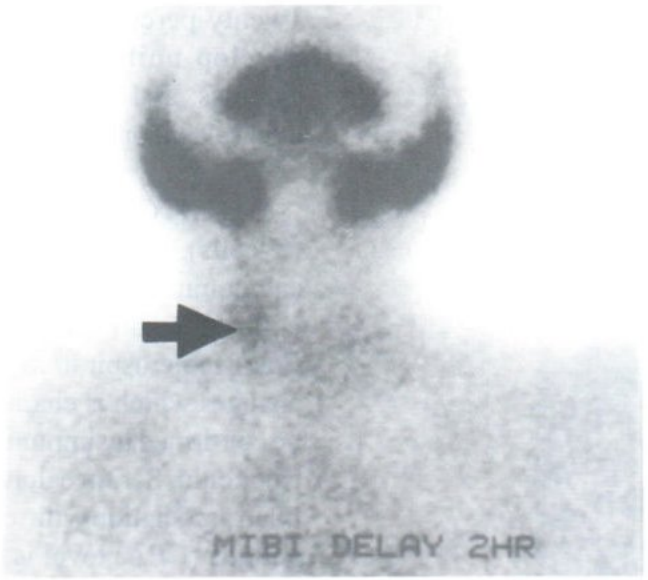

Fig. 2. Double-phase ^{99m}Tc-MIBI parathyroid scintigraphy ; The delayed 2 –hour after injection image shows intense uptake of radiotracer at the right side of lower neck (arrow).

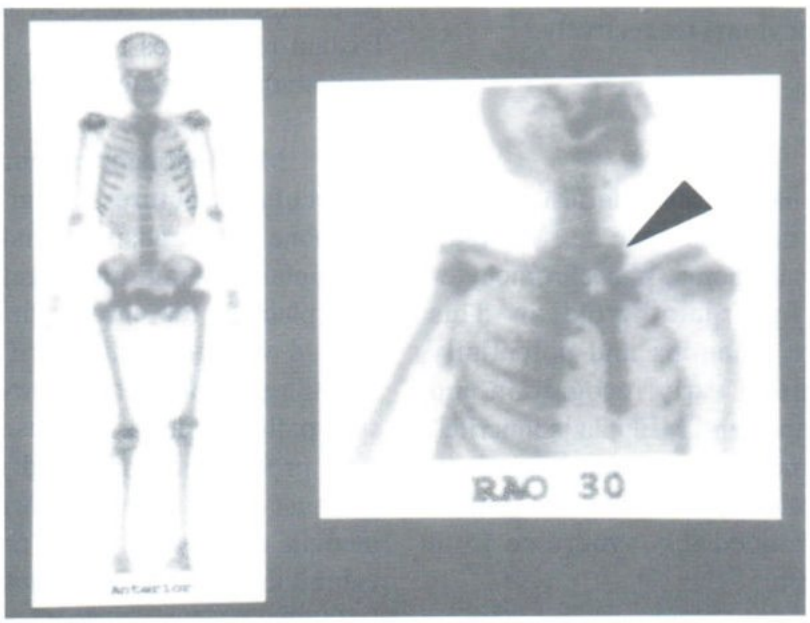

Fig. 3. ^{99m}Tc-MDP bone scintigraphy reveals normal radiotracer uptake throughout whole body skeleton but abnormal radiotracer uptake is noted at thyroid gland (arrow).

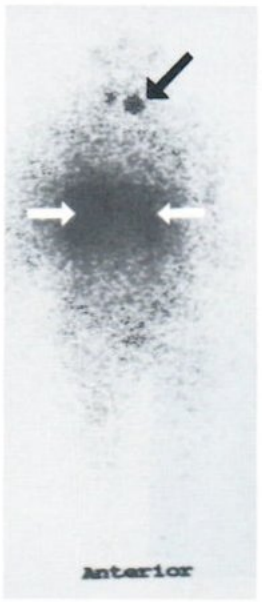

Fig. 4. Whole body ^{131}I-MIBG scintigraphy shows two focal areas of intense uptake at thyroid gland (black arrow) and both enlarged adrenal glands (white arrows), which were subsequently proved to be medullary thyroid carcinoma and pheochromocytoma respectively.

DISCUSSION

The patient had a triad manifestations of multiple endocrine neoplasia type 2a (MEN2a): medullary thyroid carcinoma, pheochromocytomas and primary hyperparathyroidism. This syndrome is a rare, complex and potentially lethal disorder, so that early recognition and diagnosis is very important. MEN 2a is inherited by an autosomal dominant mode of transmission.[2] However, many patients, including the patient reported here developed this syndrome from spontaneous mutation.

The most common manifestation and, indeed ,the hallmark of MEN 2a is hyperplasia of thyroidal C-cells, which progresses through several intermediate stages until finally developing into medullary thyroid carcinoma (MTC). Twenty percent to 50% of affected individuals develop unilateral or bilateral pheochromocytomas, and 10% to 20% develop parathyroid hyperplasia or multiple parathyroid adenoma.[3,4]

MTC originates from para-follicular cell (C-cells), which synthesize, store, and secrete calcitonin.[2] The clinical presentation is usually a unilateal or bilateral nodules or thyroid mass. A fine needle aspiration typically shows cytologic changes which is characteristic for MTC and can be confirmed by immunocytochemical staining for calcitonin. Serum calcitonin greater than 1000 pg/ml in association with elevated carcinoembryonic antigen (CEA) level is also used for diagnosis of MTC. In particular, determination of the serum calcitonin value stimulated by intravenous pentagastrin or calcium infusion is the prefered screening test for patient who is at risk for MTC.

Metastases to cervical or mediastinal lymph nodes are found in one half of the patients with a palpable enlarged MTC at initial presentation. Distant metastases to lung, liver, or bone most commonly occur later in the disease course .[5,6]

Metaiodobenzylgaunidine (MIBG) has molecular structure similar to the adrenergic hormone neurotransmitter, norepinephrine (NE). The uptake, storage and release of NE and MIBG take place in the chromaffin granules.[7] MIBG labeled with radioiodine (^{131} I or ^{123} I) can be used to image pheo-chromocytoma and other sym-patho-medulla neoplasm.[8] ^{131}I-MIBG also may protray primary[9] and metastatic MTC.[10] Because the embryonic orgin of the adrenal medulla and thyroid C-cell are similar, both may exhibit the capacity to sequester ^{131} I-MIBG.

Sensitivity of MIBG for diagnosis MTC is about 30%,but its specificity is high.[11-12] Clarke et al [11] compared the uptake of ^{99m}Tc(V) DMSA, ^{131}I-MIBG and ^{99m}Tc-MDP in patients with MTC and showed that ^{99m}Tc(V) DMSA was the most

sensitive agent for detecting sites of MTC. ^{99m}Tc-MDP is useful for evaluation of bony metastases and extraoxeous metastases in MTC.[13] Total thyroidectomy is mandatory for treatment of MTC, however, pheo-chromocytomas should be removed before thyroid surgery.[14]

MTC = Medullary Thyroid Carcinoma

The adrenal medulla in MEN2a apparently undergoes morphologic changes that are similar to those of the thyroid C-cells with diffuse or nodular hyperplasia as precursors of pheochromocytoma.[15] The early clinical features of pheochromocytoma in MEN 2a are inter- mittent headache, palpitation and nervousness ; hypertension is uncommon.[16] Increased urinary excretion of epinep-hrine and an increased ratio of epinephrine to norepinephrine excretion in 24-hr. urine sample are the first abnormalities noted.[17] In most patients with pheochromocytoma, the increase in urine metabolites such as urine VMA is considerable, often to more than three times of the normal range.[18] The specificity and sensitivity of urine VMA is 80-100% and 70-90% respectively.[19-20]

The diagnosis of pheochomocytoma is further confirmed by computed tomography (CT), magnetic resonance imaging (MRI), ^{131}I-MIBG scan. Scanning with ^{131}I-MIBG is useful for confirming the presence of functioning intra-adrenal chromaffin tissue and the exclusion of the rare extra- adrenal pheochromocytoma.[21,22] In the study of Quint LE et al,[23] MIBG scanning had a sensitivity of 100% (20/20). The sensitivity of MRI was 90% (18/20), and CT scaning was 70% (14/20). Scanning with CT is relatively insensitive in detecting extra- adrenal pheochromocytomas elsewhere in the abdomen or the chest, while MIBG scan is outstandingly sensitive in localizing pheochromocytomas in both areas.[24]

If a unilateral pheochromocytoma is found, the contralateral adrenal gland is inspected at surgery and removed only if the gland is nodular or enlarged.[25] This selective approach may prevent or postpone the necessity for glucocorticoid and mineralocorticoid replacement. Because of the 50% likelihood that nonaffected adrenal glands will develop a pheochromocytoma within 10 years, some advocate bilateral adrenalectomy at the time of first operation.[26]

Primary hyperparathyroidism is confirmed by elevated serum calcium level with an inappropriately elevated serum parathyroid hormone level.[27] Bone scintigraphy may show slight generalized increased activity with high bone to soft tissue ratio but rarely more obvious metabolic features and twenty-four–hour whole body imaging is more sensitive.[28] Because most cases of primary hyperparathyroidism are mild and asymptomatic, the high generalized uptake is not a consistent finding and the bone scan should not be used for diagnosis. In clinical practice, the detection of hyperparathyroidism is most likely occurred when a bone scan is performed as part of the investigation of hypercalcemia.[29]

An experienced surgeon will render a high cure rate (greater than 95%) in surgery for sporadic hyperparathyroidism even without preoperative steps to localize the abnormal parathyroids.[30] Success is harder to achieve in MEN, because all parathyroid tissue must be located. Preoperative localization imaging of intrathyroid parathyroid glands or extraparathyroid gland is needed before surgery.[31] Double phases ^{99m}Tc-sestamibi (MIBI) has been reported to significantly increase the reliability of scintigraphic localization of hyperfunctioning parathyroid tissue.[32-33] The mechanism is different biokinetic handling in thyroid and parathyroid tissue. The difference in uptake may be explained by the number of mitochondria in the cells where adenoma and hyperplastic gland have in large number.[34] Chiu et al [35] suggested that ^{99m}Tc-sestamibi is sequestered in the cytoplasm and

mitochondria. Joseph et al[36] showed sensitivity of double phases ^{99m}Tc-sestamibi in the detection of adenoma and hyperplastic gland to be 80% and 60% respectively. Hyperplasia is more difficult to be evaluated because of varying criteria for positive diagnosis. Strict criteria was defined that four parathyroid glands were detected scintigraphically. Loose criteria define a positive result that more than one parathyroid glands were demonstrated in the scan. Rodriquez et al[37] reported that dual phases MIBI sensitivity is greater than ultrasonography and CT, but similar sensitivity and greater specificity for MIBI, as compared with MRI. MRI has a high cost and low specificity.

Limitation of double-phases technique is related to the presence of parathyroid adenoma with a rapid ^{99m}Tc-sestamibi wash-out, similar to that of thyroid tissue; this condition can cause false-negative scintigraphic result.[38] Another limitation is related to thyroid nodules which can be ^{99m}Tc-sestamibi avid regardless of whether they are benign or malignant. Such nodules may trap and retain the tracer for a prolonged time, as do parathyroid adenoma, causing false-positive result.[39]

As we know an autosomal dominant inheritance in MEN2a, screening test should be done in all relatives of the patient. Identification of point of mutation of the RET proto-oncogene now makes it possible to identify gene carriers with 100 per cent accuracy in families with a proven mutation.[40]

In conclusion, patient with the MEN2a syndrome manifest a spectrum of endocrinologic abnormalities. Radio-nuclide imaging is useful in the detection of MTC, pheochromocytomas and, primary hyperparathyroidism. Death is related to either metastatic MTC or pheochro-mocytoma. Therefore, early diagnosis and recognition of the tumors in the patient is very important.

REFERENCE

1. Sipple JH. The association of pheochro mocytoma with carcinoma of the thyroid gland. Am J med 1961;31:163-166.
2. Raue F, Frand-Raue K, Grauer A. Multiple endocrine neoplasia type 2 : clinical features and screening. Endocrinol Metab Clin NA 1994;23:137-156.
3. Easton DF, Ponder MA, Commings T, et al. The clinical and screening age-at-onset distribution for the MEN2 syndrome. Am J Hum Genet 1989;44(2):208.
4. Steiner AL, Goodman AD, Powers SR. Study of a kindred with pheochromocytoma, medullary carcinoma, hyperparathyroidism and Cushing's disease: Multiple endocrine neoplasia type 2. Medicine 1968 ;47:371.
5. Brunt LM, Wells SA: Advances in the diagnosis and treatment of medullary thyroid carcinoma. Surg Clin North AM 1987;67 :263.
6. Duh QY, Sancho JJ, Greenspan FS, et al. Medullary thyrouid carcinoma: The need for early diagnosis and total thyroidectomy. Arch Surg 1989;124: 1206.
7. Beierwaltes WH. Endocrine Imaging Part II. J Nucl Med 1991; 32:1627-1639.
8. Shapiro B, Gross M. Radiochemis-try, biochemistry and kinetics of ^{131}I-MIBG and ^{123}I-MIBG: clinical implications and the use of ^{123} I-MIBG. Med Pediatr Oncol 1978;15:170-177.
9. Endo K, Shiomi K, Kasagi K, et al: Imaging of medullary thyroid carcinoma with ^{131} I-MIBG.Lancet 1984;2:233.
10. Sone T, Fukunaga M, Otauka N, et al. Metastatic medullary thyroid cancer: localization with iodine-131 metaiodobenzylguanidine.J Nucl Med 1985;26:604.

11. Clarke SEM, Lazarus CR, Wraight P, Sampson C, Maisey MN. ^{99m}Tc DMSA (V), ^{131}I-MIBG and ^{99m}Tc-MDP an evaluation of three imaging techniques in patients with medullary carcinoma of the thyroid. J Nucl Med 1988;29:33-38.
12. Clarke SEM. Medullary thyroid cancer. In : Murray IPU, Ell PJ. Nuclear medicine in clinical diagnosis and treatment. Churchill Livingstore, New York 1994.677-685.
13. Johnson DG, Coleman RE, McCook TA, et al. Bone and liver scans in medullary carcinoma of the thyroid. J Nucl Med 1984;25:419-422.
14. James B. Young and Lewis L. Cate-cholamines and the adrenal medulla. In: Wilson JD, Foster DW, Kronenberg HM, Larsen PR. Williams Textbook of endocrinology 9th edition 1998;13:665-728.
15. Carney JA, Sizemore GW, Sheps SG. Adrenal medullary disease in multiple endocrine neoplasia, type 2 : Pheochromocytoma and its precursors. Am J Clin Pathol 1976;66 :279.
16. Gagel RF, Tashjian AH Jr, Cummimgs T, et al. The clinical outcome of prospective screening for multiple endocrine neoplasia type 2a, An 18-year experience. N Engl J Med 1988;318:478-484.
17. Hamilton BP, Landsberg L, Levine RJ. Measurement of urinary epinephrine in screening for pheochrocytoma in multiple endocrine neoplasia type 2. AM J Med 1978;65:1027- 1032.
18. Lewis L. James BY. Pheochromocytoma. In : Isselbacher KJ, Braund-wald E, Wilson JD, Martin JB, Fauci AS, Kasoer DL. Harrison 's Principles of Internal Medicine 14th edition 1998;333:2057-2060.
19. Wittles RM, Kaplan EL, Roizen MF. Sensitivity of diagnotic and localization tests for pheochromocytoma in clinical practice. Arch Intern Med 2000;160(16): 2521-2524.
20. Peaston RT, Lennarad TW, Lai LC. Overnight excretion of urinary catecholamines and metabolites in the detection of pheochromocytoma. J Clin Endocrinol Metab 1996;81(4):1378-1384.
21. Valk TM, Frager MS, Gross MD, et al. Spectrum of pheochromocytoma in multiple endocrine neoplasia. A scintigraphic portrayal using ^{131}I - metaiodobenzylguanidine. Ann Intern Med 1981; 94:762-767.
22. Sisson JC, Shapiro B, Beierwaltes WH. Scintigraphy with I-131 MIBG as an aid to the treatment of pheochromocytomas in patients with the multiple endocrine neoplasia type 2 syndromes. Henry Ford Hosp Med J 1984;32:254-261.
23. Quint LE, Glazer GM, Francis IR, et al: Pheochromocytoma and paraganglioma. Comparison of MR imaging with CT and I-131 MIBG scintigraphy. Radiology 1987;165:89.
24. William HB. Endocrine Imaging: parathyroid, adrenal cortex and medulla, and other endocrine tumor. part II,J Nucl Med 1991; 32(8) : 1627-1639.
25. Gagel RF, Tashjian AH Jr, Cummings T, et al. Impact of prospective screening for multiple endocrine neoplasia type 2. Henry Ford Hosp Med J 1987;35:94-98.
26. Van Heerden JA, Sizemore GW, Carney JA, et al. Surgical management of the adrenal glands in the multiple endocrine neoplasia type 2 syndrome. World J Surg 1984;8:612-621.

27. Cance WG, Wells SA Jr. Multiple endocrine neoplasia type 2a. Curr Probl Surg 1985;22:1-56.
28. Fogelman I, Bessent RG, Beastall GB. Estimation of skeletal involvement in primary hyperparathyroidism. Ann Intern Med 1980 ;92:65.
29. Ryan PJ, Fogelman I. Bone scintigraphy in metabolic bone disease. Semin Nucl Med 1997;l27(3) :291-305.
30. Brennan MF. Reoperation for suspected hyperparathyroidism. In Kaplan El (ed) : Surgery of the Thyroid and Parathyroid Glands. New York, Churchill Livingstone, 1983,168.
31. Sawady J, Mendelsohn G, Sirota RL, et al. The intrathyroid hyperfunctioning parathyroid gland. Mod Pathol 1989;2: 652.
32. Taillerfer R, Boucher Y, Potvin C, et al: Detection and localization of parathyroid adenomas in patients with hyperparathyroidism using a single radionuclide imaging procedure with Technetium-99m-sestamibi (double phase study). J Nucl Med 1992;33:1801-1807.
33. Stenger A, Frilling A, Beyer W, et al. Tc-99m sestamibi imaging -A new method in localization of abnormal parathyroid glands. Eur J Endocr 1994;130:227 (abstr).
34. O'Doherty MJ, Kettle AG, Wells PC, Collins REC, Coakley AJ. Parathyroid imaging with ^{99m}Tc-sestamibi : preoperative localization and tissue uptake studies. J Nucl Med 1992;33,313-318.
35. Chiu ML, Kronange JF, Piwnica WD. Effective of mitochondrial and plasma-membrane potentials on accumulation of hexakis (2-methoxyisobutylisonitrile) technetium in cultured mouse fibroblasts. J Nucl Med 1990;31:1646-1653.
36. Joseph K, Welcke V, Hoffken H, et al : Scintigraphy of parathyroid adenomas with ^{99m} Tc-sestamibi in an endemic goiter area. Nuklearmedizin 1994;33:93-98.
37. Rodriquez JM, Tezelmam S, Siperstein AE, et al. Localization procedures in patients with persistent or recurrent hyperthyroidism. Arch Surg 1994;129:870-875.
38. Leslie WD, Riese KT, Dupont JO, et al. Parathyroid adenomas without sestamibi retention. Clin Nucl Med 1995;20:699-702.
39. Rubello D, Mazzarotto R, Casara D. The role of ^{99m}Tc-sestamibi scintigraphy in the planing of therapy and follow up of patients with differentiated thyroid carcinoma after surgery. Eur J Nucl Med 2000;27:431-440.
40. Mulligan LM. Ponder BAJ. Genetic basis of endocrine disease : multiple endocrine neoplasia type 2. J Clin Endocrinol Metab 1995;80:1989-1995.

PERICARDIAL CYST, A CASE REPORT

M. Puvaneswary MB, BS; F.R.CR.[1] G. Oldfield MB, BS; F.R.A.CP[2]

A 83 year-old woman was referred for evaluation of a left paracardiac mass. She had a history of hypertension and bronchiectasis involving the right middle lobe. The blood pressure was 160/90 mm Hg, and the heart rate was 80 beats / min and regular. The heart sounds were normal and there was no audible murmur and the jugular vein pressure was not elevated. Routine laboratory values were unremarkable.

An electrocardiogram revealed a normal sinus rhythm and left axis deviation due to left anterior hemiblock. A chest roentgenogram demonstrated mild cardiomegaly and partial collapse consolidation of the right middle lobe and a large left paracardiac mass. A computed tomographic scan (CT) of the chest demonstrated a well-marginated cyst in the anterior pleuropericardial space distinct form the adjacent heart and vasculature (Fig. 1).

The magnetic resonance imaging (MRI) demonstrated a lobulated well-marginated non-enhancing mass (Fig. 2a) measuring 7.5x12x11.5 cm in the anterior mediastinum with intermediate signal intensity in T1-weighted turbo spin echo (T1-W TSE) (Fig. 2b) and T2-W TSE sequences (Fig. 2c). The pericardium was well seen adjacent to the mass. There was bronchiectasis and collapse consolidation of the right middle lobe.

Because of the atypical features of the cystic mass an aspiration was performed under CT guidance. Approximately 300 ml of milky fluid was aspirated.

The biochemical analysis of the fluid revealed an elevated protein of 10 gm/L, CK 0/UL, LD 2u/L, cholesterol 0.1mmol/L, glucose 3.3mmol/L. Microscopy demonstrated 135x10 L white cells and 25x10 /L red cells. Microbiology and culture were unremarkable.

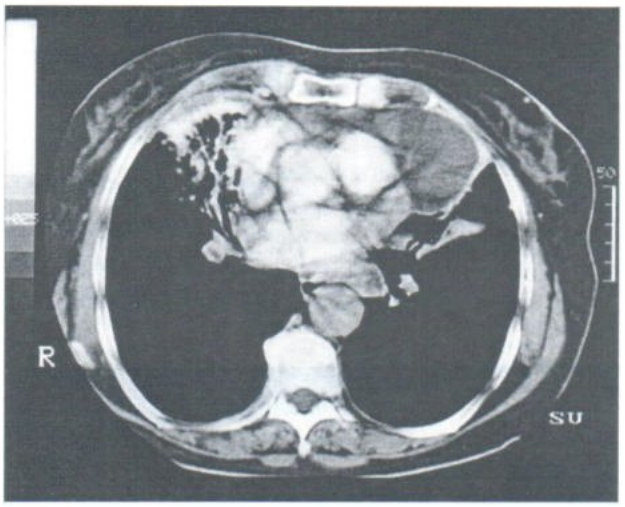

Fig. 1. Axial post-contrast CT scan demonstrates right middle lobe bronchiectasis and anterior pericardial cyst.

[1] Department of Medical Imaging
[2] Department of Cardiovascular Medicine

John Hunter Hospital, N.S.W AUSTRALIA
Correspondence: M. Puvaneswary, John Hunter Hospital, Locked Bag No 1., Hunter Mail Centre, NSW 2310, Phone 49213383, Fax 49213949

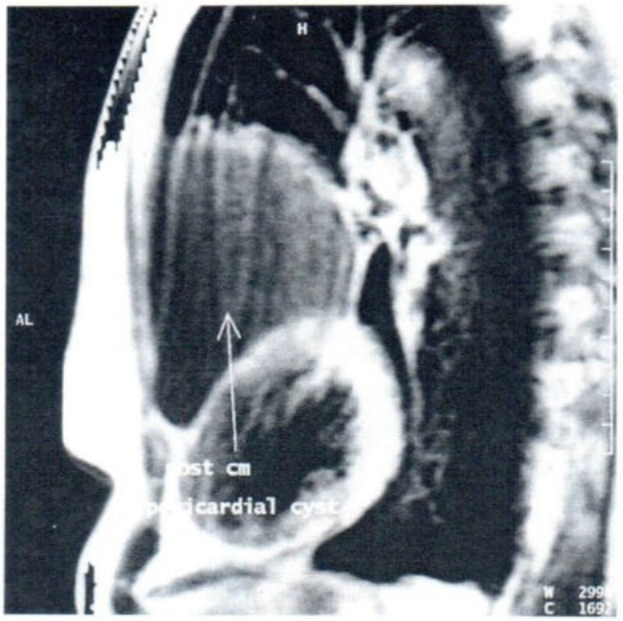

2a

Fig. 2a. Sagittal post-contrast T1-weighted MRI image. Non-enhancing pericardial cyst. (arrow), post cm pericardial cyst; post-contrast pericardial cyst.

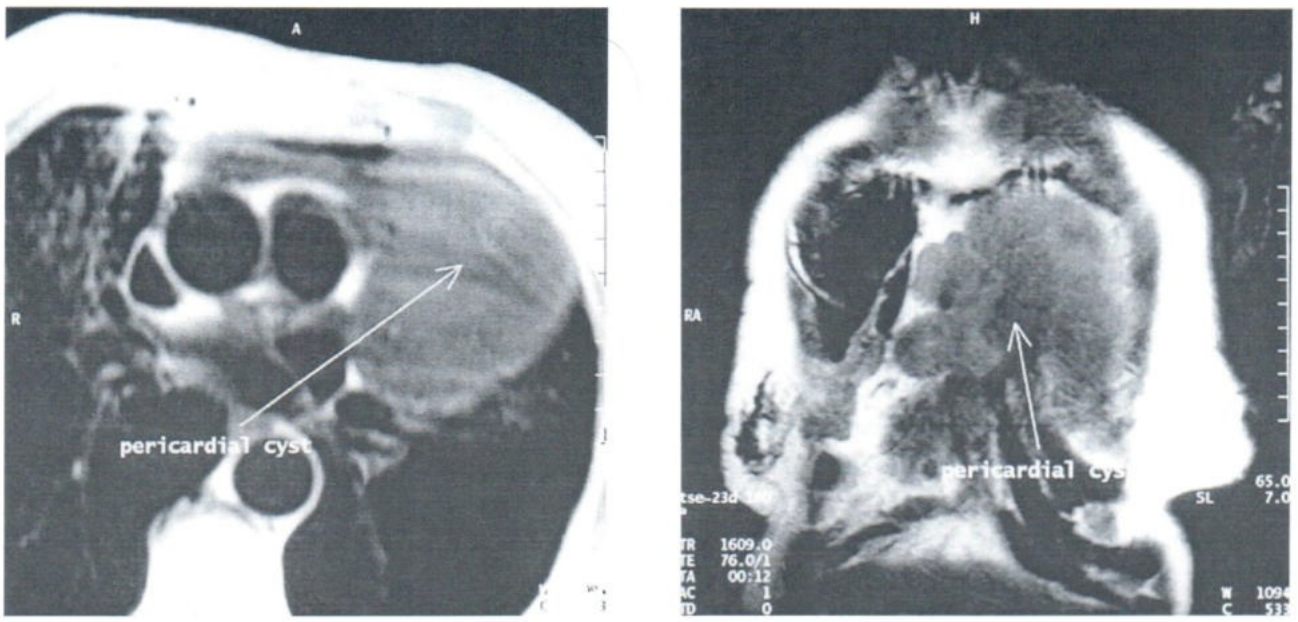

2b 2c

Fig. 2b. TSE T1-weighted axial image, **(C)** TSE T2-weighted coronal image.
Large lobulated well-marginated intermediate signal intensity anterior pericardial cyst. Right middle lobe bronchiectasis. (arrow); pericardial cyst.

REFERENCES

1. McAllister HA Jr. Primary tumours and cysts of the heart and pericardium. Curr Probl Cardiol 1979;4:1-51.
2. Maier HD: Diverticulum of the pericardium. Circulation 1957;16:1040-1045.
3. Ozasa A, Nakazawa K, Kamegai M et al. A case of epicardial cyst. Jpn Circ J 1991; 55:53-57.
4. Feign DS, Fenoglio JJ, McAllister HA, et al. Pericardial cysts; A radiologic-pathologic correlation and review. Radiology 1977;125:15-20.
5. King JT, Crosby I. Pugh D et al. Rupture of pericardial cyst. Chest 1971;60:611-612
6. Ng AF and Olak J. Pericardial cyst causing right ventricular outflow tract obstruction. Ann Thorac Surg 1997;63: 1147-1148.
7. Chopra PS, Duke DJ, Pellet J, et al. Pericardial cyst with partial erosion of the right ventricular wall. Ann Thorac Surg 1991;51:840-841.
8. Mastroroberto P, Chello M, Bevacqua E, et al. Pericardial cyst with partial erosion of the superior vena cava. An unusual case. J Cardiovascular Surg 1996;37:323-324.
9. Brunner Dr, Whitley NO. A pericardial cyst with high CT number AJR 1984;142: 279-280
10. Murayama S, Murakami J, Watanabe H, et al. Signal Intensity Characteristic of Mediastinal Cystic Masses on T1-Weighted MRI J Comput Assist Tomogr 1995;19(2):188-191.
11. Stark DD, Higgins CB, Lanzer P, et al. Magnetic resonance imaging of the pericardium : normal and pathologic findings. Radiology 1984;150:469-474.